Passive Regeneration: Long-Term Effects on Ash Characteristics and Diesel Particulate Filter Performance

by

Michael J Bahr

B.S., Aeronautical Engineering
United States Naval Academy, 2006

Submitted to the Department of Mechanical Engineering in Partial Fulfillment of the Requirements for the Degree of

NAVAL ENGINEER

And

MASTER OF SCIENCE IN MECHANICAL ENGINEERING

AT THE

MASSACHUSETTS INSTITUTE OF TECHNOLOGY

June 2013

Signature of Author: _____
Department of Mechanical Engineering
June 1, 2013

Certified by: _____
Victor W. Wong
Principal Research Scientist and Lecturer in Mechanical Engineering
Thesis Supervisor

Accepted by: _____
David Hardt
Chairman, Department Committee on Graduate Students

(This page intentionally left blank)

Passive Regeneration: Long-Term Effects on Ash Characteristics and Diesel Particulate Filter Performance

by

Michael J Bahr

Submitted to the Department of Mechanical Engineering on June 1, 2013 in Partial Fulfillment of the Requirements for the Degrees of

NAVAL ENGINEER

&

MASTER OF SCIENCE IN MECHANICAL ENGINEERING

ABSTRACT

Diesel particulate filters (DPF) have seen widespread growth as an effective means for meeting increasingly rigorous particle emissions regulations. There is growing interest to exploit passive regeneration of DPFs to reduce fuel consumption accompanying traditional active regeneration. Incombustible material or ash, mainly derived from metallic additives in the engine lubricant, accumulates in the DPF over time. This ash accumulation increases flow restriction and rise in pressure drop across the DPF. The growth of pressure drop adversely impacts engine performance and fuel economy.

This study built upon previous research to evaluate the different effects of regeneration strategy on ash packing and distribution within DPFs. Since passive regeneration relies on a catalyzed reaction, the interactions of ash with the catalyst will play an important role. Passive regeneration is specifically dependent on exhaust feed gas composition, exhaust conditions including temperature and flow rate, catalyst type and configuration, and the state of DPF loading during prior to passive regeneration. The goal of the study is to address the long-term effects of regeneration parameters on ash accumulations and the resulting impact of ash on the DPF catalyst performance. Experiments were conducted that focused on pressure drop measurements over the lifetime of diesel particulate filters with different regeneration methods coupled with post mortem ash characterization. These experiments provide insight to how these regeneration methods impact the DPF performance.

These results, among few fundamental data of this kind, correlate changes in diesel particulate filter performance with exhaust conditions, regeneration strategy, and ash morphological characteristics. Outcomes are useful in optimizing the design of the combined engine-aftertreatment-lubricant system for future diesel engines, balancing the necessities of additives for adequate engine protection with the requirements for robust aftertreatment systems.

Supervisor: Victor W. Wong
Title: Principal Research Scientist and Lecturer in Mechanical Engineering

(This page intentionally left blank)

ACKNOWLEDGEMENTS

My time at MIT will stay with me forever. Numerous people have contributed to making this experience exceptionally rewarding. This period in my life has afforded me opportunities to grow and develop on unimaginable levels, and for that I am grateful.

I would like to thank my thesis advisor, Dr. Victor Wong, for allowing me to work on a project that I truly valued. With the aid of both Dr. Wong and Dr. Alex Sappok, I was guided to develop an understanding of scientific research and a capability to critically evaluate experimental results. I would also like to thank the MIT Consortium to Optimize Lubricant and Diesel Engines for Robust Emission Aftertreatment Systems for their funding and support as well as feedback and insight at our biannual meetings.

Thane DeWitt and Raymond Phan are key to every study conducted in the Sloan Automotive Laboratory. They both work hard to support all students in every way possible, from advice, to parts acquisition and beyond. Working in the Sloan Automotive Laboratory has been rewarding and I would like to personally recognize Dr. Carl Justin Kamp, Casey Chiou, and Tim Murray for making lab work pleasurable and contributing to every aspect of my research. Our discussions and laughs will never be forgotten.

The support of my fellow 2N classmates has left me with many memories from their vast experiences in the Navy as we ventured through classes at MIT together.

I also want to thank my family and friends for their support. From motivation to mental breaks, they have carried me through this journey. I have been fortunate to have the constant support from my best friend and wife, Kathi. From the trips to the coffee shops to late night lab visits, her encouragement and patience has supported my every step, making our time here gratifying.

(This page intentionally left blank)

Table of Contents

LIST OF FIGURES

LIST OF TABLES

(This page intentionally left blank)

NOMENCLATURE

API	American Petroleum Institute
ASTM	American Society for Testing and Materials
ATS	Aftertreatment System
Ca	Calcium
C-DPF	Catalyzed Diesel Particulate Filter
CI	Compression Ignition
CO	Carbon Monoxide
CO_2	Carbon Dioxide
CT	Computed Tomography
DPF	Diesel Particulate Filter
DOC	Diesel Oxidation Catalyst
EGR	Exhaust Gas Recirculation
EPA	Environmental Protection Agency
EU	European Union
HC	Hydrocarbons
Mg	Magnesium
NI	National Instruments
NO	Nitrogen Oxide
NO_X	Oxides of Nitrogen
P	Phosphorous
Pe	Peclet Number
PM	Particulate Matter
PPB	Parts per Billion
PPM	Parts per Million
Re	Reynolds Number
S	Sulfur
SA	Sulfated Ash
SCR	Selective Catalytic Reduction
SI	Spark Ignition
SiC	Silicon Carbide
SO_2	Sulfur Dioxide
SO_4	Sulfate
SOF	Soluble Organic Fraction
SOL	Insoluable Fraction
TDC	Top Dead Center
ULSD	Ultra Low Sulfur Diesel Fuel
ZDDP	Zinc Dialkyl-Dithio-Phosphate
Zn	Zinc

A	Area
A_f	DPF Frontal Area
D	Diffusion Coefficient
$d_{Aggregate}$	Aggregate Particle Diameter
D_H	Hydraulic Diameter
d_P	Pore Diameter
$\overline{D}_p^2$	Surface Average Sphere Diameter
$d_{Primary}$	Primary Particle Diameter
k	Permeability
L	DPF Length
P	Pressure
S	Channel Perimeter
u	Exhaust Gas Channel Velocity
U_w	Filtration Velocity
v	Exhaust Gas Velocity
v_w	Exhaust Gas Wall Velocity
w	Porous Media Thickness
$Z_{in\ /\ Out}$	Channel Inlet / Outlet Friction Coefficient
ΔP_{ash}	Ash Layer Pressure Drop
$\Delta P_{Channel}$	Channel Pressure Drop
ΔP_{In}	Pressure Drop Due to Inlet Contraction
ΔP_{Out}	Pressure Drop Due to Outlet Expansion
ΔP_{Total}	Total DPF Pressure Drop
ΔP_{Soot}	Soot Layer Pressure Drop
ΔP_{Wall}	Substrate Wall Pressure Drop
ε	Porosity
μ	Dynamic Viscosity
ν	Kinematic Viscosity
ρ	Gas Density
$\rho Packing$	Packing Density
$\rho Theoretical$	Theoretical Density
τ	Shear Stress
ξ	Contraction / Expansion Loss Coefficient

1 INTRODUCTION

Diesel engines have a crucial component of the world's energy supply especially within the transportation sector. Ever since the introduction of the diesel engine in the late nineteenth century it has been an extremely popular powering method based off it's high fuel economy, reliability, durability, along with low fuel and maintenance costs. Diesel power has become the majority for commercial land and marine vehicles, and retains a significant share of personal and commercial passenger vehicles in volatile fuel markets such as Europe, with diesel vehicles comprising more than 50% of the fleet. One of the major downfalls of diesel engines is the high amount of particulate matter (PM) emissions. The bulk of these emissions is soot which has become an increasingly regulated pollutant and its carcinogenic effects have been realized. The health concerns regarding the soot emissions has prompted strict emissions regulations to protect public health.

To reduce PM emissions diesel particulate filters (DPF) have been added to aftertreatment systems (ATS) in nearly all diesel engines produced after 2007 for both United States and European uses. The DPF can trap over 99% of PM and have proven the most successful way to reach government emission regulation to date. The disadvantage of incorporation of DPF in the exhaust system results in engine backpressure reducing fuel efficiency. This encouraged optimization of ATS to further reduce losses due to emissions reduction.

1.1 Diesel Engine Fundamentals

First patented in 1892 by Rudolph Diesel the first diesel engine operated effectively in Germany in 1897. This baseline design built upon current internal combustion engine technology but used injection of fuel into air heated by compression to induce combustion, rather than relying on heat from an external source such as a spark plug. With this new design the compression ignition (CI) engine compared to the spark ignition (SI) engine yielded a doubling of efficiency when it was introduced [1].

Although diesel engine technology has advanced since its invention, the basic process remains the same; a reciprocating piston, internal combustion engine relying on high pressure air compression balanced with timed fuel injection to yield in-cylinder combustion. The compression of air prior to fuel injection enables CI engines to use compression ratios of 12-24, which is significantly higher than those in SI engines that generally fall between 8-12 [2]. With this high compression ratio, intake air is compressed to 30 to 55 bar and temperatures from 700°C to 900°C during the compression stroke [1]. Fuel injection occurs just prior to the piston's top dead center (TDC). The elevated temperatures and high pressure

causes the fuel injection to auto ignite, and thus powering the power stroke with the rapid expansion of burning fuel air mixture.

Limited by knock or auto-ignition SI engines cannot reach comparable compression ratios of CI engines. CI engines avoid knock by compressing prior to fuel being presented in the combustion chamber, so the fuel air mixture does not have the required time in chamber to auto-ignite early. Another main difference between SI and CI engines is their methods of controlling the load of the engine. While SI engines use restrictions of intake air to control the load, CI engines vary that amount of fuel injected in the combustion chamber, while not effecting intake air.[1] With these differences, CI engines have various advantages and disadvantages compared to SI engines.

1.1.1 Diesel Engine Advantages

The unique features of the diesel cycle described in the previous section provide the CI engine with a few of characteristic advantages such as greenhouse gas and hydrocarbon (HC) reduction, increased fuel economy, durability, reliability and low fuel & maintenance costs as compared to its SI counterparts [3]. Because CI engines have small pumping losses due to not having to throttle engine operation and overall lean fuel/air ratios the cycle increases the fuel conversion efficiency. These features translate to a 20-40% increase in fuel economy as compared to SI engines of similar power [4].

The lean operation of the diesel engine also gives the added benefit of reducing the unburned fuel that are present in crevice volumes of SI engine, and thus CI engines have extremely low HC emissions. Also directly related to the engine's fuel to air ratio, Carbon Monoxide (CO) emissions remain exceptionally low due to the availability of oxygen to fully oxidize the carbon to Carbon Dioxide (CO_2). The low HC and CO emissions of CI engines diminishes the need for costly ATS to minimize these gaseous emissions like the three-way catalysts used with most SI engines [1], [3].

The CI combustion process produces abundance of heat quicker and sooner in the expansion stroke than in a SI engine. Because this heat released occurs at slower engine speeds compared to SI engines, Diesel engines have a very high amount of torque in the low speed range. Slower speeds have lower frictional losses for the same power generation. CI engines eliminate the need for intricate ignition related systems such as spark plugs and distributors that are a source of wear and failure. Matched with the higher compression ratios of approximately twice that of a SI engine create a stout engine design resulting in a usable life up to four times that of a SI engine. These advantages make diesels attractive for many applications [3].

1.1.2 Diesel Engine Applications

The advantages of efficiency, fuel economy, durability, and power output continue to make diesel engines the prime mover of choice for a number of applications. These applications include construction, mining, agriculture, military, emergency power generation, and transportation. With transportation being the largest sector ranging from large commercial ships and locomotives to a growing number of light-duty passenger cars.

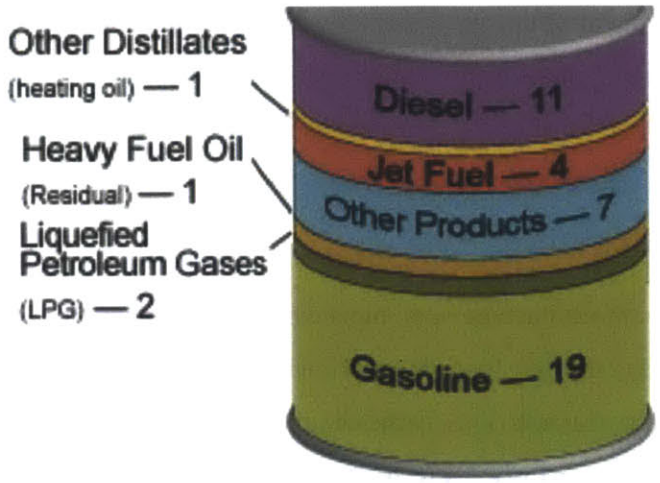

Figure 1: Products Made from a Barrel of Crude Oil (Gallons) (2011)[5]

A study performed in 2011 shown in Figure 1 above estimated that diesel fuel accounted for nearly 25% of all refined petroleum products with 94% of all diesel in America produced being used in diesel powered vehicles [5]. A study from 2000 analyzed the variety of uses of diesel applications in the United States. This showed that approximately 22% of mining equipment, 62% of school buses, 66% of agriculture equipment, 75% of inner-city rail transit, 85% of commercial trucks, 100% of commercial marine, 100% of railway freight transport, and 100% of inner city buses are diesel powered [6]. Since this study was conducted the growth of natural gas has decreased some of these values, but the percentages are still strong. As previously stated due to the fuel price volatility in Europe and Asia, many passenger vehicles are diesel powered, compared to the small percentage of personal passenger diesel vehicles in the United States. This small sector is on the upswing, growing in the United States by 80% since 2000.[4]

1.1.3 Diesel Engine Emissions

The advantages of the CI engine discussed in the prior sections come with a few key disadvantages. The robust engine design comes with a higher acquisition capital cost, low power to weight ratio, and increased noise compared to SI counterparts. These disadvantages are compromised with fact that the

diesel engine is currently the most efficient internal combustion engine available. The most technological challenge as of now comes with the emissions of the diesel engines.

Diesel Engine exhaust comes with the challenge of the high nitrogen oxides (NO_x) or PM emissions. These two emissions are closely tied, and by reducing one normally the other will increase. This is strongly correlated to the limited fuel and air mixing, high pressure, and high temperature turbulent diffusion flame of diesel combustion [1]. Nitrogen Oxide (NO) formation is dependent on both temperature and oxygen concentration, and the tendency for CI engines to form NO is substantially increased because diesel engines have higher compression ratios and run lean. PM is formed during the combustion process due to poor mixing of CI engines, and is principally unburned fuel and lubrication oil additives. Oxidation of PM can occur by increasing the cylinder temperature, but then that would have an adverse effect of increasing in NO_x emissions.

Many emission reduction methods have been employed on diesel engines. Reduction of he NO_x emissions can be achieved by retarding the fuel injection timing to lower cylinder temperature but this increases PM emissions and comes with a fuel efficiency decrease of up to 10% [1]. Reducing the temperature in cylinder also lowers the exhaust gas temperature, which creates problems for oxidation of collected soot within a DPF. Oxidation of soot requires a temperature above 600°C if the filter does not contain a catalyst [7]. Another effective method of reducing NO_X emissions is exhaust gas recycling (EGR). By diluting the fresh intake air with a fraction of exhaust gas, oxygen available to form NO_X is reduced. While this method is effective, fuel conversion efficiency of the cycle, and thus the overall efficiency of the engine are greatly reduced.

1.2 Diesel Emission Regulations

With increasing evidence of the health effects posed by diesel particulate matter, concern over diesel emissions has grown considerably. Ideally diesel fuel is a mix of hydrocarbons that when oxidized would produce CO_2 and water vapor (H_2O). Actual combustion is nowhere near ideal and produces a multitude of products.

The post combustion diesel pollutants produced are credited to an assortment of non-ideal processes during combustion (unburned fuel, combustion of lubrication and fuel additives, and high temperature and pressure mixture reactions). Many diesel emission suspected pollutants are not regulated by government bodies either due to their yet-to-be-proven adverse health effects or their abundant production in nature, but the pollutants that are widely regulated include are PM, NO_X, HC and CO.

Motivated by the growing concern over the negative environmental and human health effects posed by emissions, large reduction in allowable NOx and PM emissions from heavy-duty diesel engines have been implemented. NOx concentrations in populated urban areas contribute significantly to the development of photochemical smog and ozone [1]. Exposure to diesel exhaust has chronic long-term effects which can range from noncancerous to carcinogenic, as well as short-term effects including irritation and neurophysiological symptoms [8]. The majority of PM emitted from diesel engines is of an extremely small size (~ 0.1 μm [1]), when inhaled these particles can penetrate deep within the lung tissue. This leads to an increased likelihood of a number of health related issues such as respiratory irritation & infection, aggravation of asthma symptoms, chronic coughing, and in extreme cases lung cancer [8]. Symptoms are predominant in young children whose immature respiratory systems cannot yet repel infections and in elder members with asthma, emphysema, and heart or lung disease.

Air pollution is the total combination of a multitude of sources from power generation facilities, coal/wood stoves, internal combustion engines, municipal waste incinerators, and many more. Regulating pollutants requires knowing each source. Methane (CH_4) and nitrous oxide (N_2O) the naturally significantly exceeds the contributed by SI and CI engines and therefore are not regulated engine emission products. However for CO, HC, PM, and NO_X emissions contributions from SI and CI engines contribute greatly to the total amount and are consequently regulated engine emissions. Based off a study conducted by the Environmental Protection Agency (EPA) in 2002, the mobile sources category contribute to as much as 50% of the NO_X emissions, 70% of the CO emissions and very large shares of the HC and PM emissions in industrialized countries. Inside this mobile source category, SI engines are responsible for majority of the HC and CO emissions and CI and SI engines divide the NO_X emissions approximately 50% each. The chief contributor of PM emissions within the mobile source category is CI engines. $PM_{2.5}$ is defined as all PM smaller than 2.5μm, and approximately 75% of $PM_{2.5}$ can be attributed to CI engines [8]. The issue of PM pollution from diesel sources is more significant more pronounced in Europe, due to the larger dense number of diesel engines in operation compared to the United States [9].

In 2006 In conjunction with the tighter emissions limits the EPA also limited the sulfur contents of highway diesel fuel to no more than 15ppm [9]. The use of this ultra-low sulfur diesel fuel (ULSD) aside from helping reduce overall particle emissions, more importantly it enables the use of advanced ATS which are deactivated by high fuel sulfur levels. With a growing surge of non-road diesel engines moving

to ULSD in 2010, as well as railroad locomotive and marine diesels in 2012 advanced ATS could cover a greater range of diesel engines [10].

Figure 2 graphically displays the historical U.S. heavy duty emission regulations.

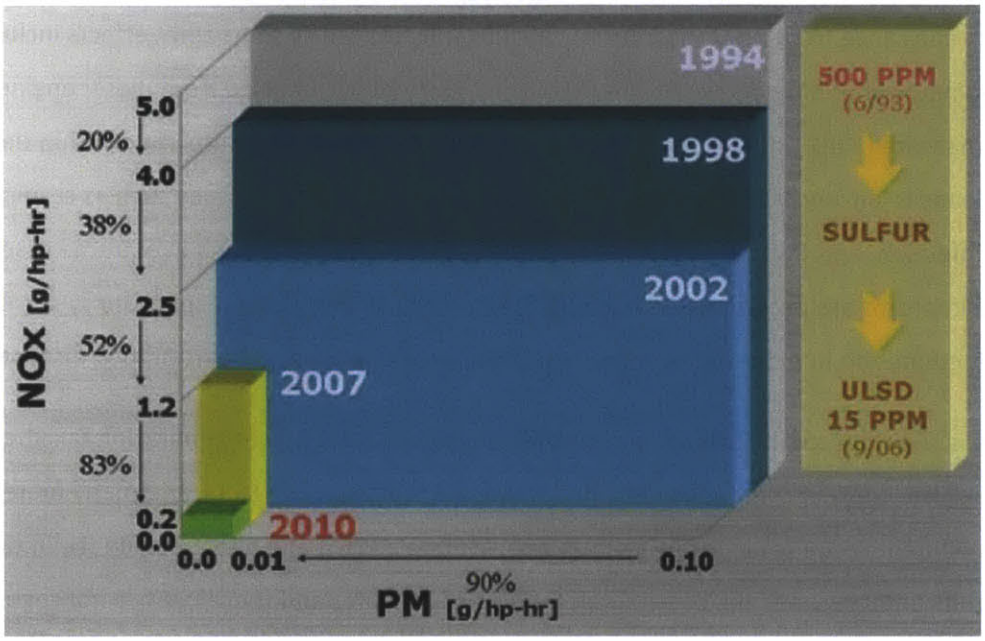

Figure 2: United States Heavy Duty Diesel Engine Emission Regulation [11]

The U.S. and the E.U. have employed strict and rapid emission regulations in order to greatly reduce the amount of PM and NO_x emitted into the atmosphere. A 90% PM emissions reduction was required for U.S. heavy duty diesels, a standard change from 0.10 g/hp-hr (grams per brake horsepower per hour) to 0.01 g/hp-hr between the years 2002-2007. Further for U.S. heavy duty diesel engines NO_x emission, a 52% reduction was required from 2002-2007 from 2.5 g/hp-hr to 1.2 g/hp-hr. Followed by further regulation the reduced the allowable limit another 83% between 2007-2010 from 1.2 g/hp-hr to 0.2 g/hp-hr.

In addition to adverse health effects, black carbon (soot) emissions is one of the largest contributors to global warming, only second to CO_2. Reliant on temperature of formation, diesel PM ranges between 70%-90% carbon [1]. Soot has a global warming contribution factor of around 60% of that of CO_2 [8]. Elemental carbon is a strong absorber of solar radiation, and while a large fraction of these black carbon emissions, around 30% are due to the use of biomass for heating and cooking in developing countries, diesel engines produce significant amounts in developed nations. CO_2 may remain in the atmosphere for

years, while the lifespan of soot is on the order of a week. This is the reason reduction of soot emissions produces almost immediate environmental benefits.

1.3 Diesel Emission Reduction Methods

The two primary missions of concern from diesel engines are PM and NO_X, since NC and CO emissions from diesel engines are normally low and below regulated levels. There are in-cylinder methods as previously described of reducing unwanted diesel emissions but this typically results in a permanent engine configuration along with a fuel efficiency consequence. Another method of reducing diesel emissions is with the installation of an exhaust ATS. This adds additional components to the exhaust system to reduce emissions as the engine produces them. The most widely accepted and effective method to reduce PM emissions has been the addition of a DPF to the ATS. Using a porous substrate DPF physically trap PM while exhaust is flowing thru the filter. Once mass begins to increase in the filter the flow resistance and backpressure on the engine increases. This causes a fuel efficiency reduction, so using a catalyst or increasing the temperature of the DPF the soot trapped will be oxidized resulting in the emission of CO_2. This practice is referred to as filter regeneration and will be discussed in more detail in later sections. As soot is oxidized, incombustible ash is left behind, and this slowly accumulates over time building the pressure penalty of the DPF. Since 2007, DPF have become standard to meet the stringent PM regulation of 0.01 g/hp-hr. Although these systems are highly effective at removing PM from diesel exhaust, the optimization of these systems is necessary to mitigate efficiency penalty that grows with the backpressure on the engine. The optimization and further understanding of DPF aging is the motivation for this research.

(This page intentionally left blank)

2 DIESEL PARTICULATE FILTERS

As discussed in the previous section, the implementation of diesel ATS, specifically DPFs has become extremely attractive with the stringent PM emissions regulations. First used in 1980 in a non-road vehicle use of DPFs have grown rapidly in recent years with PSA Peugeot Citroën being the first auto manufacture to make them standard in 2000 on all passenger cars to prepare for Euro V emission standards [12]. In the United States since 2007 all new diesel vehicles have DPF systems standard, and it has also become an effective retrofit solution on diesel produced earlier. DPFs prevent emissions of harmful PM emissions by collecting solids contacted in the exhaust gas flow with the porous material of the filter.

2.1 Fundamental DPF Operation

A number of geometries and materials have been researched for DPF construction. Wall-flow, ceramic, cellular, monolith filter has become the most popular with the most usage due to its high trapping efficiencies and relatively low cost. Constructed from a porous ceramic with channels running longitudinally along the DPF. Alternating ceramic plugs are placed at either inlet or outlet side designating it an inlet or outlet channel. The inlet and outlet channels are placed next to one another along the filter creating the wall flow structure. Figure 3 displays an actual image of a creaming wall flow DPF as well as an artist's rendition of the wall flow filtration process. As engine-out exhaust that is saturated with PM reaches the filter face, it flows into the inlet channels. The exhaust gas is forced through the porous channel walls before it exits the filter, since each inlet channel is plugged on its outlet end. As gases passes through the walls, high percentages of the PM collects within and on the ceramic filter walls.

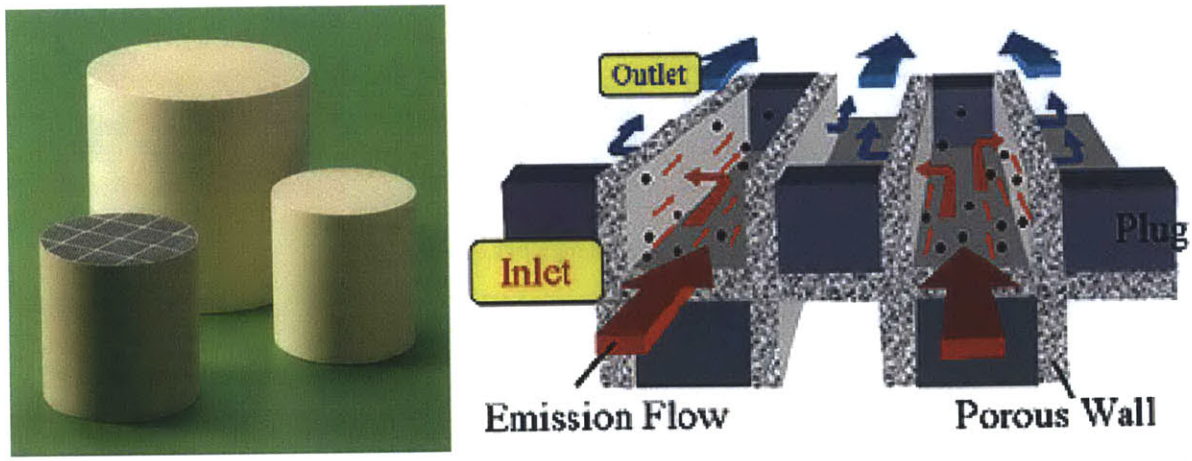

Figure 3: Ceramic DPF image and rendition of wall-flow filter [13], [14]

The combustible portion of PM can be oxidized at temperatures of 150°C -650°C based on type of filter (catalyzed or not) and volatility of the combustible PM fraction. Oxidations are classified by the method of regeneration regime and period. Method refers to passive regeneration relying on catalytic oxidation and active regeneration based on high temperature oxygen based burning of the PM. Period is the classification if the oxidations are continuous or periodic. Once the filter has trapped PM, this added medium increases the DPF's filtration efficiency, which is an inherent advantage of the wall-flow filtration method [15]. However, this added accumulation increases the flow restriction of the ATS translating to a higher exhaust backpressure, thus decreasing engine efficiency [16]. PM within the filter is mainly soot, with an approximately a hundred to one compared to inorganic sulfated ash [17]. With complete regeneration, the combustible soot is oxidized to CO_2 and the incombustible PM (ash) remains in the channels. Figure 4 shows the PM distribution throughout a filter channel with concentrations of ash and a dusting of soot, while Figure 5 exhibits a cross section view of the ash build up overtime in a few channels of a ceramic wall flow DPF.

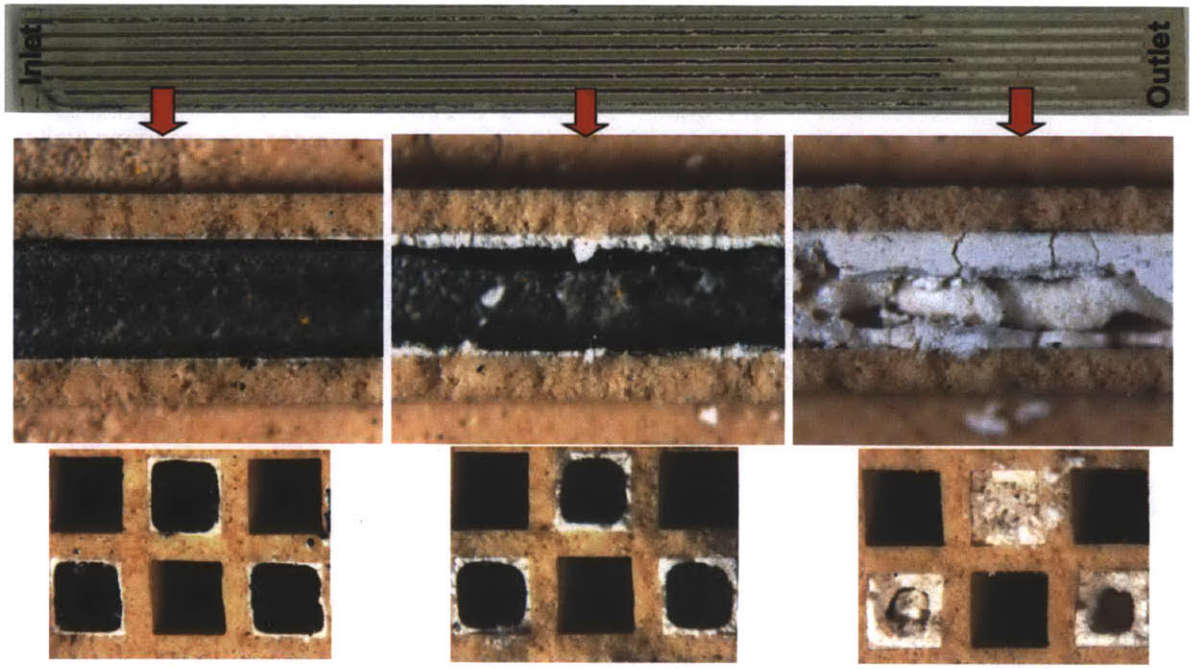

Figure 4: PM distribution along a DPF channels [18]

Figure 5: Display of ash distribution in DPF [19]

Ash accumulation eventually leads to irreversible clogging of the DPF. This will cause the filter to require extensive cleaning or expensive replacement, or will result in extensive engine backpressure build-up or failure. The details of the ash deposition process will be discussed in later sections but note that ash deposits differ greatly from filter to filter and even channel to channel as seen in an X-Ray CT Scan of ash end-plugs in Figure 6. Basic ash distribution is a thin layer on the channel walls along the length of the filter as well as an ash plug located on the outlet end of the filter channels. As ash accumulates the wall layer along the channel thickens thus reducing the hydraulic diameter and open frontal area of the channels. The filter's operational length reduces as the ash plug on the outlet end of the filter channels develops over time. These ash distribution characteristics alter the fluid dynamics of the exhaust gases directly affecting the pressure drop through the filter [17].

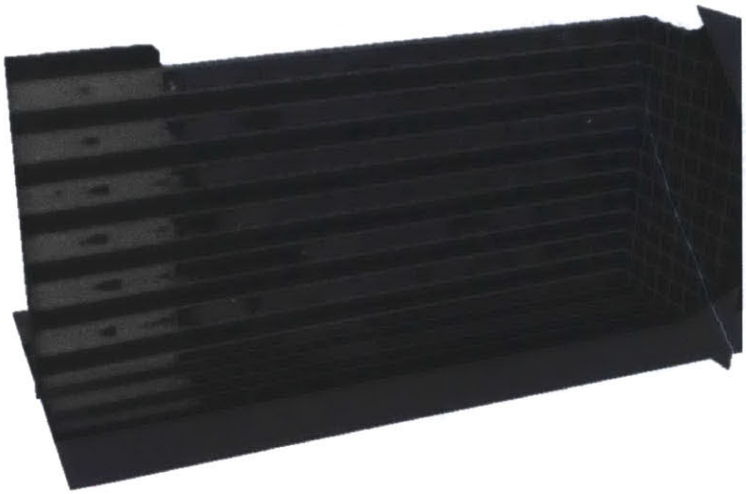

Figure 6: X-Ray CT Scan of ash deposit in end-plugs [20]

2.1.1 Passive Regeneration

Passive regeneration makes use of catalyst to oxidize soot at a lower temperature than with active regeneration. In catalyzed diesel particulate filter (C-DPF), the catalyst is applied to the filter to stimulate chemical reactions amongst exhaust gas and the soot of the exhaust and accumulated in the filter. This catalytic range is normally between 300 and 400°C, therefore typically within the exhaust temperatures ranges experienced during routine operation of the engine. In comparison, with active regeneration temperatures between 550 and 650°C are needed for oxygen based reactions to occur at an acceptable rate. These conditions can only be reached at engine full load condition or with external energy introduced into the system [21].

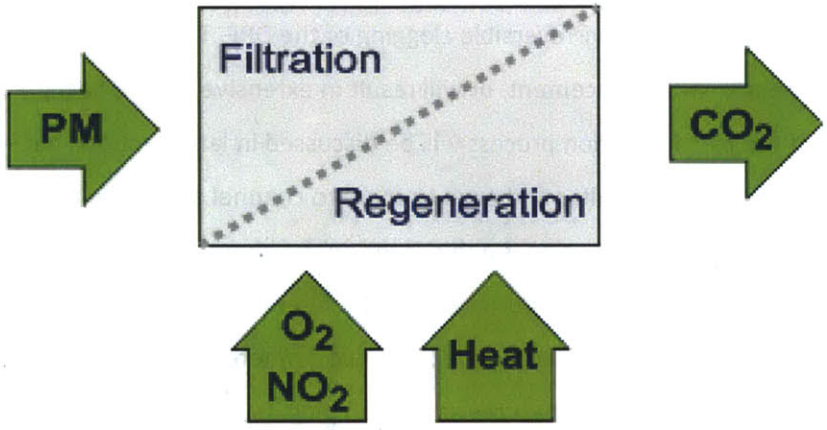

Figure 7: Simple Regeneration Model [22]

Figure 7 shows a simple model that satisfies both active and passive regeneration. The filter captures PM, and then oxygen and heat in active regeneration transforms the carbon to CO_2. With passive regeneration the oxygen is replaced with NO_2. In reality the transformations or regenerations are more complicated. Active regeneration is still fairly straightforward. CO and HC oxidation simply follow Eq 1 and Eq 2. Soot oxidizes completely by Eq 3, but can also partially oxidize to CO.

Eq 1

$$CO + \frac{1}{2}O_2 \rightarrow CO_2$$

Eq 2

$$HC + O_2 \rightarrow CO_2 + H_2O$$

Eq 3

$$C + O_2 \rightarrow CO_2$$

The means of catalytic oxidation of PM are intricate, and are not completely understood. Different reactions occur in parallel and can be stimulated by various catalysts. The mechanisms focus around Eq 4, with the oxidation of NO to its high unstable form NO_2.

Eq 4

$$NO + \frac{1}{2}O_2 \rightarrow NO_2$$

The NO_2 reacts then with the solid carbon of the soot to form CO/CO_2 and recreates the NO molecule as seen in Eq 5. NO gets recycled with the catalyst.

Eq 5

$$C + 2NO_2 \rightarrow CO_2 + 2NO$$

This is again a simplification, these are thermal processes and the oxidation of gases or particles can create limited zones of increased temperature because of the exothermal heat of reaction. These regions can reach active regeneration temperatures to support thermal oxidation of the soot. Once reactions begin they can become change modes as concentrations of soot are ignited. Catalyst can be significantly effective at producing NO2 to oxidize the PM available in the DPF, as seen in Figure 8, the catalyst produced NO2 can be an order of magnitude larger than engine out exhaust within the catalytic range.

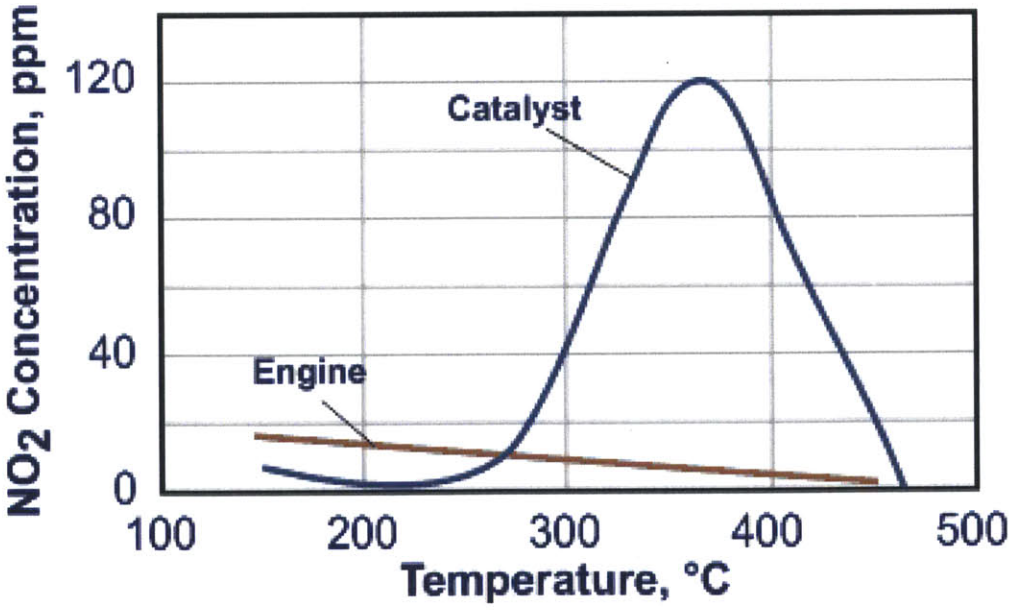

Figure 8: Display of NO_2 exhaust levels [21]

2.1.2 Diesel Oxidation Catalyst (DOC)

The diesel oxidation catalyst (DOC) is a portion of many diesel ATS based on promoting oxidation of exhaust gas components. These systems have traditionally been flow thru based catalyst centered on the oxidation of CO, HC, and the organic fraction of diesel particulates. This system again follows Eq 1 and Eq 2 for the conversion of carbon monoxide and hydrocarbons. Representative conversion percentages of these gases can be seen in Figure 9.

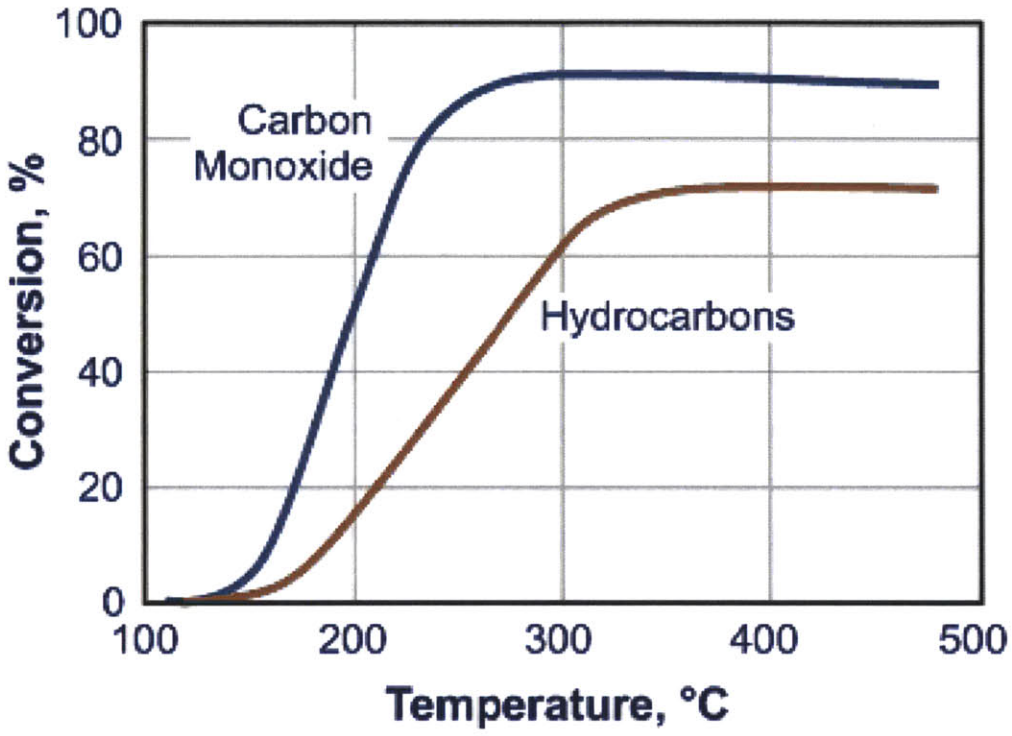

Figure 9: Representative conversion percentages for DOC [23]

The DOC also supports the NOx reaction, Eq 4, which before the use of DPFs was an adverse affect of the DOC, since NO_2 is more toxic than NO. With the incorporation of DPFs the NO_2 production can then be used to oxidize soot at lower temperatures.

2.2 Ash Sources

The small ash deposits of the PM emitted from the diesel engine pose a major problem for DPF lifecycle. While ash is a small portion of the emitted PM, it becomes permanent within the DPF during normal engine operation, and procedures such as filter removal & cleaning or replacement of the DPF is both costly and time consuming. Ash in the DPF comes from a number of sources including engine wear, corrosion particles, trace metals found in diesel fuels, and mainly from lubricant additives (in cases where fuel-borne catalysts are not used [24], [25]). Diesel engine lubricants are normally comprised of

70-83% organic base stocks and 5-8% viscosity modifiers, it is the residual 12-18% of the oil, consisting of a mostly inorganic additive package, that is the source of the majority of the ash emissions. While combustion of diesel lubricant undesirable, it is unavoidable throughout engine operation. This is caused by to small amounts of oil that enters the combustion chamber by bypassing by the piston rings and from the cylinder wall liner. After the combustion the organic portions are oxidized while the incombustible ash remain.

Performing a number of beneficial functions lubricant additives are essential in the engine and are used for wear protection, deposit and corrosion control, soot dispersion, and anti-oxidant functions. Some of the most commonly used additives are calcium- and magnesium-based detergents, and zinc dialkyl-dithio-phosphates (ZDDP) for anti-wear and anti-oxidant. Lubricant-derived ash is composed primarily of Ca, Zn, Mg, P, and S in compounds of phosphates, sulfates, and oxides [26], [27], [28]. Recently the CJ-4 oil specification was developed to minimize ash impacts on ATS systems by introducing limits on the lubricant shown in Table 1.

		Content Limitations		
Specification	Year of Introduction	Sulfated Ash	Sulfur	Phosphorus
API CJ-4	2006	1.00%	0.40%	0.12%

Table 1: CJ-4 oil specification [29]

The effects of specific species on ATS performance are still not well understood even with the introduction of the CJ-4 oil specification. Following the ASTM D876 specification, lubricant sulfated ash is described as the solid remaining after the oil has been mixed with sulfuric acid and heated until the weight of the residual material remains constant [30]. This does not support the method of ash formation in a DPF, and thus does not describe the possible ash formations with the DPF.

2.3 Ash Effects on DPF Performance

Recent years have shown much effort to identify how lubricant additives negatively affect the performance of diesel ATS. Many intricacies are still unknown even though fundamental results have are commonly accepted. These intricacies are necessary to fundamentally understand differences in ash distributions and flow restrictions. Below is a list of a few of the fundamental results from previous studies on ash accumulation.

- DPF ash rises with oil consumption and lubricant ash content [27], [28], [31].

- Ash from lubricant additive is mostly composed of Zn, Mg and Ca sulfates, phosphates and oxides [26], [27], [28], [31], [32], [33].
- Lubricant consumption over-estimates ash buildup because of lubricant volatility [18], [31], [33].
- Ash levels produced widely varying pressure drops [18], [28], [34].
- Plug formation and wall distributions greatly affected by regeneration strategy [35].

Even with significant advancement, the ultimate mechanisms accountable for the results listed above are unknown. An example is the factors affecting ash deposition, migration, and accumulations within the channels, have slight understanding. This is specific to plug formation, uniform distribution, and ash bridging. Explanations for the factors that determine ash packing density, and ultimately pressure drop are still required. The ash composition, morphology and distribution within a DPF is greatly effected by the lubricant additive package and the regeneration strategy. The details of the ash formation in turn effects the extent of the filter's pressure differential with an increasing ash load [36].

2.3.1 DPF Pressure Drop

With the introduction of any restriction, even as simple as a bend in the exhaust piping to as complicated as a filter, a flow restriction is added to the system which causes an exhaust backpressure. With most filters as the filter accumulates debris over time, the filtration area decreases causing the flow restriction to increase. This flow restriction causes a differential pressure between the inlet and outlet of the filter, and it is commonly referred to as the filter's pressure drop. This is the same for a DPF, and PM is the debris the filter accumulates. Soot periodically between regenerations and ash over the long-term life of the filter. Since this pressure drop effects engine efficiency this is one of the primary focal areas of research involved with the DPF. Figure 10 shows a number of experiments that have been preformed to explore the effects of ash on engine backpressure from the DPF.

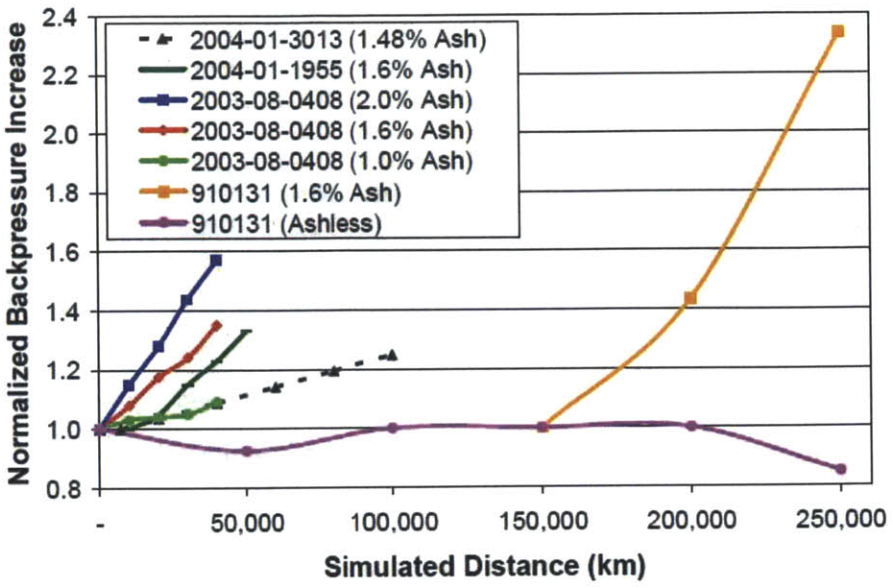

Figure 10: Exhaust backpressure as a function of simulated driving distance (ash load)[24]

As ash load increases, so does the exhaust backpressure, as seen in Figure 10. This figure also shows that ash level does not directly affect the backpressure. In many cases lower ash percentages produced higher backpressures. This shows the importance of ash composition and morphology. Further there are beneficial affects of ash shown in Figure 11.

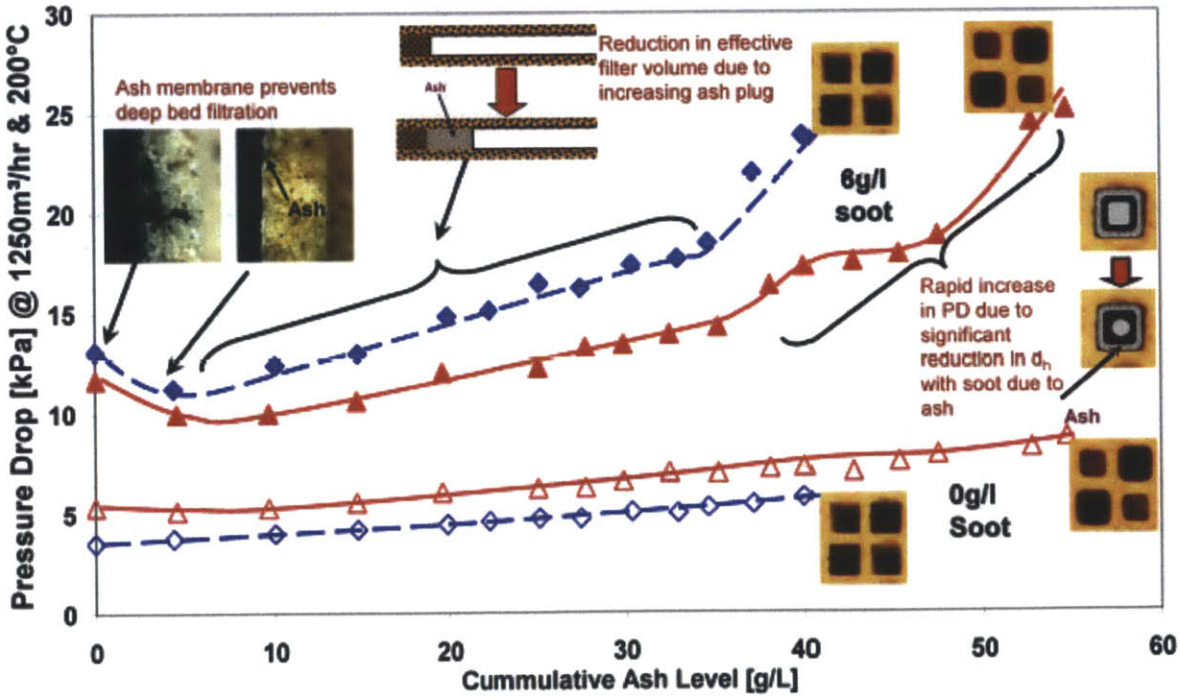

Figure 11: Normalized pressure drop variation with ash in filter [19]

This beneficial affect comes to play with the addition of soot to a filter already containing ash. The ash acts as the filter medium and can reduce the backpressure of the filter under similar soot loads when compared to a clean DPF for lower ash loads.

2.3.2 Operating Conditions and Ash Distribution Effects on Pressure Drop

The operating conditions and regeneration strategy have an important impact on ash morphology and distribution. The distribution of ash throughout the channels influences pressure drop. Figure 12 displays a comparison of ash distribution profiles from a periodic regenerated filter on the left and a continuously regenerated filter on the right. The periodic regeneration tended to generate plugs of ash, while the continuous case has ash dispersed evenly down the walls of the channel with little plug formation.

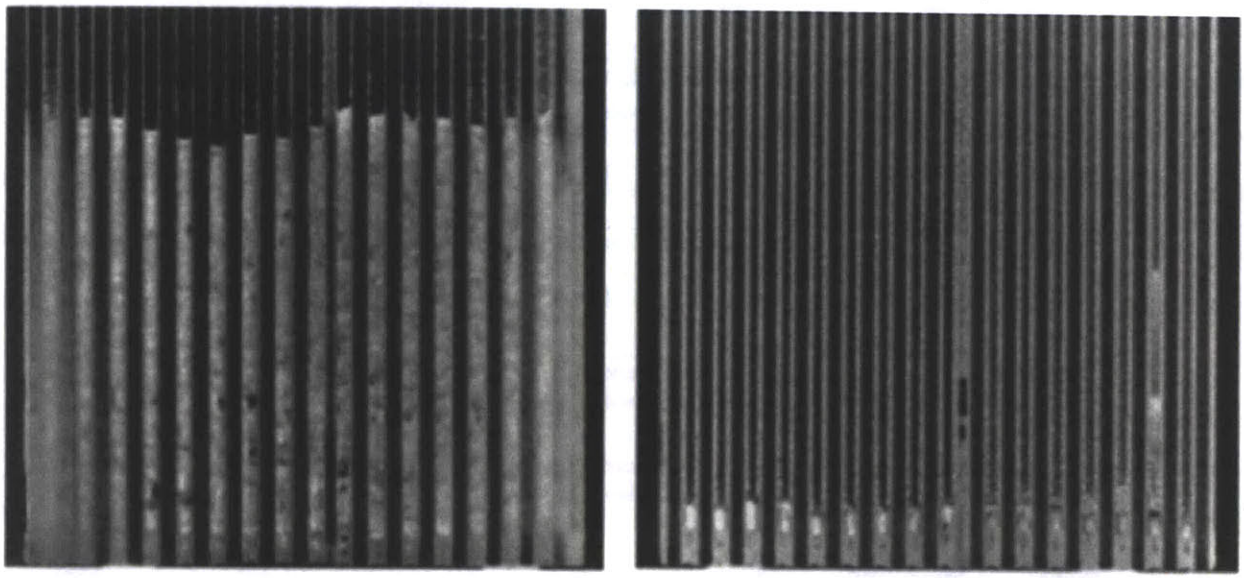

Figure 12: Ash distribution comparison periodic on left continuous on right [35]

When a DPF experiences continuous regeneration and soot is continuously oxidized, the ash is accumulated directly on the filter walls. Accumulation of this fashion seems to adhere securely to the walls of the filter. This produces a fairly even ash layer along the channel length. Whereas in periodically regenerated filters ash accumulated is disseminated in a soot layer that builds along the channel walls. Once the DPF is regenerated and the soot is oxidized the remaining ash agglomerated are a loose network and are not secure to the filter walls. It is thought that these ash formations will move to the plug of the filter because of there formation.

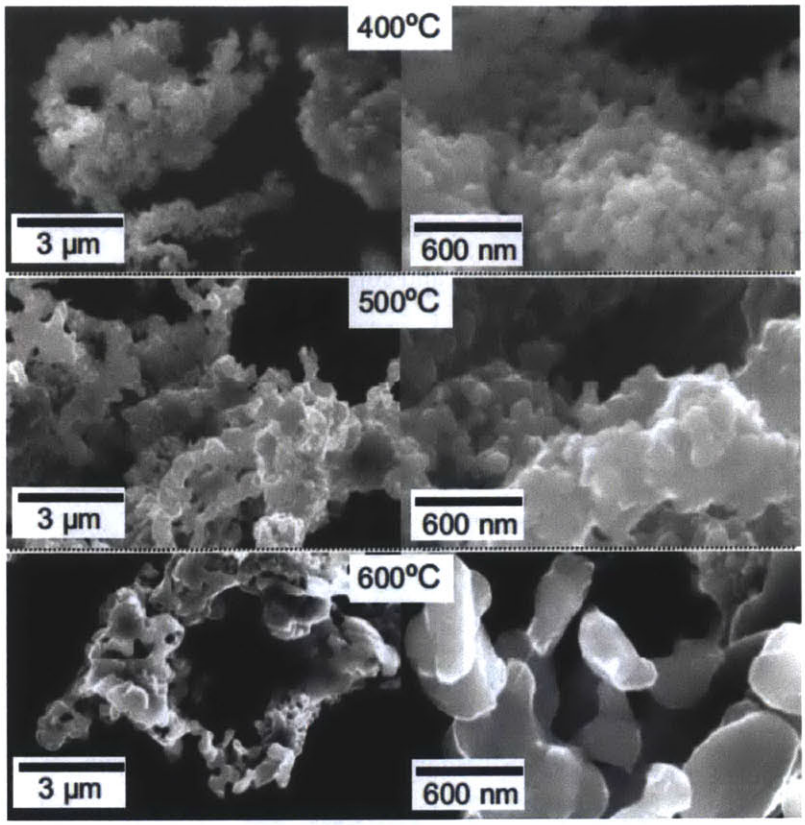

Figure 13: Ash characteristic based on temperature [19]

The varying temperatures the ash formations experience can greatly affect the ash formations as well. Figure 13 shows how increasing the temperature can transform the ash formations. At high temperatures ash agglomerates and sinters. The larger agglomerates have higher permeability since they cannot pack as closely as the smaller particles and agglomerates.

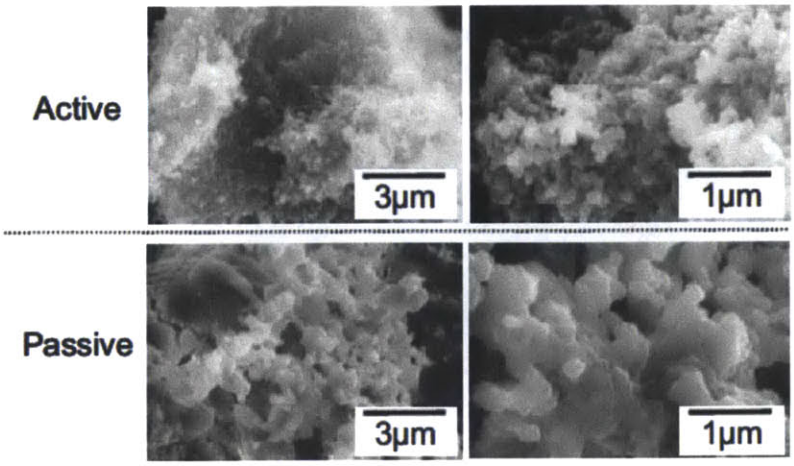

Figure 14: Ash characteristic based on regeneration method [19]

Active and passive regeneration can produce substantially different ash formations. Figure 14 and Figure 15 portray this theory. Similar to the continuous versus periodic case above, this study believes that passive regeneration creates uniform ash layers distributed along the channel walls, while active regeneration focuses the ash agglomerates toward the filter plug. This theory is describes active regeneration producing ash that is beneficial to pressure drop of the filter, because these large agglomerates are pushed to the rear of the filter and continuous to have high permeability. An artist rendering can be seen in Figure 16. This theory is based on the higher temperature active regeneration experiences and the expectation that passive regeneration builds up little PM between regenerations. This is not necessarily true, and will depend on the regeneration method chosen.

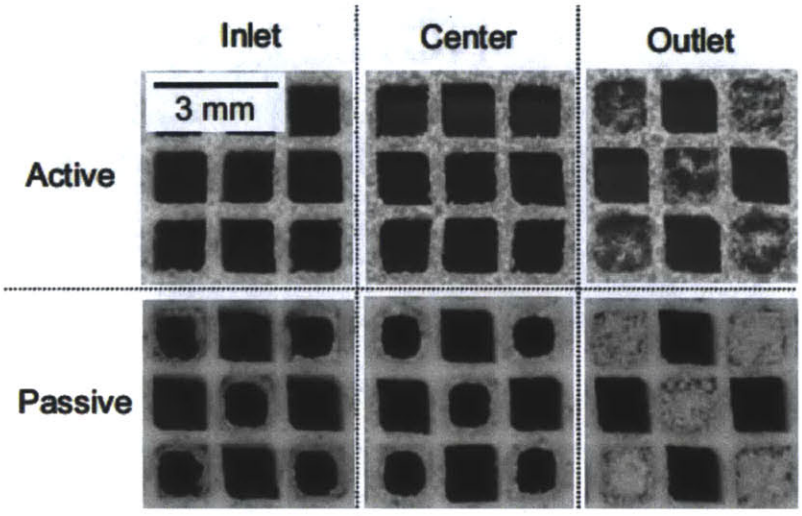

Figure 15: Ash distribution based on regeneration method [19]

With the observed differences in ash distribution between these different studies, it is clear that the resulting pressure drops will differ greatly based on the exhaust conditions and ultimately the regeneration strategy. Level of PM buildup between regeneration effects ash morphology independent of regeneration method.

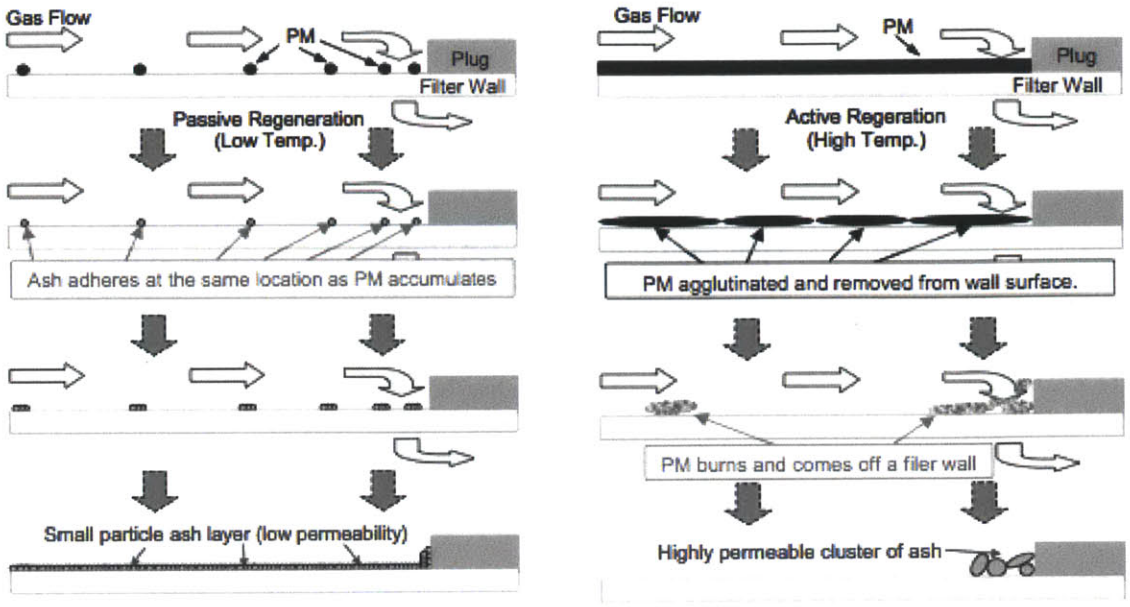

Figure 16: Ash formation theory based on regeneration method [19]

2.4 Project Objectives

There is swelling interest to exploit passive DPF regeneration to reduce the fuel consumption penalty associated with more traditional active approaches. Previous research indicates different regeneration strategies (active vs. passive) may result in differences in ash packing and distribution within the DPF. These studies did not decouple periodic and continuous methods or other regeneration strategies. Increased use of passive regeneration also places additional emphasis on the role of the catalyst and potential ash-catalyst interactions. The primary objective of this project is to further the knowledge on how individual regeneration parameters affect ash properties and accumulation, distribution, and morphology. This will then lend material to explore the impact of the resulting ash on DPF and catalyst performance in a future study. By understanding these affects on DPF performance, the optimization of advanced diesel ATS can be further developed. Three different passive regeneration cases are explored completely aging DPFs to decouple the differences in each method. This focuses on periodic versus continuous regeneration and the affect of a DOC. This evaluates the thermal effects of soot accumulation on ash history and how the DOC role in the ash accumulation.

(This page intentionally left blank)

3 FUNDAMENTAL UNDERSTANDING

Stated in preceding sections, the DPF produces an unavoidable backpressure on the diesel engine. Exhaust gas properties, system configuration, DPF geometry, and distribution and morphology of soot and ash contained in the filer all effect the backpressure of the system. Further understanding how each parameter impacts differential pressure provides greater support to the individual role of ash formation and properties.

3.1 DPF Pressure Drop

Before a DPF is loaded with soot and ash, still in its clean state, it introduces a flow restriction to the diesel exhaust system. The loading of soot and ash reduce the filtration area seen by incoming flow by decreasing each channel's hydraulic diameter and the available channel length. A DPF's pressure drop and flow resistance is directly affected by the characteristics of the accumulated PM. A description of the alterations soot and ash accumulation in the DPF's channels is displayed in Figure 17. Diesel exhaust gas continues to flow through the DPF after significant soot and ash accumulation, due to the porous nature of the PM.

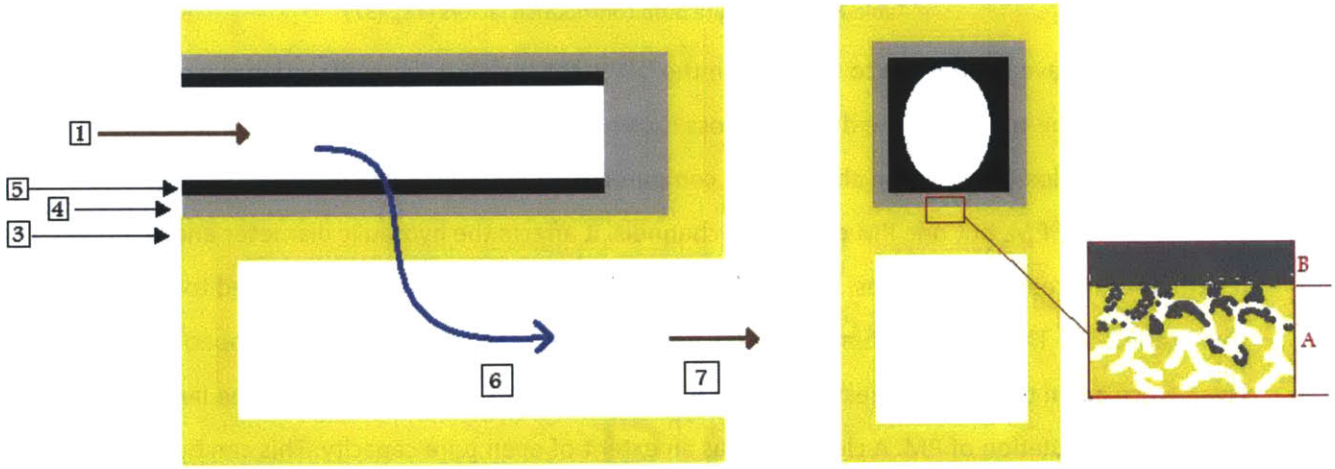

Figure 17: PM accumulation in DPF channel model, numbers correspond to Table 2 [37]

Sappok et al. produced a table of pressure drop contribution variables and their relating parameters. Table 2 exhibits this data with numerical resemblance to Figure 17 [18], [37]. Combining ash, soot, and the wall as one porous medium; follow through this medium accounts for the largest total percentage of pressure drop.

Pressure Drop Contribution Variable		Key Parameters	Controlling Properties	Reynolds Number (Re)	Pressure Drop Contribution %
1	Inlet Losses (Contraction)	Open Frontal Area	Filter Geometry, Ash and Soot Layer Thickness	Transition	<3%
2	Frictional Losses Along Inlet Channel Walls	Channel Hydraulic Diameter	Filter Geometry, Ash and Soot Layer Thickness	< 2,100	5% - 30%
		Available Channel Length	Filter Geometry, Ash and Soot End-Plug Formation		
3	Frictional Losses from Flow Through Channel Wall	Channel Wall Permeability	Filer Properties, Extent of Ash and Soot Depth Filtration (A)	<<1	50% - 90%
		Channel Wall Thickness	Filter Geometry		
		Available Filtration Area	Filter Geometry		
4	Frictional Losses from Flow Through Ash Layer	Ash Permeability	Ash Porosity, Pore Size		
		Ash Thickness	Ash Packing Density		
		Available Filtration Area	Ash Layer Thickness, End-Plug Formation		
5	Frictional Losses from Flow Through Soot Layer	Soot Permeability	Soot Porosity, Pore Size		
		Soot Layer Thickness	Soot Packing Density		
		Available Filtration Area	Soot Layer Thickness		
6	Frictional Losses Along Outlet Channel Walls	Channel Hydraulic Diameter	Filter Geometry	<2,100	~ 5%
		Available Channel Length	Filter Geometry		
7	Outlet Losses (Expansion)	Open Frontal Area	Filter Geometry	Transition	<3%

Table 2: DPF Pressure drop contribution factors [18], [37]

Exhaust gases have to contract to flow within the DPF's channel, but this contraction is a minimal percentage of the total pressure drop. This loss is comparable to expansion losses on outlet side of the filter. Frictional losses along the channel are comparable for both the inlet and outlet prior to the accumulation of PM, but one PM enters the channels, it affects the hydraulic diameter and channel length, thus increasing the losses. PM is extracted from the gas as the exhaust is forced to flow through the filter media. This filter medium is actually both the filter wall as well as any developed ash/soot layer. Once again this is the largest percentage of pressure drop, and it experiences the largest growth with the accumulation of PM. A clean DPF has an extent of open pore capacity. This can hold much of the initial PM accumulation in the DPF, and this preliminary depth filtration occurs with the filling of the pores of the substrate. Figure 17 shows the depth filtration with part **A** along the inlet channels. Depth filtration produces a sharp climb of the pressure drop over a minor amount of mass accumulation. As the PM enters these porous structures it alters the permeability and porosity of the filter substrate causing this initial rise in flow restriction. Part **B** of Figure 17 depicts the thin layer of distributed PM that forms following the depth filtration. This next step is called cake filtration. Cake filtration rapidly increases the filtration efficiency, with the addition of additional porous media thickness. The cake filtration layer actually in a sense becomes the filter. This is a less drastic increase in flow resistance and

can be fairly linear. Figure 18 depicts these filtration means and their corresponding affect on pressure drop over the loading time of the filter.

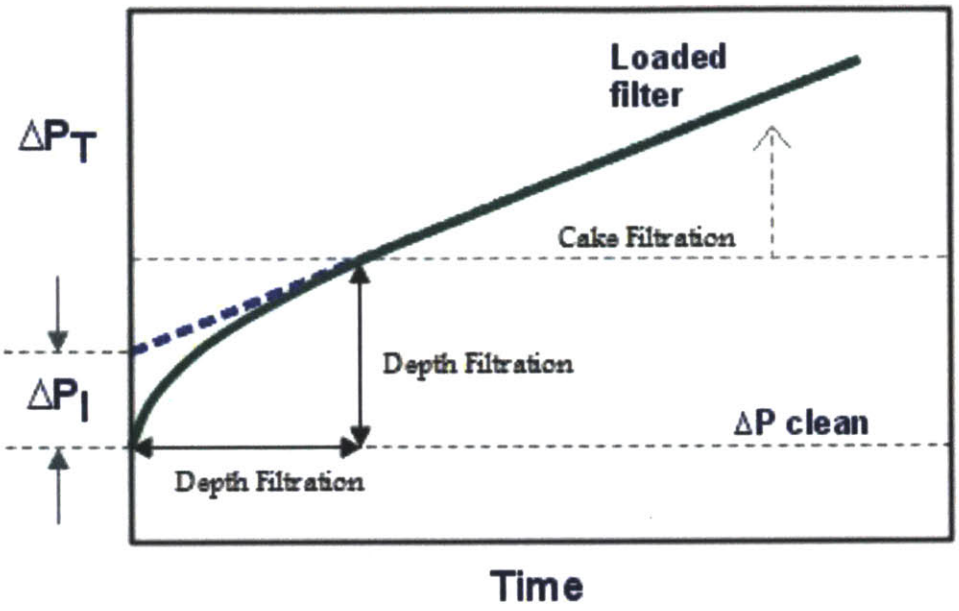

Figure 18: Pressure from as a function of filtration (depth and cake) [38], [39]

Figure 18 is consistent with the majority of studies covering DPFs. The depth filtration of PM presents a sudden non-linear increase in pressure. A closely linear pressure drop increase is observed, as the depth filtration tapers off and a cake layer builds. The non-linear increase due of depth filtration introduces difficulty in estimation of pressure drop modeling because of its highly dynamic nature. Over time various parameters fluctuate and change, but ultimately result in the total pressure drop of the DPF. The fundamentals of these parameters are critical to comprehension of the lifecycle of a DPF.

3.1.1 Zero-Dimension DPF Pressure Drop Model

A zero-dimension pressure drop model captures the significant aspects contributing to the total pressure drop across the DPF. This fundamental, widely used model will help highlight the underlying properties, shown in Figure 17 and Table 2, which affect the total pressure drop of a DPF and support further research and progressive modeling. Mathematically, the total pressure drop can simply be split into six general variables and is portrayed as:

Eq 6

$$\Delta P_{Total} = \Delta P_{In} + \Delta P_{Out} + \Delta P_{Channel} + \Delta P_{Wall} + \Delta P_{Ash} + \Delta P_{Soot}$$

Where $\Delta P_{In/Out}$ is the pressure drop related with the contraction and expansion of the diesel exhaust gases entering and exiting the DPF, $\Delta P_{Channel}$ is the pressure drop associated with the frictional losses along the channel walls, and $\Delta P_{Wall/Ash/Soot}$ contribute to the losses connected with the flow through the porous media layer comprised of substrate, ash and soot.

The pressure drop associated with the contraction and expansion of the inlet and outlet exhaust gases can be described as:

Eq 7

$$\Delta P_{In/Out} = K_{In/Out} \times \frac{\rho V^2}{2}$$

Where ρ is the exhaust gas density, V is the exhaust gas velocity and $K_{In/Out}$ explains the frictional coefficients for inlet contraction and outlet expansion as:

Eq 8

$$K_{In} = \left(-0.415 \times \frac{A_F}{A} + 1.08\right)$$

Eq 9

$$K_{Out} = \left(1 - \frac{A_F}{A}\right)^2$$

The area terms in Eq 8 & 9 refer to the open frontal area, A_F, and total surface area, A of the filter face. These equations are associated with frictional losses due to laminar flow which is not always the case., but it is a conservative estimate. The frictional coefficients for turbulent flow are approximately half of laminar flow proving that the laminar assumption but may be an overestimation. If flow is known to be turbulent or transitional the appropriate frictional coefficients shall be used [40].

Pressure drop from frictional losses occur as the gases pass over the channel walls down the length of the filter. These frictional losses are described as:

Eq 10

$$\Delta P_{Channel} = 4f \frac{L}{D_H} \times \frac{\rho V^2}{2}$$

Where D_H is the channel diameter or hydraulic diameter once the filter is loaded, L is the channel length, ρ is the exhaust gas density, V is the exhaust gas velocity and f is the dimensionless Fanning friction factor is estimated as:

Eq 11

$$f = \frac{K}{Re}$$

Where Re is the exhaust flow's corresponding Reynolds number and K is a constant coefficient of 14.23 for channels of square cross sectional opening and 16.00 for round cross sectional openings [40]. Though the pressure drop from channel friction is typically a small percentage of the DPF total pressure drop, as the hydraulic diameter is noticeably reduced it role increases. This is observed with highly loaded ash and soot filters. Additional note is that the cross sectional channel opening generally evolves from square to circular as the ash load of the filter increases [37].

Mentioned previously, the major contributor to the total pressure drop of the DPF is due to the flow through the porous media layer of soot, ash, and substrate. This contribution can be explained in totality through the Forchheimer-extended Darcy equation as:

Eq 12

$$\Delta P_{Wall} = \frac{\mu}{K_p} v_w w + \beta \rho (v_w)^2$$

Eq 12 takes into account the laminar to turbulent flow transition by including an additional inertial term. The Reynolds numbers associated with the flow through our porous media layer are generally much smaller than one. Because of this the inertial terms are approximated as a first order term resulting in a simplified from of Darcy's Law described as:

Eq 13

$$\Delta P_{Wall} = \frac{\mu}{K_p} v_w w$$

Where μ is the dynamic viscosity of the exhaust gas, v_w is the velocity of the exhaust gas across the porous media layer, w is the thickness of the material layer consisting of substrate along with ash and soot if present, and K_p is the bulk permeability of the porous media layer. As PM accumulates within the DPF, the material thickness, w increases. For a clean DPF, K_p is solely the permeability of the substrate but as soot and ash are deposited within the bulk material, the permeability is altered. The permeability

is significantly affected by both depth and cake filtration, therefore it changes throughout the filters life [39].

The bulk permeability of the porous material layer is a changing variable with the DPF's lifecycle. Permeability, K_p, is a function of porosity and pore diameter. For the substrate wall this calculation is characterized by the Kozeny-Carman correlation:

Eq 14

$$K_w = \frac{1}{5.6}\varepsilon^{5.5}{d_p}^2$$

Where K_w is the permeability of the substrate wall, ε is the porosity of the substrate, and d_p is the pore diameter. Normally the pore size for the substrate has variation and the average pore size is used in Eq 14. Average pore size and substrate porosity are parameters specified by the manufacturer. With soot and ash accumulation along a DPF's channel walls the specific permeability can be described by:

Eq 15

$$\varepsilon = 1 - \frac{\rho_{Packing}}{\rho_{Theoretical}}$$

Where $\rho_{Theoretical}$ is the powder's true density based off its material composition and $\rho_{Packing}$ is its packing density inside the DPF. The packing density directly impacts the ash layer characteristics, hydraulic diameter, and occupied volume. PM enters the DPF pores during depth filtration, and this causes the filter substrate's permeability, porosity and mean pore size change.

The understanding of these parameters regarding ash is still in its preliminary stages, although broad energy has been dedicated to understand the properties of soot layers and its formation principles. Furthering the understanding of these properties and characteristics of ash formation Sappok et al. noted that these parameters change with exhaust conditions as well [36], [37].

3.2 Material Properties

The prior section defined how various material properties of both the DPF substrate and accumulated soot and ash affect the total pressure drop across the filter. A great deal of research has been devoted to determining and understanding these properties. The manufacturer typically specifies the filter substrate's material properties, but as PM accumulation occurs these properties change drastically. The properties of ash and soot layers have been studied in recent year but a complete understanding has yet

to be found. The subsequent section is a brief discussion of the properties and their impact on filter pressure drop.

3.2.1 DPF Substrate Properties

As stated the material properties and characteristics of the DPF substrate are generally well understood and manipulated by the manufactures, prior to PM loading. The two most common types of substrate used in DPFs are cordierite, a ceramic composition, and silicon carbide (SiC). Neither of these are a perfect combination of features. An arrangement of relative parameters for both SiC and cordierite filters can be seen in Table 3.

Property	Cordierite	SiC
Channel Width (mm)	1.3 -2.1	1.0 - 1.6
Wall Thickness (mm)	0.3 - 0.5	0.3 - 0.8
Permeability ($x10^{-12}$ m^2)	0.5	1.24
Porosity (%)	45 - 50	42 - 58
Mean Pore Size (μm)	13 -34	8 - 17
Melting Temp (°C)	1450	2400
Thermal Expansion (1/°C)	0.7×10^{-6}	4.5×10^{-6}
Elastic Modulus, Axial (Gpa)	4.7	33.3
Strength, Axial (Mpa)	2.6	18.6
Thermal Shock Parameter	790	124
Thermal Conductivity (W/mK)	<2	20
Relative Cost	Low	High

Table 3: Typical properties of DPF substrates cordierite and silicon carbide [39]

Only the melting temperature is not affected by PM loading. The rest of the parameters change with the addition of soot and ash loading. Mean pore size governs the size and mass of PM that can fill the pores of the DPF. The porosity is the quantity of open volume space that could be occupied with PM. From Table 3 both cordierite and SiC are approximately 50% porous, which due to the involved network of pores that is distributed throughout the DPF's channel walls.

There are also a number of developmental DPF materials, but they will not be discussed here, as they are still in research phase and have not received wide use [41], [42], [43].

3.2.2 Ash Properties

With the goal of entirely understanding of how ash determines the performance of a DPF, it is key to measure important ash properties then associate them to DPF flow restriction. This knowledge then helps understand how specific exhaust conditions, regeneration strategies, and lubricant chemistries

alter these ash properties. An understanding of this ash characteristics and flow restriction relationship will foster the optimization of DPF design and operation. Several lab and field examinations have been accomplished within the last 15 years have measured these ash properties such as packing density, porosity, and permeability; this data has been reviewed in Table 4.

Source (SAE Tech Paper)	Theoretical Density (g/cm^3)	Packing Density (g/cm^3)	Porosity (%)	Permeability (m^2)	Test Type
2000-01-1016	---	0.4 - 1.0	---	$2.8 - 7.4 \times 10^{-14}$	Lab
2001-01-0190	3.13	0.54	83	---	Field
2004-01-0948	2.5	0.4	85	$\sim 5 \times 10^{-12}$	Field
2005-01-3716	2.85	---	---	---	Field
2006-01-3257	---	0.31 - 0.52	---	---	Field
2008-01-0331	---	0.45	---	---	Field
2009-01-1086	---	0.17 - 0.34	90 -95	---	
Field Test -A	---	0.34		---	Field
Field Test -B	---	0.17		---	Field
Field Test -C	---	0.18		---	Field
Lab Test -A	---	0.26		---	Lab
2010-01-1213	3.4	0.3	91.1	---	Lab

Table 4: Ash Properties [34], [36], [36], [41], [44], [45], [46], [47]

The above ash properties directly relate to the variables contributing to the total pressure drop of the DPF, as explained mathematically by the equations in the previous section. Understanding the related properties will produce an improved understanding of how the total pressure drop is affected. Further, two significant ash properties are particle size and ash layer thickness. The previous discussed mathematical equations presented that the hydraulic diameter and porous media thickness directly influence the total pressure drop on a DPF. Ash deposits are understood to be composed of micro-sized structures forming agglomerates of smaller particles. Particle size likewise affects pressure drop by relating to the amount of depth filtration, and substrate permeability/porosity variation that can occur. The particle size and layer thickness measurements from literature can be seen in Table 5.

Source (SAE Tech Paper)	Particle Size (μm)	Layer Thickness (μm)
2000-01-1016	1 - 10	---
2001-01-0190	$d_{primary}$ 0.1 - 0.5	---
2004-01-0948	2.4 - 37.6	---
2004-01-3013	---	73 - 298
2005-01-3716	0.4 - 8	---
2006-01-0874	1	---
2006-01-3416	---	44 - 94
2010-01-1213	---	200

Table 5: Ash particle size and layer thickness [25], [31], [33], [36], [41], [44], [45], [46]

It should be mentioned that the various measuring methods and experimental procedures impact the large variation of values reported in Table 5. The extent of PM loading directly affects the ash layer thickness along the channel walls as well.

Apart from ash deposit thickness, the location and distribution of the ash accumulated within the filter considerably affects filter flow restriction. Studies have indicated that ash generated during periodic regeneration tends to collect in ash plugs in the back of the filter, compared to ash accumulated during continuously regenerating conditions is distributed along the channel walls with little to no ash plug formation. This distinction in the ash distribution could significantly alter the ash effect on DPF pressure drop [35]. The dynamics governing the location of ash mobility and deposition within the filter remain unambiguous.

Literature presents a clear case that based on the ash property measurements; lubricant chemistries have strong influence on ash properties. Nevertheless, exhaust conditions are equally important in determining ash mobility, deposition, and packing characteristics. To understand the underlying mechanisms responsible ash effects on DPF performance, it is crucial to comprehend the effects of these parameters.

3.2.3 Soot Properties

Unlike to the factors affecting ash properties, soot layer properties and the controlling parameters affecting these properties are much better understood. Soot particles are smaller than ash particles from a particle size viewpoint. Similar to ash, soot particles follow a bimodal size distribution with primary particles ranging from 10 -40nm while agglomerated particles on the order of 100nm [48], [49]. Soot particles are smaller almost by an order of magnitude when comparing these measured soot particles sizes with those for ash found in Table 5.

Soot packing densities are approximately of 0.1 g/cm^3 and layer permeability varies from 1.5 x 10^{-14} m^2 to 3.3 x 10^{-14} m^2 [44], [50]. Ash packing densities are 2 to 5 times that of soot, and ash layer permeability values vary from 2 to 100 times that of soot, compared to the figures for ash in Table 4.

A 2002 study reported that soot packing density and permeability were a function of the flow's Peclet number (Pe), which a measure of inertial versus diffusional deposition:

Eq 16

$$Pe = \frac{U_w \times d_{Primary}}{D}$$

Where U_w if the filtration velocity, $d_{Primary}$ is the primary particle diameter and D is the diffusion coefficient. High Pe signals primarily in inertial deposition which results in a more densely packed later and low Pe represents particles primarily deposited by diffusion resulting in a more loosely packed layer [68]. This is highly dependent on the exhaust flow rate which effect space velocity of the DPF. Many mathematical relationships have been completed and reported in the literature resulting in soot permeability calculations and a better understanding of how soot directly affects pressure drop. Since this study is in regards to exhaust condition effects on DPF performance, these aspects will not be explained.

3.3 Deposition Mechanisms and Cake Filtration Theory

Even though DPF are fairly new, cake filtration theory has been studied for over a century and is understood well. Particles are collected along the cell channel wall, and thus an ash layer is generated. The method of particle deposition controls the ash layer's properties. Many theoretical and experimental studies have developed an understanding of these phenomena.

In the 1980s Houi et al performed a simulation experiment in which a statistical model was used to describe the particle deposition mechanisms and cake layer growth. Two simulations were preformed. In the first simulation, using only a small number of particles (1000) was used to determine deposit. The second simulation used a larger amount of particles to determine the macroscopic structure of the cake layer. Both simulations were based off random, Brownian motion (diffusive) and the results are shown in Figure 19.

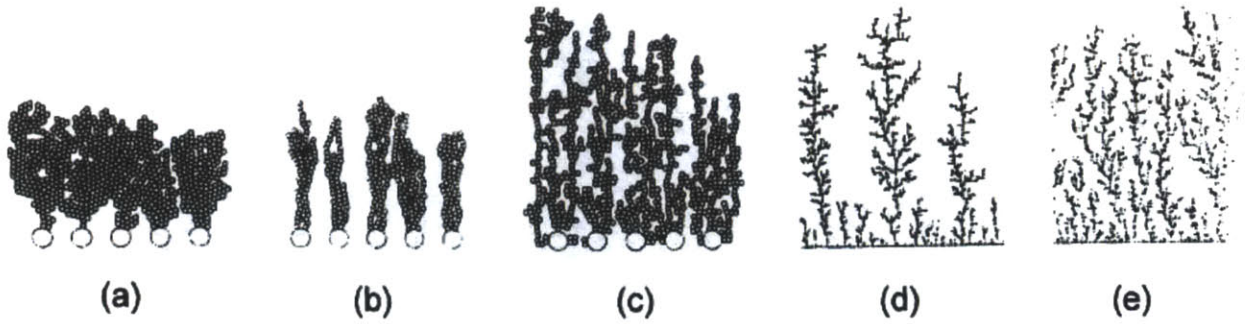

Figure 19: Simulation for 1000 particle deposited on individual collectors (a-c) and macroscopic structure cake layer formation (d,e) [51]

The results exhibited in Figure 19(a-c) characterize particle deposition for particles with much smaller diameter than the filter pores. This is similar to the case of soot and ash deposition in a DPF. The outline circles on the bottom of Figure 19(a-c) represent the collectors, representing the filter surface. Figure 19(d, e) portrays the macroscopic formation and growth of the cake layer. The simulations show that the ash and soot particles are accumulated on the cake layer to form tree-like structures that develop over time. This describes a "sticking probability" which governs whether particle collides to attach itself to the structure or bounces off. The sticking probability is constructed from the angle of incidence of the individual particles within the exhaust flow and the collision with the cake layer. As the particles move from a range of these tree-like structures of the cake layer, the particles will eventually land in a ultimate spot. Since these particles do not attached to the initial structure they strike, the complete density of the cake layer growths. But as the tree-like structures grow they eventually become unstable and colliding particles or the exhaust flow can cause them to collapse. This collapse can create ash bridges. Ash bridges can branch filter pores keeping PM from entering this pores [51].

Other studies have determined that the cake layer growth is associated to the flow's Peclet number (Pe). The tree-like particle formations begin to appear as the Pe decreases. The density of the cake layer deceases and the layer becomes thicker. Also, as the angle of incidence is amplified, comparable tree-like deposits are produced building a more open structure. But as the flow velocity is increased, the layer density is increased and the layer thickness decreases [52], [53]. Figure 20 visually portrays the morphology of the ash layer produced during various conditions.

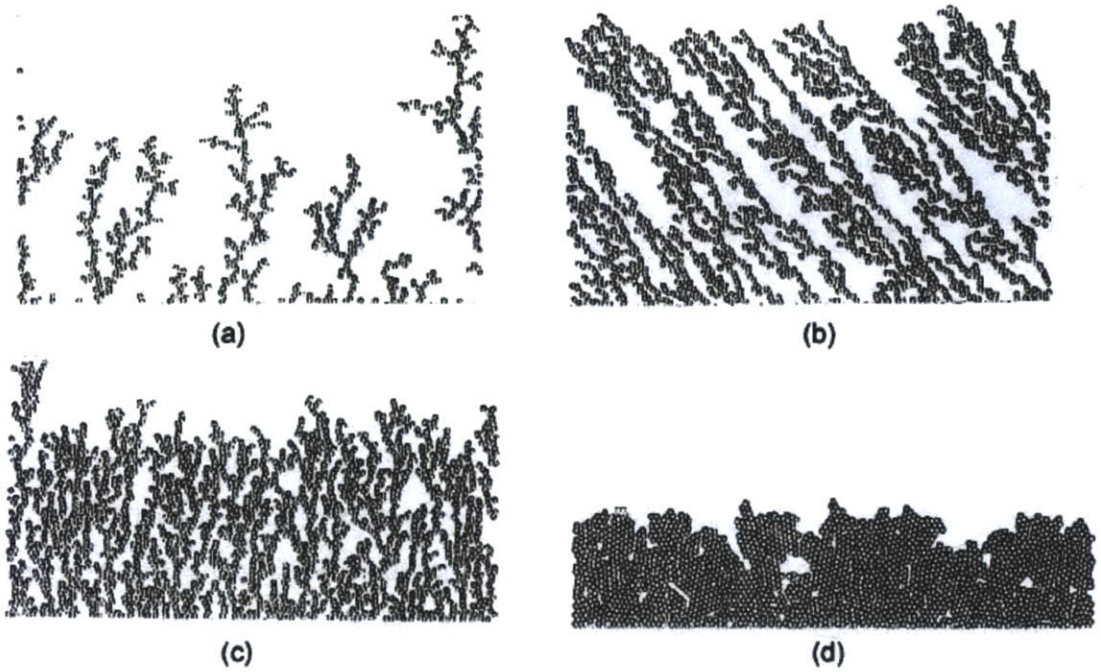

Figure 20: Particle deposition and filter cake layer growth for pure diffusional deposition (a), ballistic deposition at 60 incident angle (b), ballistic deposition normal to the filter surface (c), and ballistic deposition with particle restructuring (rolling events) (d) [53]

Figure 20(d) presents an ash layer produced with multiple "rolling events", or deposit restructuring, transpiring. This occurs when the tree-like structures become unstable and collapse causes them to break and be re-deposited which produces a more densely packed cake layer.

Results have presented that primarily the ash accumulation in a diesel particulate filter will begin by penetrating within the pores of the filter (depth filtration). This leads to a sharp rise in pressure drop and modifies the porous filter's permeability and porosity. Following this deposition in the pores of the DPF, a cake layer begins to build which produces in a smaller linear pressure drop increase. Furthermore as ash accumulation reduces the available filter area, thus resulting in increased gas velocities throughout the filter walls. This increasing the velocity of the particles entrained in the exhaust gas stream. The reduction of the channel hydraulic diameter due to the ash accumulation can also promote an increase in the incident angle of the particles. The following alteration of ash morphology, incidence angle and flow velocity can greatly affect the cake layer morphology which is directly related to the total filter pressure drop.

3.4 Additional Ash Property Considerations

The fundamental equations were defined in previous sections concerning the effects that ash properties have on total DPF pressure drop. Widespread studies have been performed for clean DPF operation and

the effects of soot accumulation, but the effects of ash is lacking. This type of understanding is needed to fully understand aging of DPFs.

A 2003 ash transport model proposed an ash "stickiness factor" to describe ash re-entrainment in the DPF channel flow as a function of the flow shear stress along the channel walls. This "stickiness factor" is correlated to the tendency of tree-like ash deposits reaching their critical shear stress and being re-entrained in the exhaust flow. The critical shear stress of the ash was predicted to be a function of the ash thermal history and properties defining the "stickiness factor". Figure 21 provides simulation results for ash transport for ash of varying "stickiness" [54].

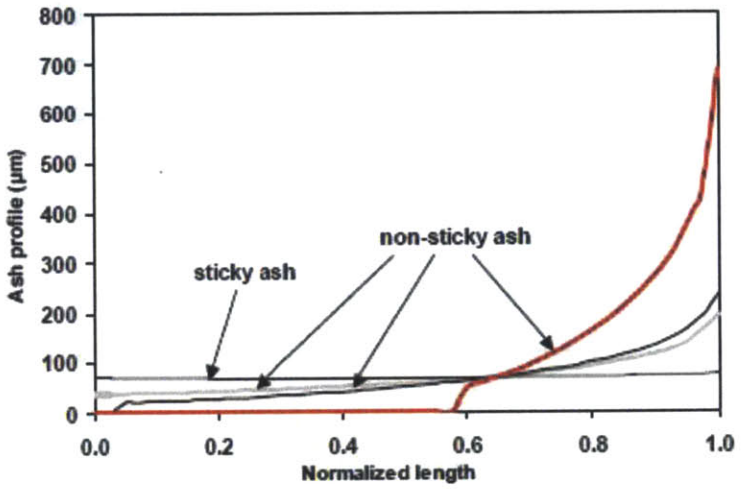

Figure 21: Simulated ash deposition profiles for varying levels of ash stickiness along the DPF length [54]

Figure 21 shows that as ash stickiness increases, the cake layer thickness increased producing little ash end plug. Naturally this is clear that if it is less sticky ash, it will shear from the cake layer and be accumulated near the back of the filter. Ash composition and morphology is influences ash stickiness, and thus provides motivation for the conducted research in determining how exhaust conditions affect the ash "stickiness" and resulting ash profile.

3.5 Ash and Soot Distribution and Modeling

Fundamental equations described at the beginning of this chapter proved that ash morphology and distribution relate directly with the total pressure drop of a DPF. This relationship is of special interest because of the manner in which both ash and soot are deposited in the filter. Although PM distribution is frequently non-uniform both along the channel length and radially, the general deposition trends stand [36], [37], [44].

Particulate matter is initially trapped in the surface pores of the porous media of a clean filter. Mentioned previously this early depth filtration has a large effect on DPF pressure drop. The extent of depth filtration is normally small only occurring at particulate loads less than 5 g/L [36], [37]. Depth filtration is represented with SEM images in Figure 22.

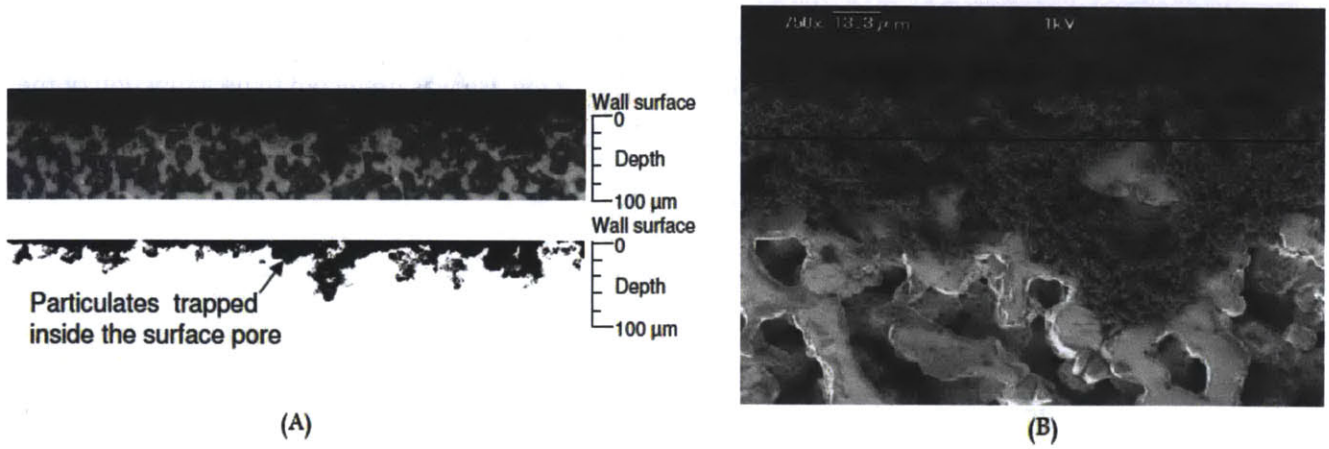

Figure 22: SEM images of depth filtration of a SiC DPF [55]

Figure 22(A) shows depth filtration inside the filter matrix. Some depth filtration reaches deep inside the matrix of filer surface, but most is limited to surface pores. Figure 22(B) displays increased magnification of depth filtration within the filter matrix similar to Figure 22(A). This depth filtration again occurs a PM loads on the order of 5g/L and lower and produces a sharp rise in DPF pressure drop. This is shown in the three experimental test cases in Figure 23 by three steep initial slopes. While depth filtration doesn't change channel geometry, it greatly alters the porosity and permeability of the porous filter matrix.

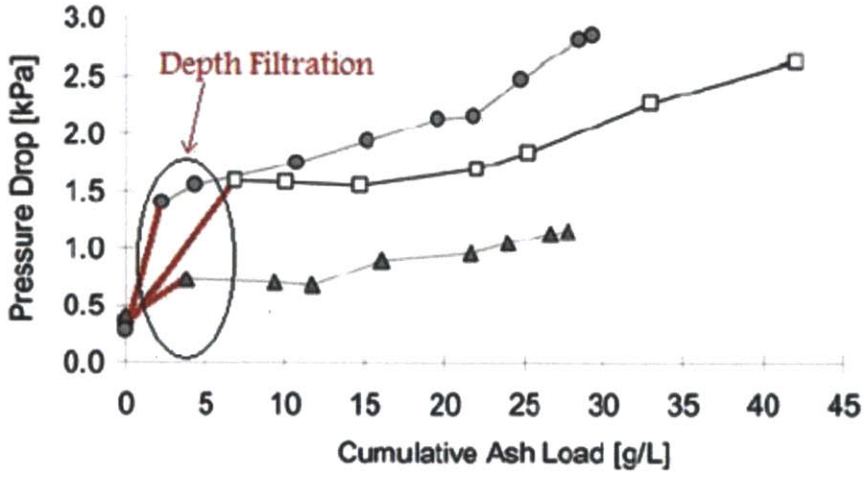

Figure 23: Pressure drop due to depth filtration highlighted [36]

Filling the surface pores with soot and ash or bridging of the pores ends depth filtration. Once depth filtration has ended, cake filtration occurs which builds a layer of soot and ash down the filter channels. This formation alters the channel geometry reducing the channel's hydraulic diameter. The decrease in channel diameter greatly influences the flow characteristics. The filters trapping efficiency increases, because as the cake layer builds the available porous media for filtration grows. But as the cake layer reaches a "critical thickness" and the max allowable shear stress is reached, the ash layer can shear and move to the end of the filter. This builds an ash plug that seems to arise at ash loads on the order of 12 g/L, mainly this does not become a significant issue until much larger ash loads are reached (approximately 20g/L) [36], [37]. Figure 24 displays cross-sectional views of filter channels with ash layers and end plugs.

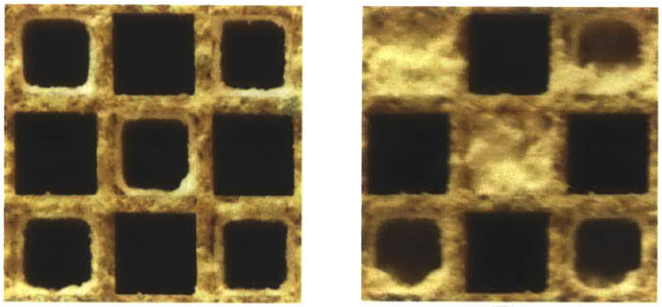

Figure 24: Cross section of channel views displaying ash layer and end plug [37]

As the cake filtration layer is form it changes the channel geometry and produces a larger porous matrix that the exhaust gas is forced to flow through. This increases the resistance as the ash end plug begins to form and the available channel begins to decrease in length. The available filtration area of the channel reduces. The increased resistance is not as extreme as depth filtration. Cake filtration and end plug formation has a fairly linear increase in pressure drop as the accumulated ash mass within the DPF rises. Figure 25 focuses on the cake filtration region.

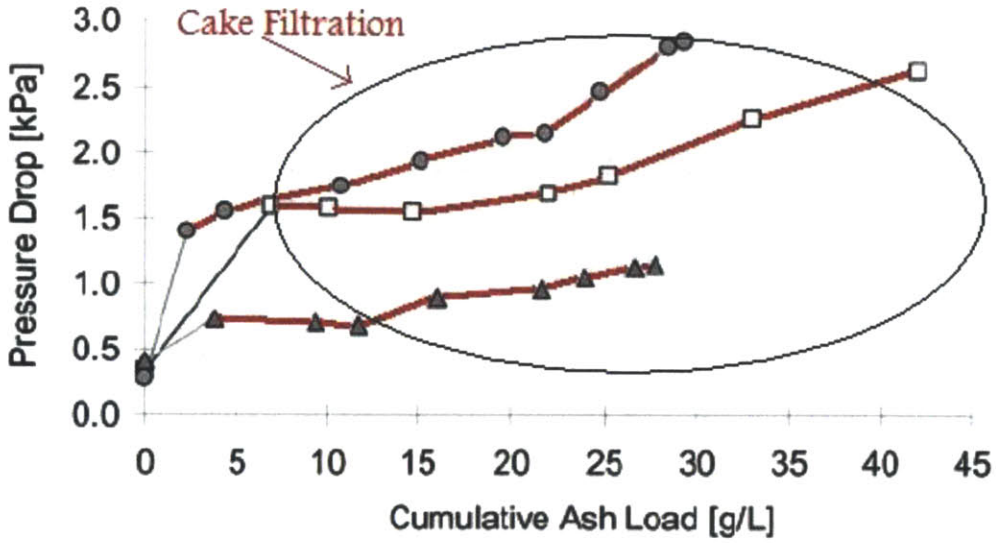

Figure 25: Pressure drop highlighting cake filtration [36]

The outlet channels stay clean although the inlet filter channels collect PM. This yields an error in the zero dimensional model as described earlier in this section but is accepted due to its insignificant nature.

A simple fraction relationship is used for both soot and ash. An end plug volume fraction is used to measure the amount of PM collected within the cake layer vice the end plug in the back of the filter. This plug fraction is defined as:

Eq 17

$$End\ Plug\ Fraction = \frac{Volume\ End\ Plug}{Total\ Volume}$$

This equation is the ratio of the volume of ash or soot accumulation in the end plug to the total volume of ash or soot accumulated in the filter. The volume of ash accumulated in the filter is reliant on the ash packing density. Pressure drop models must reflect that end plug and channel wall ash accumulation packing densities vary along with the end plug fraction variable [36], [37]. Although it is not the focus of this study, progressive accurate models are needed fully understand the dynamic process of PM accumulation in a DPF.

3.6 Modeling Ash Properties

As previously stated ash properties such as packing density, porosity and permeability, impact the pressure drop of a DPF. While packing density is somewhat easy to measure permeability is not straightforward. A primary focus of this research is to enhance the understanding of regeneration methods and exhaust conditions relates to these ash properties influencing DPF pressure drop. Permeability is a product of porosity and mean particle diameter. Porosity and particle diameter can be resolved by experimental procedures, and then permeability can be computed. Permeability relationships developed are described below.

The Rumpf & Gupte relationship is most likely the most commonly used permeability relationships in DPF technology (substrate, ash and soot layers). The relationship was created by randomly packing spherical particles with porosities (ε) ranging from 0.35 – 0.7, Reynolds numbers (Re_P) ranging from 10^{-2} – 10^{2}, and particle diameters with $D_{P,max}$ / $D_{P,min}$ ~ 7. The Rumpf & Gupte relationship is defined as:

Eq 18

$$k = \frac{\varepsilon^{5.5}}{5.6}\overline{D}_{P2}{}^{2}$$

Where k is the calculated permeability, ε is the measured porosity, and $\overline{D}_{P2}$ is the surface average sphere diameter. If the porous layer has a higher permeability ($\varepsilon \geq 0.8$), the Carman-Kozeny equation is used:

Eq 19

$$k = \frac{\varepsilon^{3}}{180(1-\varepsilon)^{2}}\overline{D}_{P2}{}^{2}$$

In conditions in where the ash formations are highly porous (permeability greater than 0.95) these relationships are not valid. When this is encountered, "flow around submerged structures" relationships are utilized instead of "flow through porous media."

(This page intentionally left blank)

4 EXPERIMENTAL SET-UP AND APPROACH

The primary goal of this study is to establish the composition and morphology of ash derived from specific regeneration strategies, and then relate these ash properties to their negative effects on DPF performance. This would be difficult to conduct in the field using fleet data it would take upwards of 150,000 on road miles with constant engine monitoring techniques [28], [36]. This makes it more effective to create and utilize an accelerated ash loading system with in situ monitoring procedures. For the experiments conducted through this research, a simple diesel generator and a specially designed accelerated ash loading system coupled to the engine's exhaust set-up was used. The accelerated ash loading system has been historically proven to generate and deposit realistic engine-out ash.

4.1 Approach

While analyzing field aged DPFs produces the greatest representative data pertaining to DPF operation, it is impractical due to the time and measurement constraints. This makes the use of accelerated loading techniques extremely beneficial to produce time critical results to determine the underlying means of long-term DPF ash loading and performance degradation. Lab produced samples have the benefit of pinpointing underlying mechanisms by controlling properties that would be nearly impossible in the field. Through experimental controls the formation of ash properties can be analyzed more easily.

4.1.1 Accelerated Ash Loading Methods

Different accelerated ash loading systems exist with varying results. These have different formations compared to field results. Mainly ash is generated by increasing the amount of lubricate consumed in the cylinder. The most established technique used is by doping lubricant into the engine fuel. It has been noticed that fuel doping differs from natural oil consumption in at least four ways [24]:

1. Fuel doping only increase one of two oil consumption methods, the flow around the top piston ring. This method accounts for 60% of natural oil consumption when compared to evaporation [56].
2. Fuel doping changes the soot to ash ratio in the "exhaust", therefore neglecting any reaction that takes place between the two especially during regeneration.
3. Fuel doped oil is burned in the diffusion flame front instead of the air rich regions it would normally occupy.
4. Oil doping may disturb the micelles within the lubricant, creating a percentage of unburnable sludge of metallic compounds [55].

Recent studies regarding elemental oil consumption disparities due to volatility differences are neglected by fuel doping. It is key to understand the morphology of field generated ash, so it can be compared and studied against lab created ash when lubricant compound consumption variations are not fully understood. In a recent study a high sulfated ash lubricant (2.23%) was doped in fuel, the axial ash deposit profile was fairly constant along the filter's length. But when compared to a low sulfated ash lubricant (0.63%) that was doped in fuel or when a high sulfated ash lubricant was strictly used in the sump without doping, ash deposits tended toward the end of the filter and varied along the filters length [57]. Fuel doping accelerated ash method, although effective with its shortcomings it must be critiqued.

Another method in addition to fuel doping, researchers have also injected oil mist into the intake manifold to accelerate oil consumption and DPF ash loading. A 2004 study injected oil at a rate of 1.5 ml/min using a standard SAE 15W-40 1.5% sulfated ash oil. After 165 hour DPF ash loading was concluded the results compared to a 1,118 hour un-accelerated test. The ash from oil mist injection was thicker and less porous but exhibited similar ash deposition [31]. More recent studies operated intake manifold oil mist injection with an 88% undersized DPF to supplement the accelerated ash loading. The tests increased oil consumption by 20 g/hr beyond the normal engine oil consumption rate for a test duration of 120 hours. The experiments produced a non-linear effect of ash loading on backpressure, with a small pressure drop increase until much higher levels of ash loading were established [33], [58]. Although the oil misting method better resembles natural oil consumption when compared to fuel doping, it is not representative of typical diesel engine operation and an alternative should be explored.

4.1.2 MIT Approach

No acceleration system will completely resemble ordinary diesel and after-treatment system operation, however the system used in this research has proved to provide accurate results in a relatively brief time. In the past years an accelerated ash systems were built and tested at the Massachusetts Institute of Technology, which closely parallels the results found from field study analysis. The chief advantage of the system developed is the flexibility to independently change a number of variables during testing. Variable that can be manipulated are listed below:

1. Exhaust temperature
2. Flow rate
3. Oil consumption rate
4. Lubricant chemistry consumed

5. DPF size
6. DPF material
7. Soot and ash interactions throughout the test duration

This flexibility delivers the capability to help isolate individual fundamental mechanisms of ash generation and their consequential effect on DPF performance. This study attempts to quantify the ash morphology of various regeneration methods and their negative effect on DPF performance.

4.2 Accelerated Ash Loading System

The DPF volume used in most MIT studies was 2.47 liters. This volume is relatively small compared to a full size DPF. The initial ash loading system was designed to ash load a conventional D5.66" (14.38 cm) x 6" (15.24 cm) DPF to 40g/L in approximately 100 hours. This is a substantial amount of accelerated ash accumulation considering 40g/L ash corresponds roughly to 300,000 on-road miles [18].

The first accelerated ash loading system used at the MIT utilized a Cummins ISB engine and a diesel combustion chamber to load the DPF with PM. A schematic of the accelerated ash loading system can be seen in Figure 26.

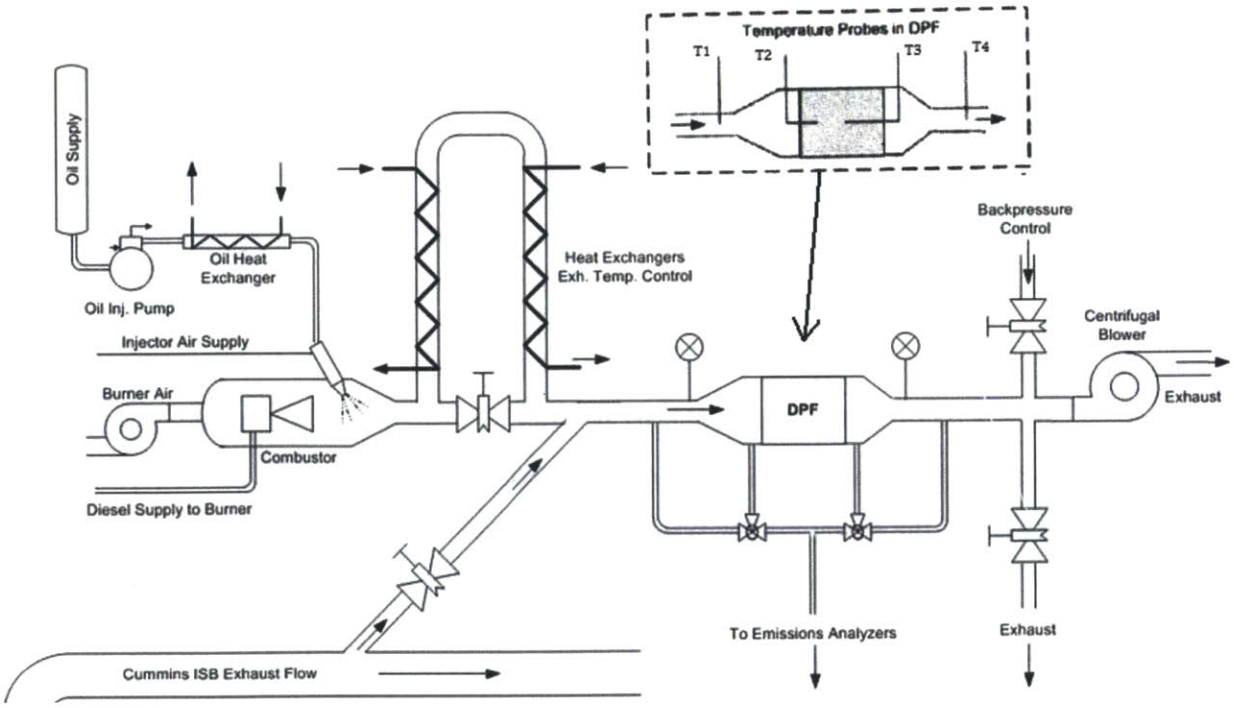

Figure 26: First MIT accelerated ash loading system [37]

The Industrial diesel burner with a custom combustion chamber is used to burn lubrication oil and deposit ash in the DPF. The Cummins ISB engine was used in the initial system to deposit realistic exhaust gas, primarily soot, into the filter. These two systems are operated independently. Figure 27 shows the system diagram of the second accelerated ash loading system created at MIT adapted from the proven operation of the original. Images of the test setup and facilities can be seen in the Appendix Figure 54 and Figure 55.

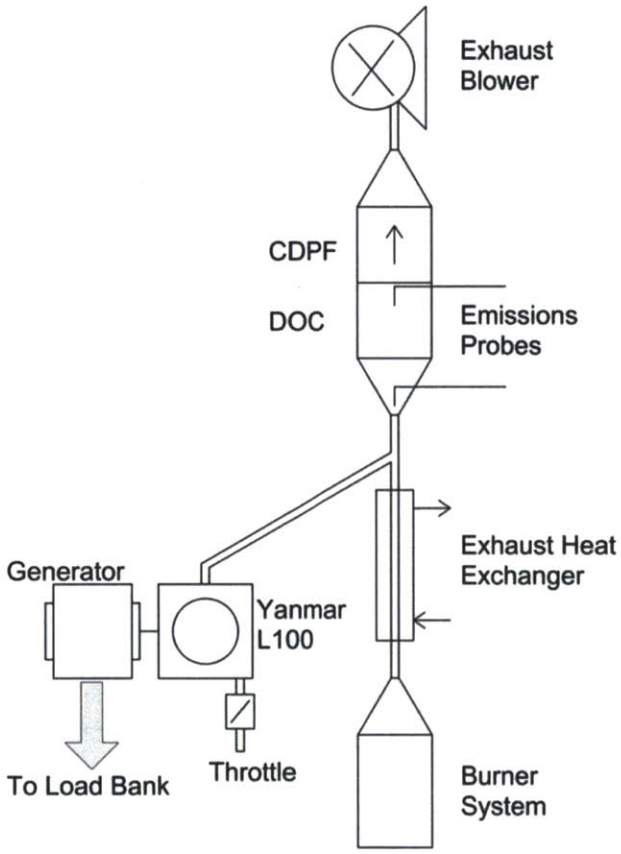

Figure 27: Accelerated ash loading system

This system is very similar to the first generation accelerated ash loading system, but uses a more affordable Pramac S5500 Yanmar L100V6-1 generator in place of the Cummins ISB. The only other primary difference is that the newer loading system adds a higher loading capability to load to 25g/L ash in approximately 25 ash loading hours. This is approximately 187,500 on road miles.

Table 6 displays the ash loading system's operating specifications utilizing the Beckett NX Oil Burner.

System Parameter	Description
Fuel Consumption	1.5 - 7.6 L/h
Oil Consumption	0.94 - 9.4 ml/min
Injection Pressure	700 - 1400 kPa
Air Flow	266 - 3114 slpm
DPF Inlet Temperature	225 - 800 °C

Table 6: MIT accelerated ash loading system specifications [37]

This system creates much flexibility. The oil is delivered by an air assisted oil injector located atop the custom diesel burner and is fed by a computer controlled constant volume pump. This allows different oils can be studied including base oil, individual additives and combinations along with fully formulated oils. This study focuses on regeneration methods and controlling exhaust conditions, so the standard CJ-4 oil is used.

The combustor air flow and oil injection properties gives minimal control over combustion quality. However the exhaust heat exchanger post combustion chamber is used to control the combustor exhaust temperature independent of burner settings with ease of temperature control. This heat exchanger can regulate DPF inlet temperatures between 225 and 800°C enabling ample control over regenerations. A small amount of soot is produced while ash loading since the diesel combustor operates by igniting diesel fuel. By varying the heat it is possible to oxidize this unwanted soot when pure ash loading is desired.

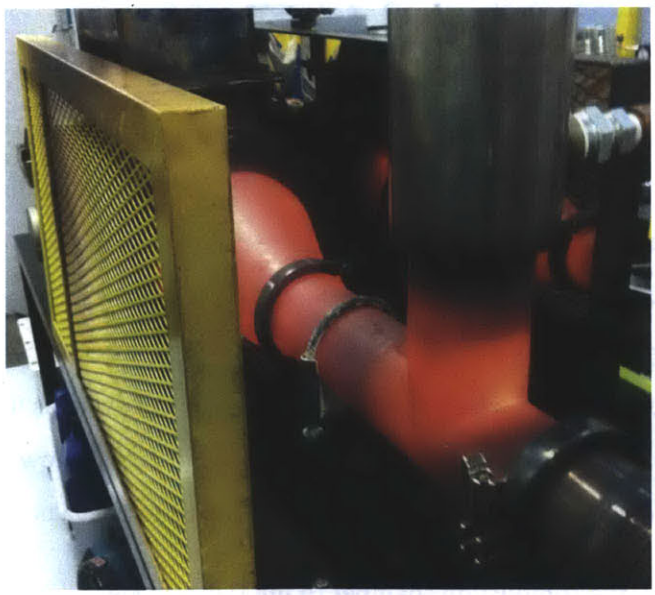

Figure 28: Accelerated ash burner in operation

Figure 28 shows the burner in operation with the vertical split off of the exhaust heat exchanger. Downstream of the system's exhaust heat exchanger but prior to the mounted DPF there is a connection stemming from the diesel generator. This enables the possibility of loading the mounted DPF with a portion of the engine's exhaust flow. This is primarily used to load the DPF with soot. Because these two systems are separate (but can be run together), soot can be loaded onto a filter, which already contains any amount of accumulated ash. This leads the better possibility of understanding the synergistic effects of ash and soot on DPF performance.

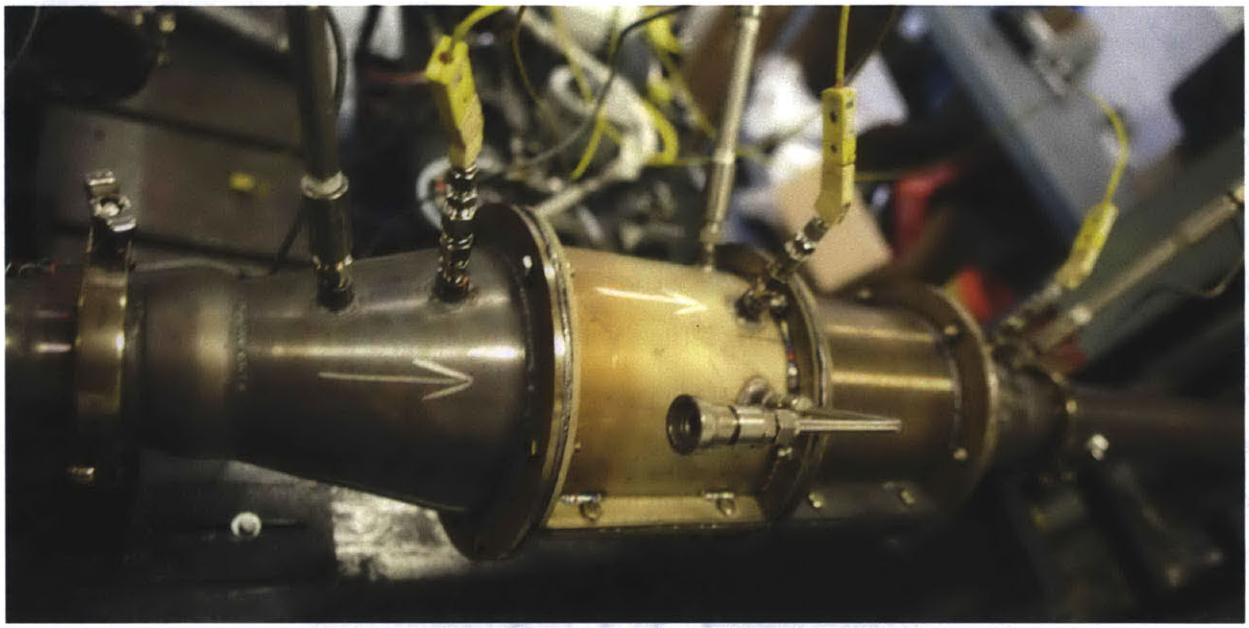

Figure 29: DOC and DPF can connected

Figure 29 shows the DPF is positioned downstream of the heat exchanger with three thermo couples and three pressure ports attached. This step up shows a DOC C-DPF combination, so there are three measuring locations: inlet to DOC, between DOC and C-DPF, and outlet of the C-DPF. In the case without the DOC, measurements are taken before and after the C-DPF, with the DOC spacer removed. The system also has exhaust gas sampling ports prior to ATS inlet and post DOC. Downstream of the mounted DPF is a centrifugal blower, which provides addition control over gas flow rates through the DPF while PM loading. This centrifugal blower provides the majority of the flow rate through the system. When not loading, this blower is used to conduct space velocity tests to evaluate DPF pressure drop.

The amount of piping from the combustion chamber to the DPF provides a lot of surface area for PM collection. This undesirable loss of PM within the system piping, and not the DPF, however this loss is unavoidable, but does not change the accuracy of the DPF accumulation measurements.

4.3 Engine Specifications and Capabilities

The accelerated DPF ash loading system includes a single cylinder Pramac Yanmar diesel generator shown in Figure 30 and Table 7.

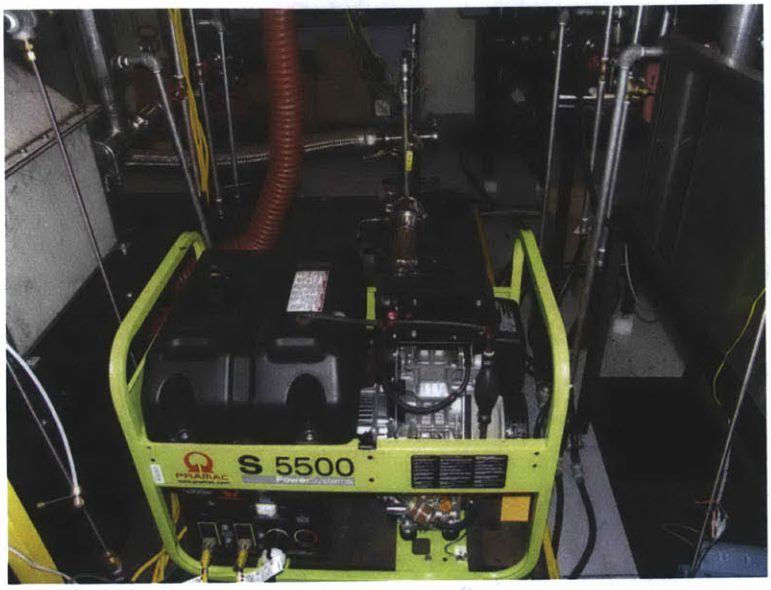

Figure 30: Pramac S5500 Yanmar L100V generator

Model	L100V
Maximum Continuous Power	5.0 kW @ 3600 rpm
Maximum Surge Power	5.5 kW @ 3600 rpm
Number of Cylinders	1
Aspiration	Natural
Displaced Volume	0.435 liters
Compression Ratio	21.2:1

Table 7: Pramac S5500 Yanmar L100V generator specifications [59]

The stock diesel generator is piped into the exhaust system to accumulate soot in the test DPFs. The exhaust system is outfitted with pressure and temperature sensors to monitor the engine exhaust. The generator is connected to a load bank comprised of simple space heaters. These heaters are dual setting heaters and can be set to either 1350 or 1500 W. These heaters can be energized to load the generator from 27 to 90 percent load in set increments. Further information regarding the Yanmar L100V can be seen in Appendix Table 14. This engine is rated by the EPA to 6.3 g/kW-hr NO_x emissions and 0.61 g/kW-hr PM emissions [60].

4.3.1 Particulate Matter Emissions Sampling

Engine PM emissions were collected on Teflon and Quartz filters in order to establish PM emission rates by gravimetric analysis as well as to examine PM composition and ash content. Particulate samples were

collected directly from the engine and were sampled from the raw and undiluted exhaust to preserve particulate matter composition. These samples were gathered on 47 mm Pallflex filters (seen in Figure 31), and the amount and rate of PM emission were establish gravimetrically. Post weight measurements composition of the exhaust particles collected on the quartz filters were analyzed with Horiba's MEXA 1370 PM analyzer. Total particulate mass (TPM) was measured in three categories: soluble organic fraction (SOF), sulfate fraction (SO4), and an insoluble fraction (SOL).

Figure 31: PM sampling [61]

4.3.2 Gaseous Emissions Sampling

Exhaust concentrations of HC, CO_2, CO, O_2, NO, NO_2 were measured both prior to the ATS and after installed DOC (after the exhaust passed thru with a particle filter). These emissions were measured using a MKS MultiGas FTIR Analyzer. This was conducted to verify the rated NO_x emissions rate of the engine and to examine the DOC conversion percentage.

5 EXPERIMENTAL TEST MATRIX AND PROCEDURES

This chapter outlines the experimental parameters, test matrices and test procedures conducted for this study. Various passive regeneration strategies were tested to quantify the ash effect on DPF performance. Details of the lubrication, fuel, filter specifications, and arrangement along with the experimental procedure conducted are explained following.

5.1 Lubricant and Fuel Specifications

The goal of this research was to determine how the regeneration methods effect DPF performance degradation. Much research has been conducted on the effects on lubricant chemistry, but to decouple variable standard CJ-4 was used to focus on the regeneration effects. Sappok et al conducted an elemental analysis of CJ-4. The specifications of the lubricant oil can be seen below in Table 8.

Lubricant	B [ppm]	Ca [ppm]	Fe [ppm]	Mg [ppm]	P [ppm]	Zn [ppm]	S [ppm]	Mo [ppm]
CJ-4	586	1388	2	355	985	1226	3200	77

Table 8: ASTM D5185 lubricant specification [37]

Conventional ultra-low sulfur diesel (ULSD) was used in the experiments, both for the diesel generator and the accelerated ash burning system. ULSD by definition contains no greater than 15 ppm of sulfur. An elemental analysis of the fuel was conducted by Sappok et al. to ensure that the fuel had no contribution to SA production. The results of the elemental analysis can be found in Table 9.

Element	Ca	Mg	P	Na	K	Zn
ULSD [ppb]	<97	<56	<1180	<2010	<2690	<155

Table 9: ASTM D5185 fuel specification [37]

In all test cases the trace metals were below the minimum detectable limits of the analyzer, which ranged from 100 to 1,000 ppb depending on the element [37].

5.2 Aftertreatment Systems

This study focuses on passive regeneration systems to compare to previous active regeneration studies conducted to determine regeneration effects on ash aging diesel particulate filters. Figure 32 shows the experiments conducted during this study.

	Target PM	Configuration	Temperature
	g/L		°C
Case A	Ideal Passive Regeneration Case		
	0	DOC+CDPF	350
Case B	Effect of PM Level at Start of Regeneration on PM/Ash Mobility		
	4	DOC+CDPF	250-400
Case C	Effect of NO_2 from DOC vs NO_2 from CDPF on PM/Ash Mobility During Oxidation		
	4	CDPF	250-400

Space Velocity 50,000 hr^{-1}
Target Ash Level 25 g/L

Figure 32: Test Matrix

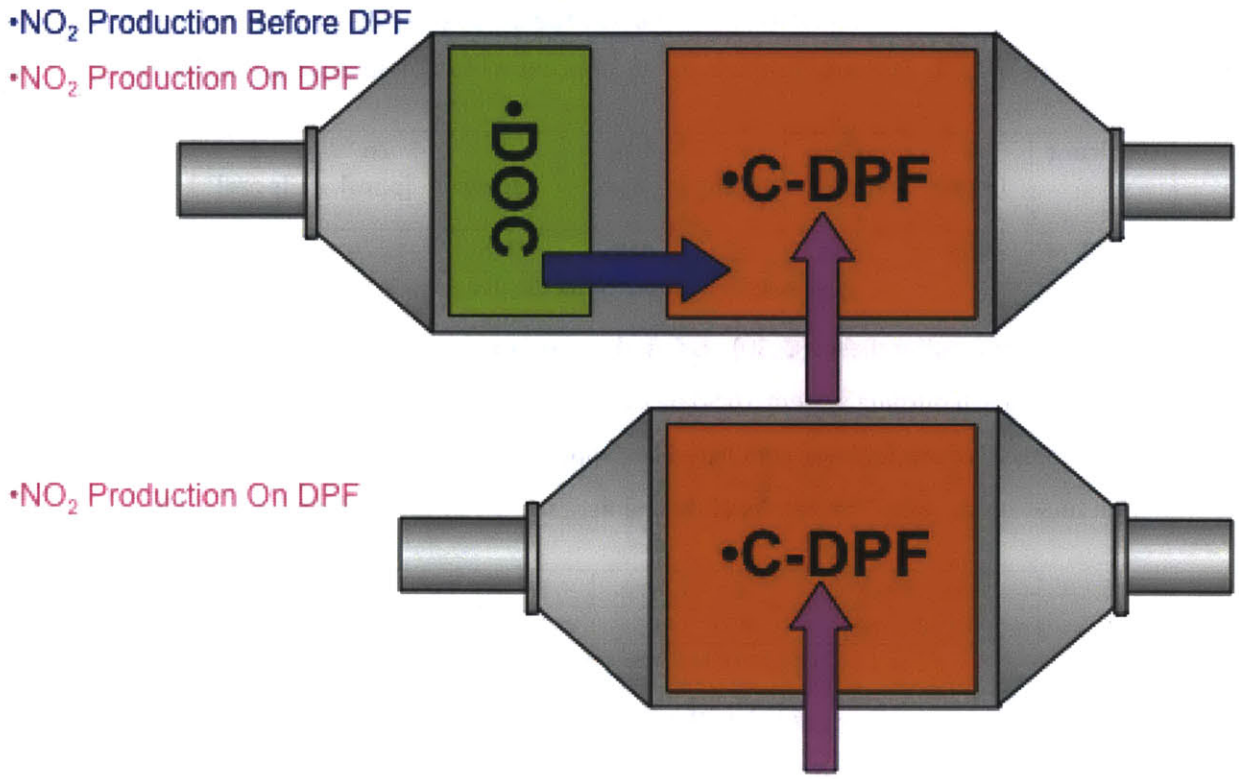

Figure 33: Test aftertreatment system layout

Figure 32 shows the layout of the experiments conducted and Figure 33 shows the two system configurations tested. Case A conducts an exploration of continuous passive regeneration, while both Case B and C experience periodic passive regeneration, with periodic soot loadings. Case A and B follow the top system layout of Figure 33, while Case C experiences the lower layout without the DOC. This matrix offers unique look at the long-term effects of ash development of a DOC C-DPF combination and continuous/periodic regeneration.

5.2.1 Particulate Filters

Conventional cordierite DPFs produced in the same batch were used this research. The filter geometry was 200 cells per square inch with wall thicknesses of 0.012 inch (200/12). The filters also contained a platinum-based catalyst. Table 10 displays details on the filter geometry and specifications.

Substrate	Catalyst	Dimensions	Cell Density	Wall Thickness	Filter Volume
Cordierite	Pt	D5.66" x 6" (D14.38 x 6.60 cm)	200 cpsi (31 cells/cm^2)	0.012" (0.03mm)	2.47 L

Table 10: Properties of DPF used in this research

5.2.2 Diesel Oxidation Catalyst

Conventional ceramic flow through DOCs produced in the same batch were used this research. The DOC contained a platinum-based catalyst. Table 11 displays details on the DOC geometry and specifications.

Type	Catalyst	Dimensions	Cell Density	Filter Volume
Ceramic flow though honeycomb	Pt	D5.66" x 2.6" (D14.38 x 15.24 cm)	400 cpsi (62 cells/cm^2)	1.07 L

Table 11: Properties of DOC used in this research

5.3 Accelerated Ash Loading

Validated by previous research conducted at MIT the accelerated ash system used in these tests follows the same previous procedures. The procedure entailed of filter preparation, ash loading, and intermittent soot loading with measurements of various parameters conducted throughout. The PM loading conducted on the DPF was to quantify the performance degradation the soot and ash contributes over the aging of the filter.

5.3.1 Aftertreatment System Preparation

The first part of the experiment begins with preparation of the C-DPF and DOC if the case calls for one. These items need to be wrapped in the proper matting and canned. Once the C-DPF and/or DOC is surrounded by matting and properly placed into its supportive containment canning, it is necessary to "degreen" the filter. This consists of heating the ATS and supportive canning to a raised temperature for a period of time. This process guarantees that proper thermal expansion of the matting occurs and ensures the exhaust flow is directed through the ATS and not around the outer surfaces. The degreening procedure consisted of increasing the filter's temperature for a specified period of time as follows:

1. ~300°C for 20 minutes
2. ~400°C for 20 minutes
3. ~500°C for 20 minutes
4. ~600°C for 80 minutes

Following this procedure ensured the matting is slowly expanded creating optimal flow for testing. After the degreening process the filter is ready to be loaded.

5.3.2 Ash Loading

A completely loaded filter is considered on the order of 25g/L ash during this research. To accumulate this mass of ash, the accelerated loading previously described was used in conjunction different regeneration methods shown in Figure 32. This mass of ash roughly equates to 35-45 hours of loading and the consumption of approximately 4.5 gallons of lubrication oil. This procedure roughly equated to 175,000 miles or 4,500 hours of DPF operation.

For Case A, being continuously passively regenerated the DPF filter face was held at approximately 300°C throughout the ash loading process. Case B and C periodically regenerated for switching inlet filter face temperatures of approximate 250°C during soot loading and 400°C during ash loading and regeneration. This ensures the filters are clearly within catalytic range for ash loading and regeneration.

At regular intervals during the loading process the filter assembly is removed from the system and weighed on the Acculab VA-12KG balance with a 0.02g resolution. When weighing the filter it is essential to ensure the entire filter is at a temperature above 100°C producing the inability for water vapor collection to occur which would create inaccuracies in the ash load determination. The filter assembly weight determines the mass of accumulated ash load. At the same intervals as the weight measurements once the filter assembly is cooled, a room temperature space velocity test was performed to determine the DPF's pressure drop.

5.4 Soot Loading

Soot loading with the diesel generator was conducted for the periodic regenerated filters of Case B and C. These soot tests were performed around 5g/L ash increments to a total of 4g/L soot. Soot loading occurred at in three ash loads at approximately 0, 5, 10, 15, 20, and 25g/L ash loading. The soot loading procedure consisted of four stages of soot loading which can be seen in Table 12. The engine loading provided a method to equate the negative effects of PM and a means to test ash loaded filters with real engine exhaust.

Soot Stage	Loading Duration	Engine Load	Approximate Soot Load	Approximate Soot Loading Rate
1	60 minutes (60 total)	90%	1 g/L	1.0 g/L per hr
2	60 minutes (120 total)	90%	2 g/L	1.0 g/L per hr
3	60 minutes (180 total)	90%	3 g/L	1.0 g/L per hr
4	60 minutes (240 total)	90%	4 g/L	1.0 g/L per hr

Table 12: Approximate soot loading procedure

Just like during ash loading, after each soot loading stage the filter was weighed above 100°C to verify the extent of PM accumulation. Again the corresponding room temperature space velocity test was conducted to determine a DPF pressure drop associated with the extent of PM loading.

(This page intentionally left blank)

6 EXPERIMENTAL RESULTS

This chapter presents and describes the experimental results produced from this study. Table 5.6 describes the four test cases that were conducted and analyzed. The regeneration methods used were chosen to expand on the research conducted in the MIT Sloan Automotive Lab. The results for the laboratory aged DPFs are described by ash effects on pressure drop and pressure drop sensitivity to soot loading with ash load.

6.1 Variability of Pressure Measurements

Before the experimental results are presented, it is important to determine and quantify any variability that may influence the accuracy of the results. Variability tests of pressure measurements were conducted daily during the experiment to determine confidence interval of the pressure drop measurements. The 95% confidence interval was found to be 0.1 kPa for pressure drop measurements.

6.2 Passive Regeneration Method Effects of on Pressure Drop

As previously mentioned, this research expands on other work conducted at the MIT Sloan Automotive Lab. The experimental methodology and procedure were similar creating a valid nature of comparison to the previous sets of results. Table 13 presents the test cases:

Case	Lubricant	Filter Type	Ash Load	Regeneration Type	Regeneration Method
A	CJ-4	DOC & C-DPF (Pt)	25.2 g/L	Continuous	Passive
B	CJ-4	DOC & C-DPF (Pt)	25.0 g/L	Periodic	Passive
C	CJ-4	C-DPF (Pt)	24.6 g/L	Periodic	Passive

Table 13: Test compared in this research

All cases used the same lubricant oil, fuel, and C-DPF and approximate ash loading space velocities of 35,000 to 50,000 hr^{-1}. Pressure drop velocity sweep measurements were conducted at 25°C, and are presented at 20,000 hr^{-1}.

6.2.1 Periodic vs Continuous Regeneration

The effect of regeneration type derived ash on DPF pressure drop can be seen in Figure 34. The three tests compared the effects of continuous verses periodic passive regeneration independently at ash loads from 0 g/L to approximately 25 g/L. The three curves are very similar until the 15 g/L measurement, when the continuous passive regeneration study takes a 1.92kPa jump. The flow resistance for this continuous case then increases at a much higher rate than prior to the half load point. At the full load condition Case A ends at approximately 1.5kPa above the other two cases. Continuous

passive regeneration might have produced wall ash layers to thick to allow passive oxidation and soot pockets could have developed.

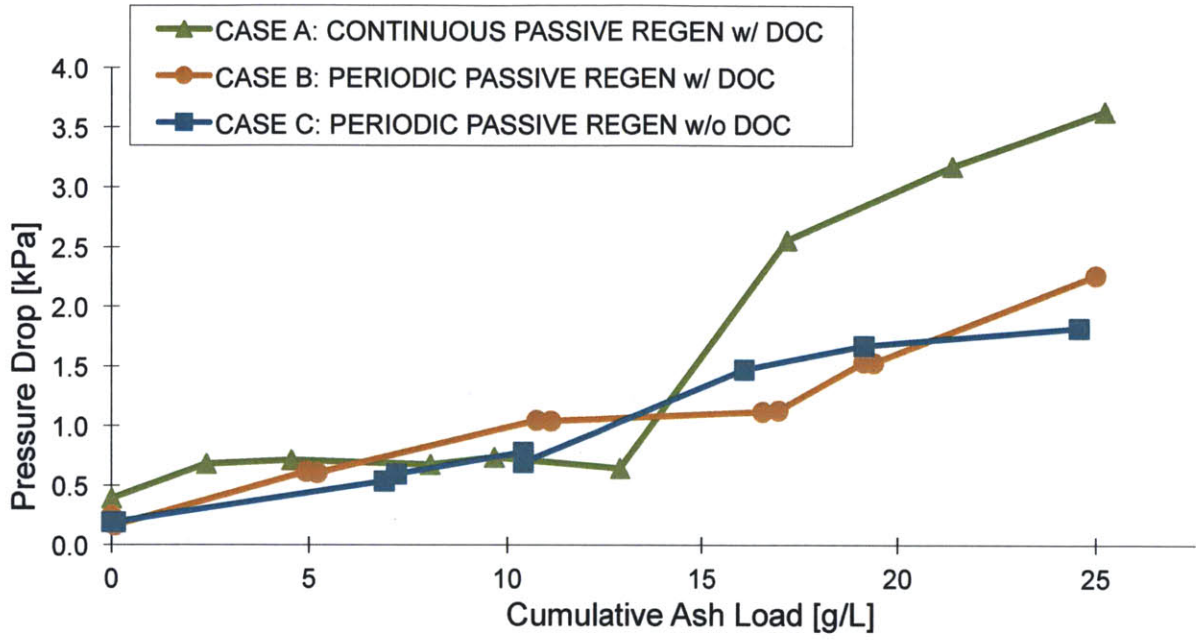

Figure 34: Pressure drop comparison to ash load between continuous and periodic regeneration

Figure 34 shows a comparison to a prior continuous active regeneration experiment conducted at MIT.

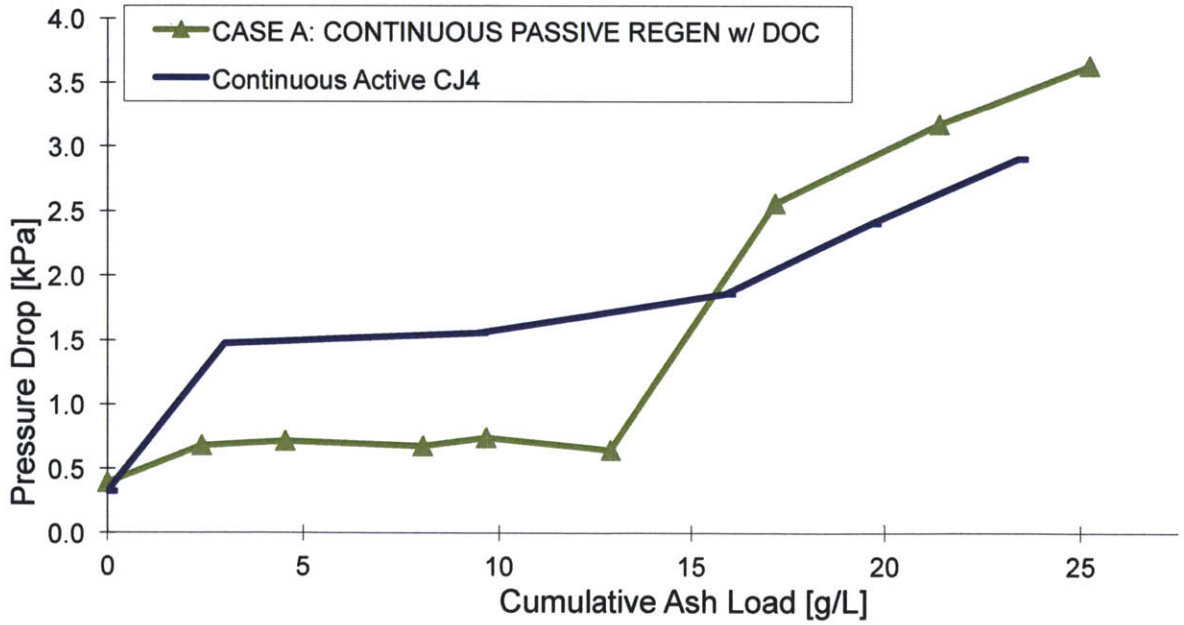

Figure 35: Pressure drop comparison to ash load from previous active continuous regeneration [36]

The passive continuous regeneration case seems to not experience as much depth filtration and move to cake filtration earlier. Both of these continuous cases experience a significant jump in pressure drop slope around 15 g/L, although the passive case is much more significant surpassing the active case. This could be due to soot layers that built up unable to be oxidized passively due to their location.

6.2.2 Effect of the DOC

The effect of a DOC on DPF pressure drop can be seen in Figure 36. The two similar periodic tests compared were the effects passive regeneration with and without a DOC at ash loads from 0 g/L to approximately 25 g/L.

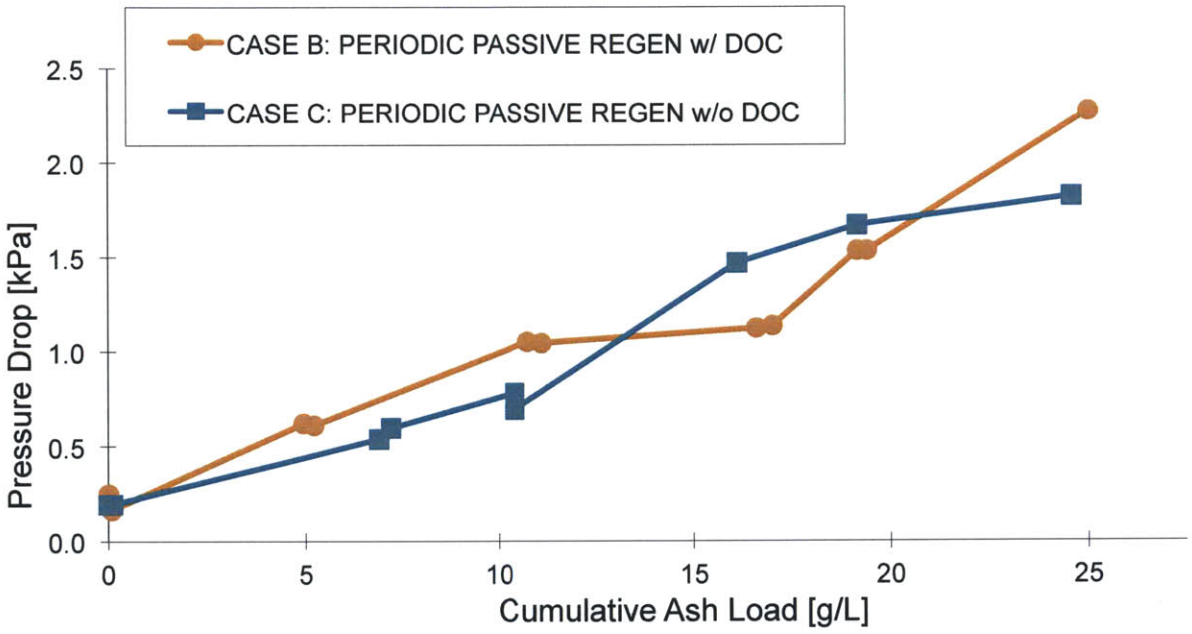

Figure 36: Pressure drop comparison to ash load between periodic regeneration with and without a DOC

Presented in Figure 36 the difference between pressure effects of a DOC is hard to see. The two pressure drops vary three different times over the aging. Early life seems to support operation without a DOC, but the midrange DOC operation seems beneficial. At full load the DOC case has step pressure drop increase that greatly surpasses the case without a DOC present. These differences are minor and show that the DOC does not significantly alter the thermal effects of soot accumulation and oxidation.

6.2.3 Active and Passive Regeneration Effects on DPF Pressure Drop

Traditional DPF follow periodic regeneration since they spend time at partial load below active and passive regeneration regimes. At higher loads or with added energy they are pushed into the regeneration modes and the oxidation of soot reduces the pressure drop in the filter. Figure 37 shows a

comparison of periodic regeneration test conducted at MIT covering both active and passive regeneration.

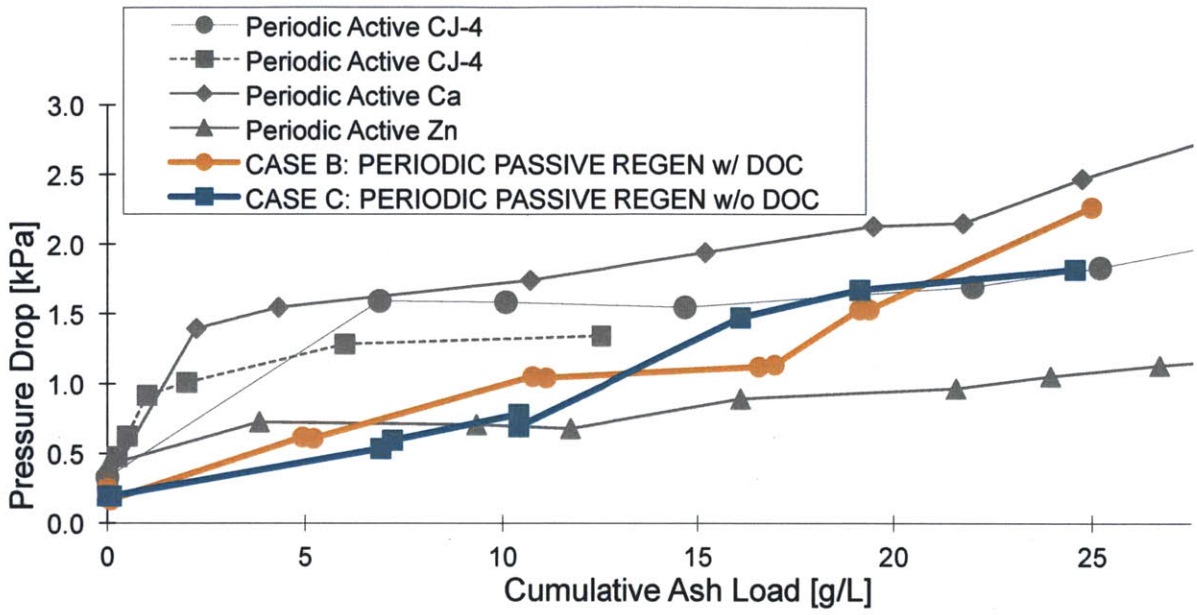

Figure 37: Pressure drop comparison to ash load between active and passive regeneration [37]

The passive cases seen in Figure 37 look very beneficial early during aging especially below 10 g/L with minimal pressure increase due to depth filtration. But even approaching 15 g/L the passive regeneration methods seem to be advantageous with lower flow restrictions than the other CJ-4 aged DPFs. After this point the passive case without a DOC, Case C, is almost overlaid on the previous CJ-4 sample. Case B's flow restriction starts increasing rapidly following the loading at 15 g/L.

6.3 Combined Soot and Ash Effects on DPF Pressure Drop

As previously discussed, the majority of the PM from engine exhaust is composed of soot. For continuous regeneration ideally soot never builds up in the filter and is oxidized as it enters the filter. For periodic regeneration as the soot is trapped in the DPF, the pressure drop across the filter is affected. During engine operation periodically the soot is regenerated and the incombustible sulfated ash remains and builds a cake layer along the channel walls. While this ash is preserved in the filter, soot is continuing to be deposited on top of the ash layer. This action makes it important to determine the synergistic effects of how soot ensnared in an ash loaded DPF affects the filter's pressure drop.

During the initial loading stage, a steep climb in pressure drop is seen due to soot depth filtration. As a cake layer of soot begins to form and grow, the pressure drop gradually increases with the addition of

PM at a rate substantially less than that observed during depth filtration. When soot is loaded on a clean DPF, the pressure drop follows a similar trend to that described during ash loading as seen in Figure 38. This represents the DPF pressure drop as a function of PM load on a clean filter with no substantial ash accumulation, but to not the pressure drop is much more significant for soot than ash per mass.

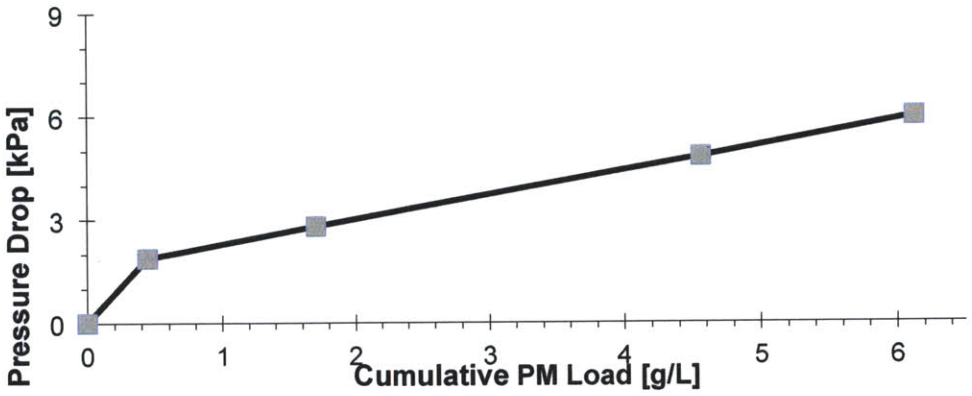

Figure 38: Typical pressure drop trend as a function of PM load for a DPF with no ash accumulation [38]

Ashes produced from passive regeneration contain different material properties and packing characteristics than that from active regeneration due to the lower heat they experience. Even between passive cases, the effect of the DOC can greatly alter ash production. These different ash characteristics likely influence the synergistic affects on DPF performance that soot has on ash cake layers. Only Case B and C are investigated for soot loading, since Case A was continuously regenerated and ideally no soot was accumulated. Figure 39 and Figure 40 show the soot loading of Case B and Case C at the clean filter situation and then in approximately 5 g/L increments to full load. As seen the lower ash loads decrease the pressure drop for a given soot load due to the ash acting as the filter medium, but between the 10 and 15 g/L mark the restriction due to the ash becomes too high and is no longer beneficial. One note is that the soot accumulation between Case B and C differed greatly due to the presence of the DOC in Case B. Without the DOC in Case C soot loading was much more rapid. This was due to the oxidation of SOF and a percentage of the soot present in the exhaust during the loading with a DOC in Case B. Further soot and ash loading comparisons are displayed following these two figures.

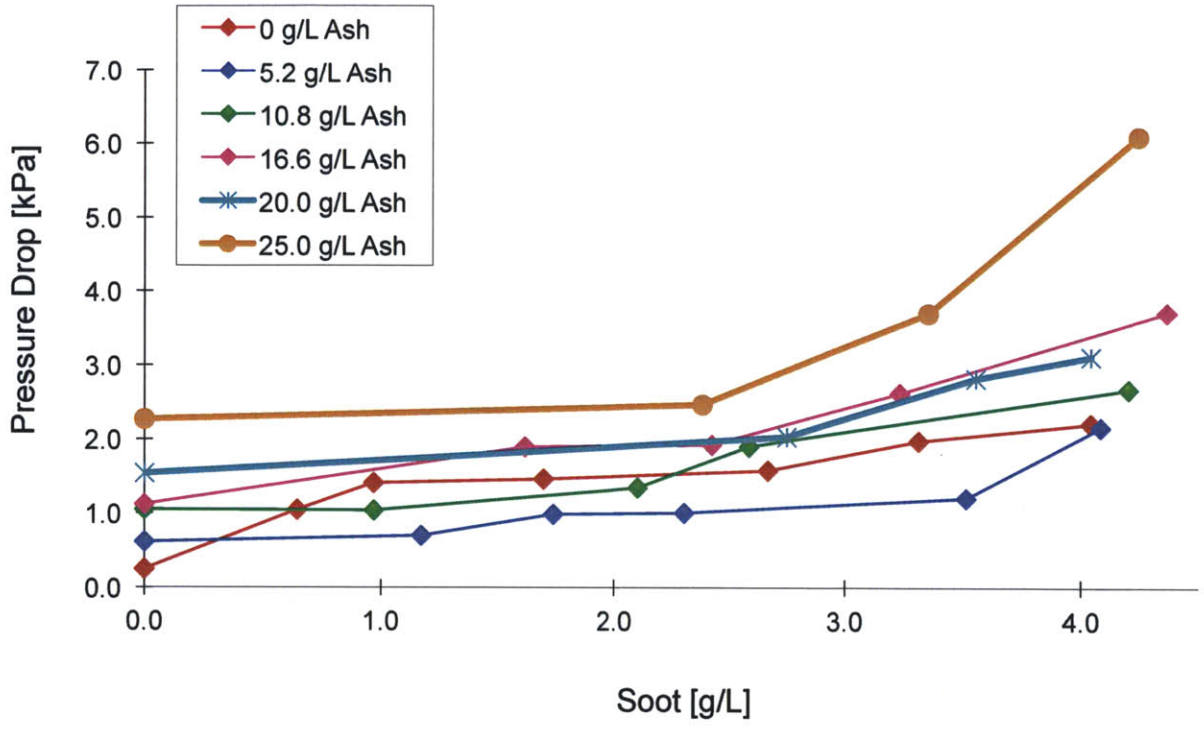

Figure 39: Case B soot loading pressure drop

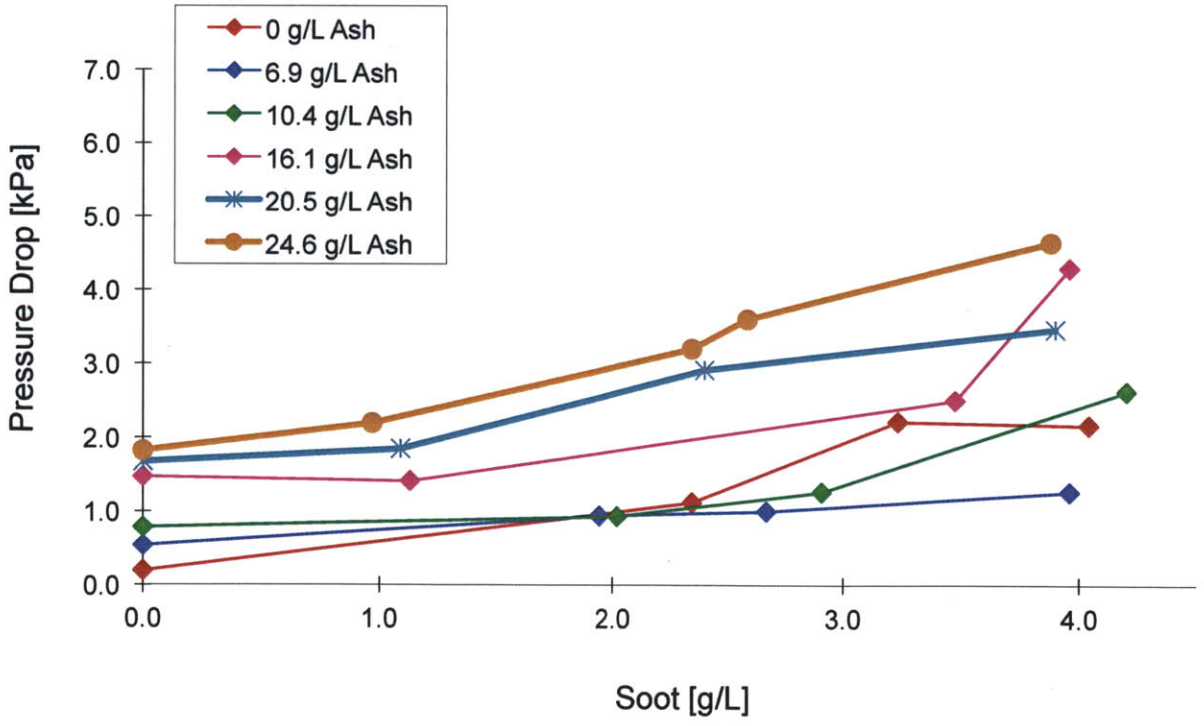

Figure 40: Case C soot loading pressure drop

Figures 41 through 46 shows the graphs produced exploring pressure drop at various ash loads for Case B and C. These show the individual soot loading pressure drop data at 5g/L ash accumulation increments. Figure 41 shows that the original clean DPF soot loading still showed the traditional depth filtration, but the 5g/L and further loading produced a more linear pressure drop trend. Similarly pressure drop curves comparing ash loadings at a give soot load are outlined in Figures 47 through 51. These will become more useful in future studies after exploring the individual ash properties of the DPFs. The trends are similar showing insignificant differences between the two loading conditions.

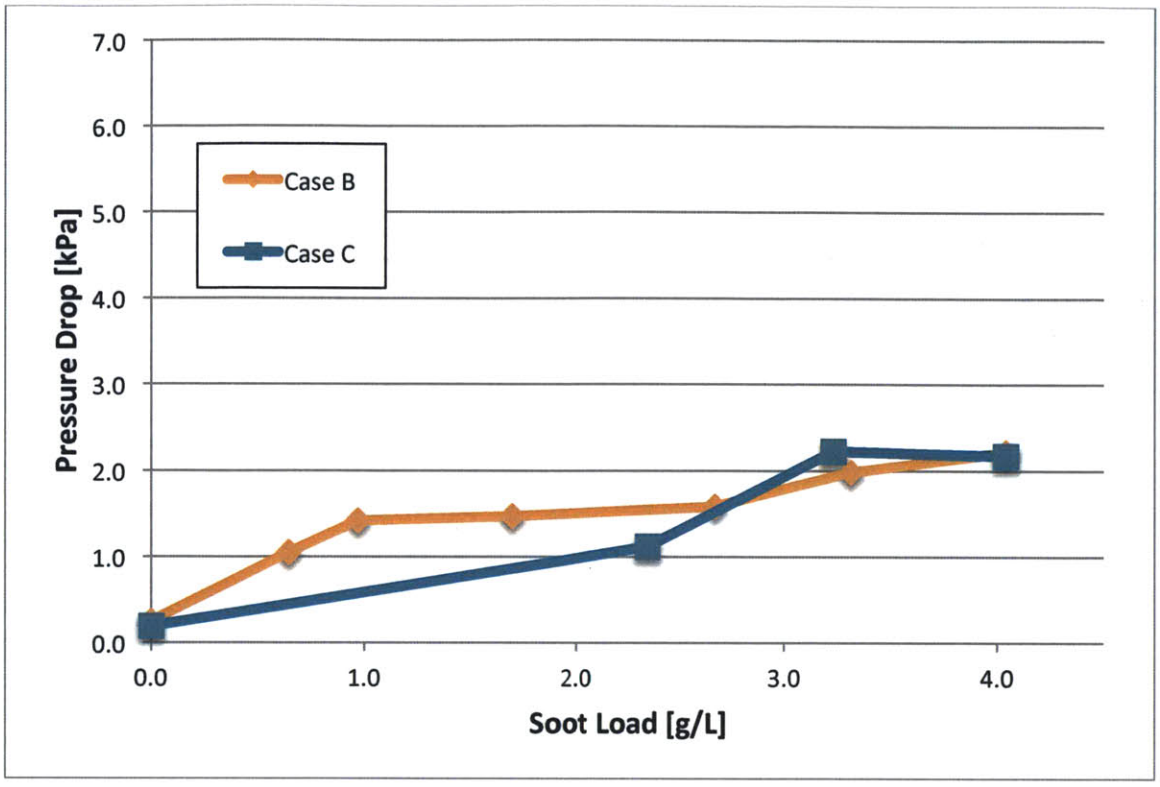

Figure 41: 0 g/L Ash samples soot loading

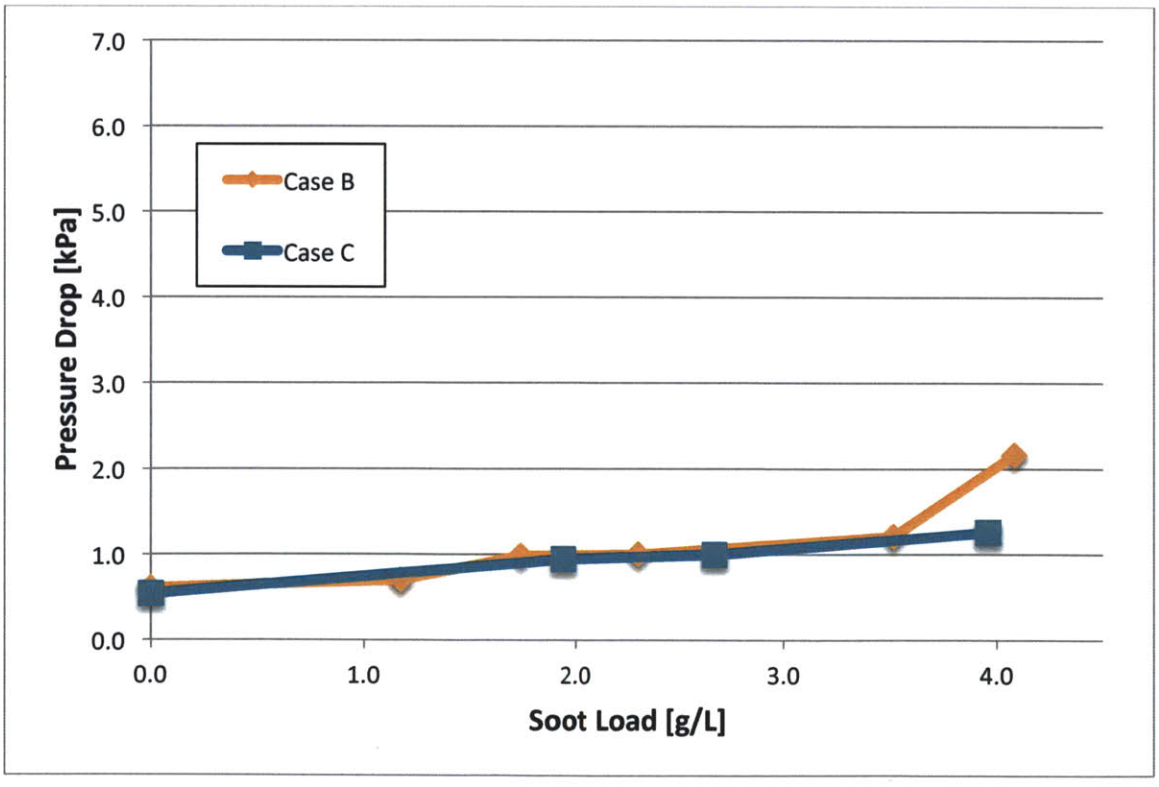

Figure 42: 5 g/L Ash samples soot loading (Note Case B is 5.2 g/L Soot and Case C is 6.9 g/L)

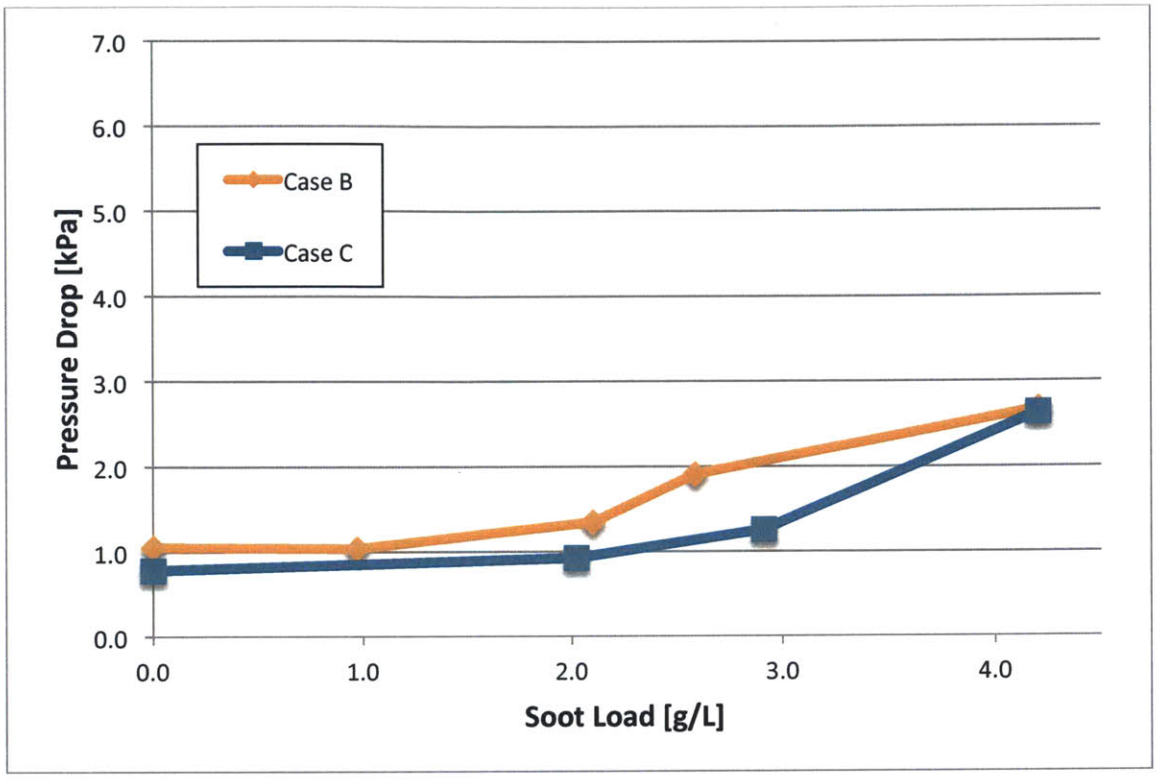

Figure 43: 10 g/L Ash samples soot loading (Note Case B is 10.8 g/L Soot and Case C is 10.4 g/L)

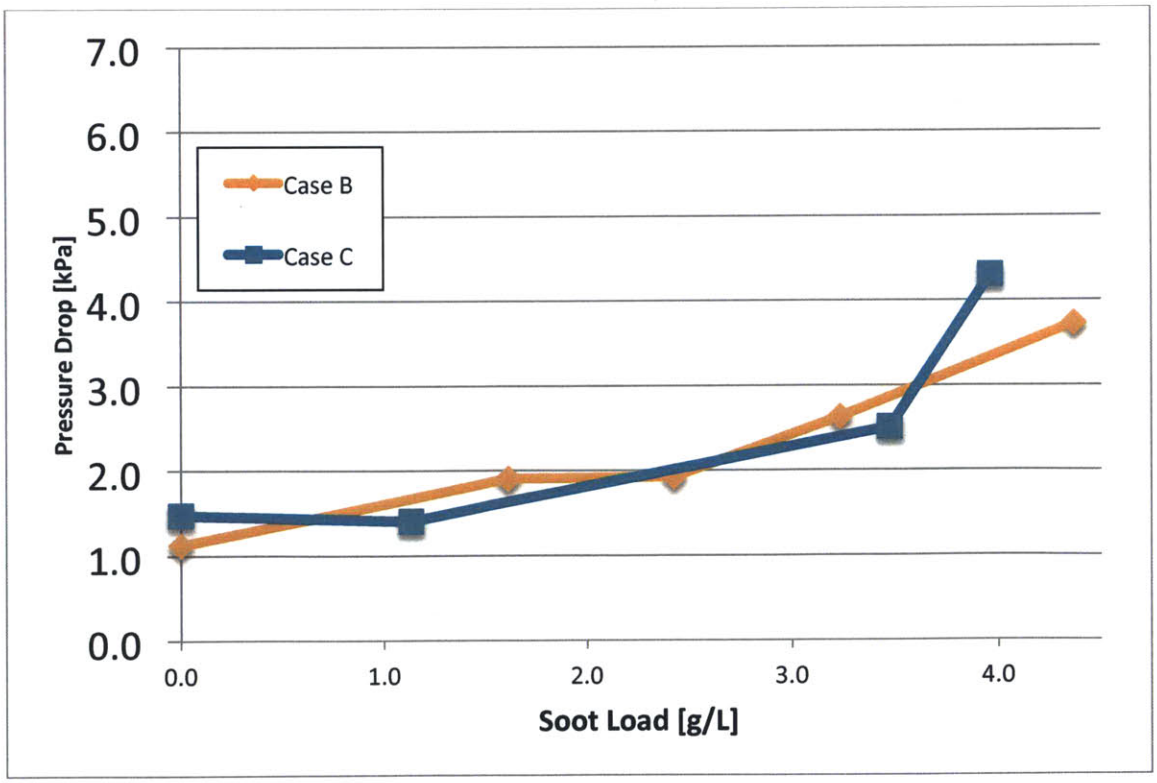

Figure 44: 16 g/L Ash samples soot loading (Note Case B is 16.6 g/L Soot and Case C is 16.1 g/L)

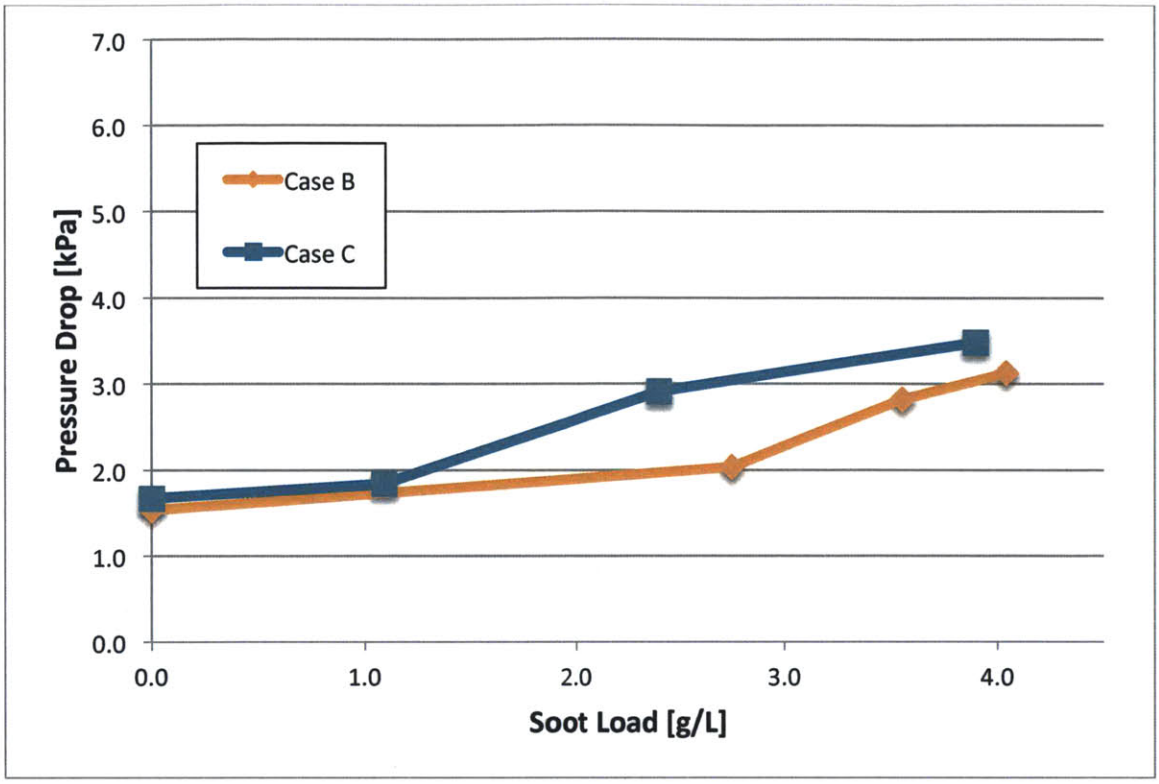

Figure 45: 20 g/L Ash samples soot loading (Note Case B is 20.0 g/L Soot and Case C is 20.5 g/L)

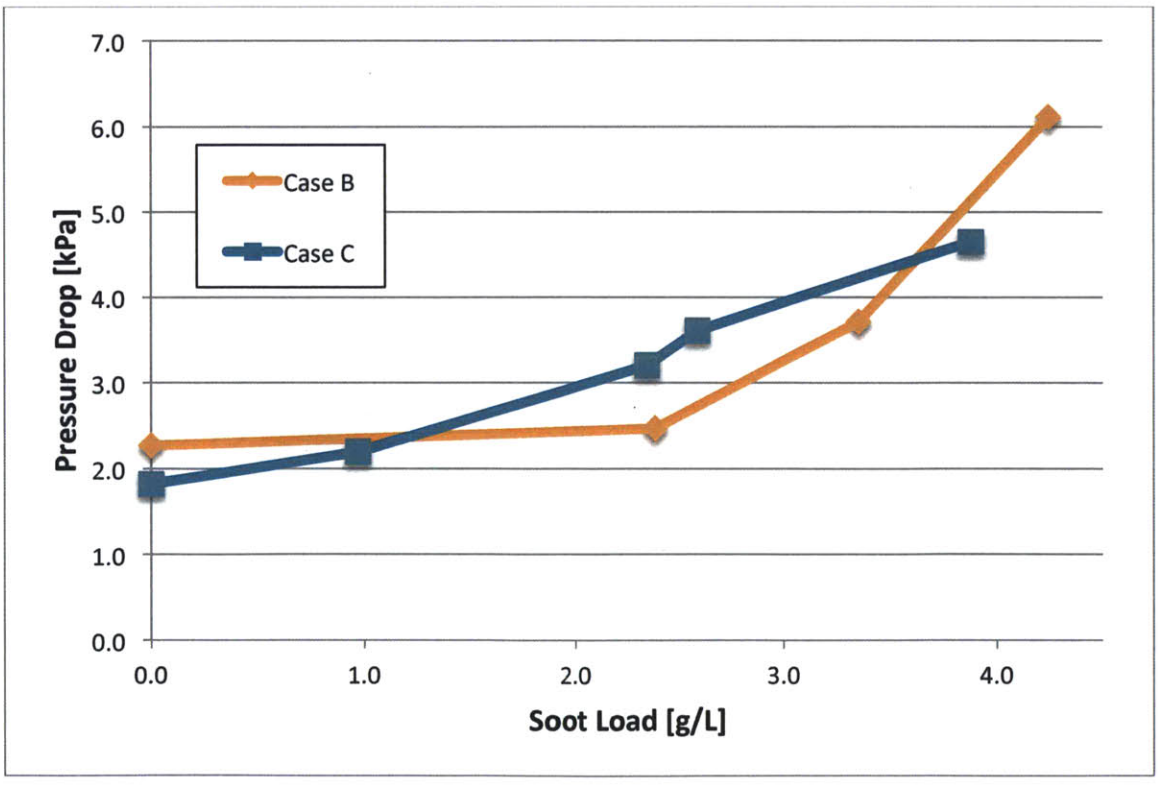

Figure 46: 25 g/L Ash samples soot loading (Note Case B is 25.0 g/L Soot and Case C is 24.6 g/L)

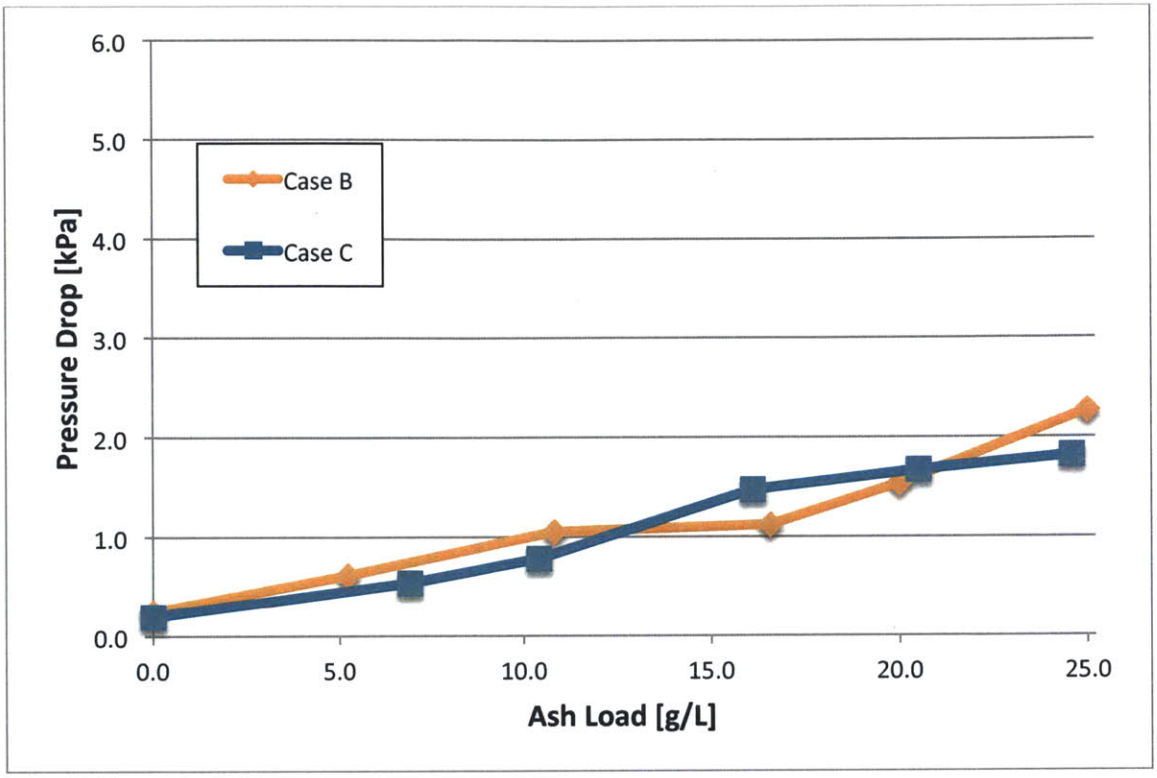

Figure 47: 0 g/L Soot samples ash effects

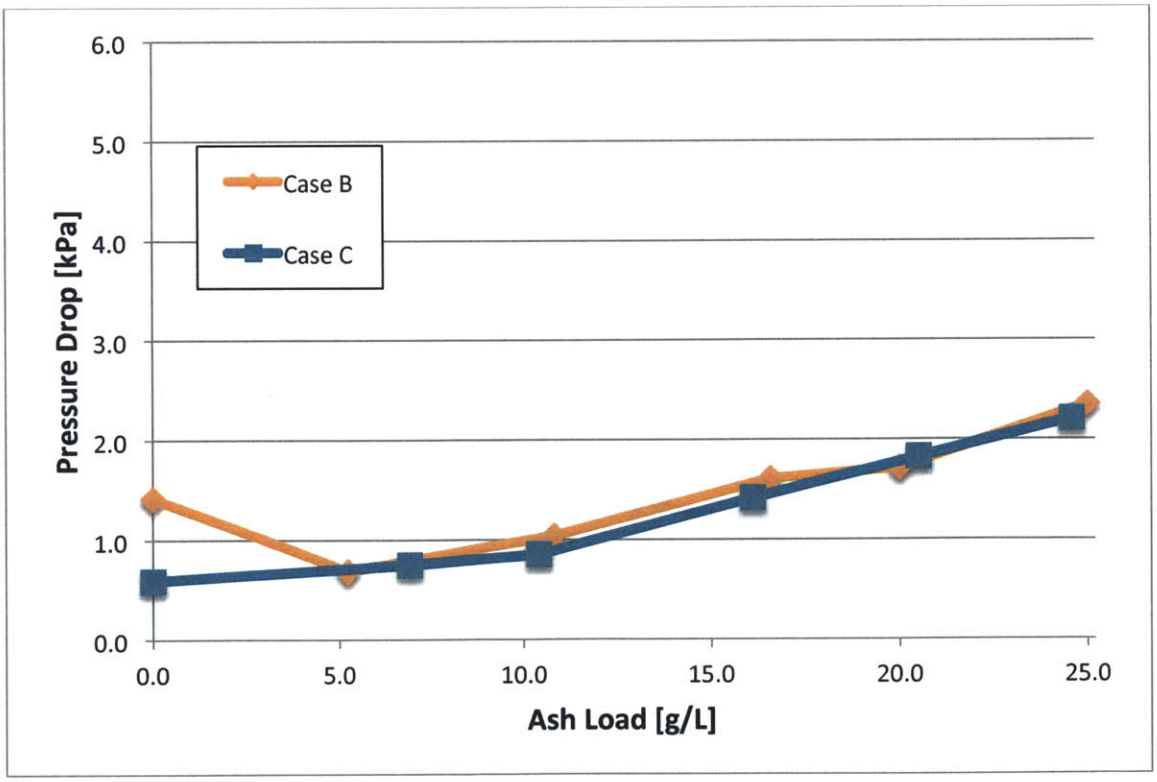

Figure 48: 1 g/L Soot samples ash effects

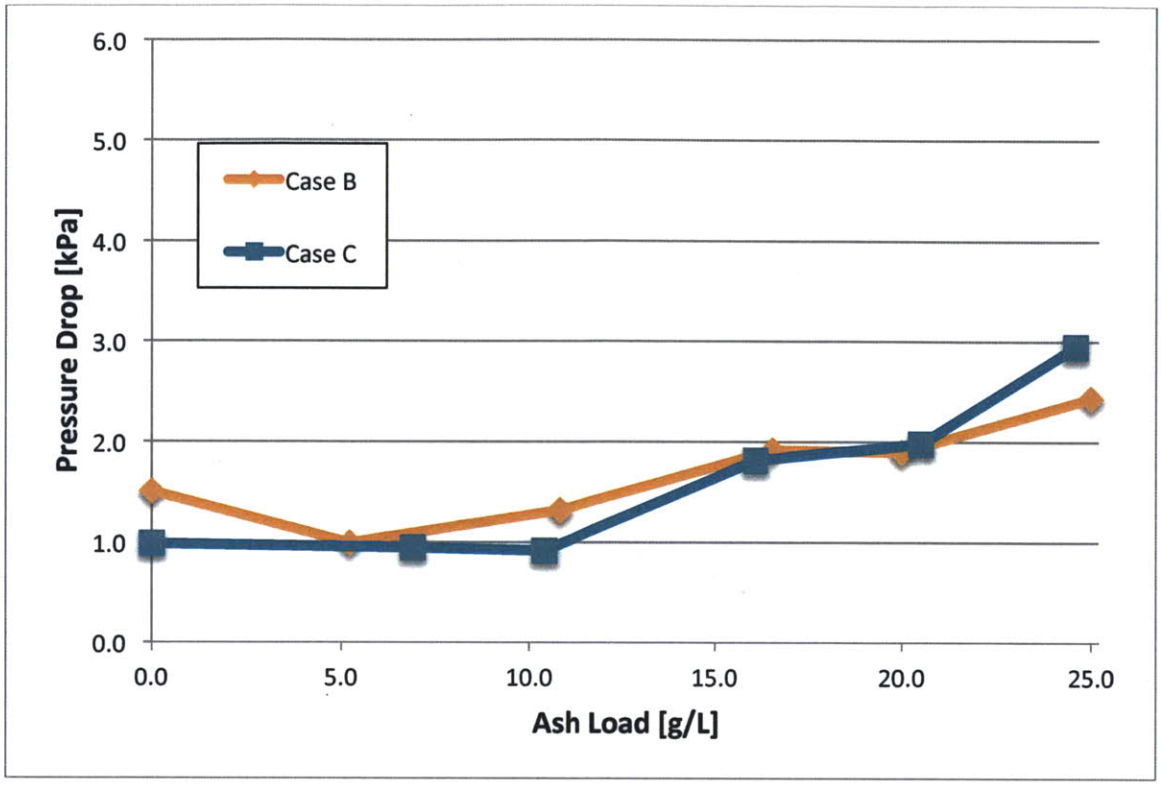

Figure 49: 2 g/L Soot samples ash effects

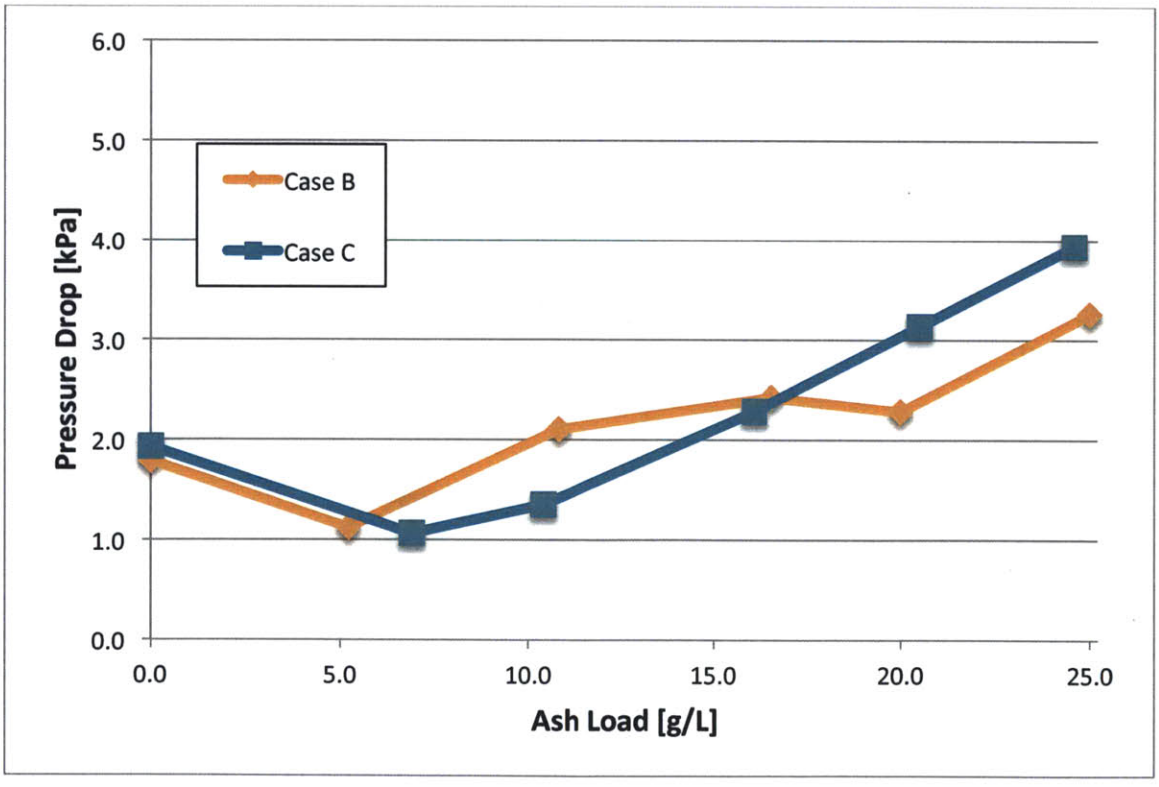

Figure 50: 3 g/L Soot samples ash effects

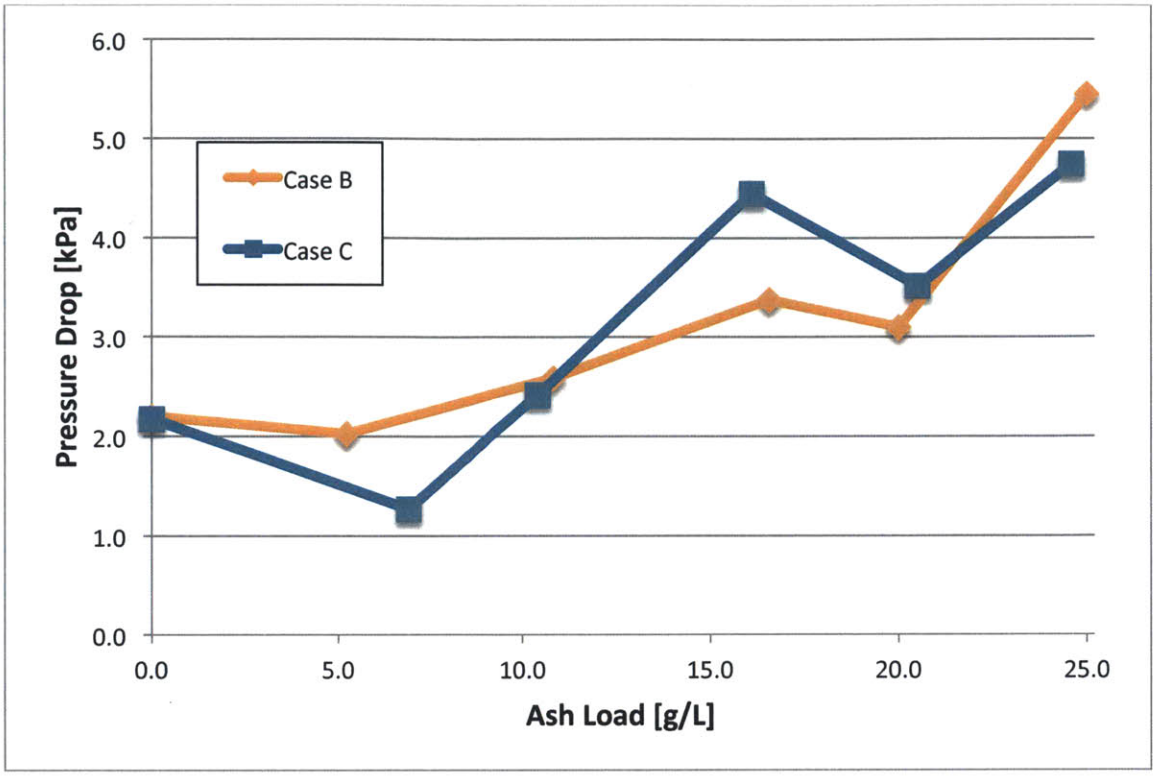

Figure 51: 4 g/L Soot samples ash effects

(This page intentionally left blank)

7.0 CONCLUSIONS

Results of this work concerning how the ash derived from differing regeneration methods adversely affect diesel particulate filters are important to understand how ash negatively affects diesel aftertreatment performance over a minimum DPF service life of 150,000 miles. Exhaust conditions play an important function in the creation of ash and how ash affects the pressure drop across a DPF. By conducting experiments with varying regeneration methods the individual and synergistic effects of the passive regeneration can be studied and analyzed. The results of this study provide practical information to engine manufactures and aftertreatment designers to diminish the unfavorable effects of ash accumulation within a DPF.

7.1 Passive Regeneration Method Effects on Pressure Drop

Continuous active regeneration is not practical or beneficial but has been included in this study for comparison. Continuous passive regeneration, seen in Case A, has beneficial pressure effects early in DPF lifetime. Past midlife continuous passive regeneration becomes detrimental. Flow restriction become much greater than previous studied DPF samples.

Case B and C also have early lifecycle benefits. The pressure drop curves show very little depth filtration effects compared to previous periodic active regeneration methods. Given that the fidelity of pressure drop points are not numerous enough to judge the scale of depth filtration. It can neither be stated that depth filtration is short in duration or that it is longer in duration but has less effect on flow restriction. During the cake filtration stage of Case B and C the pressure increase is again very advantages compared to active studies until the midlife stage. The cake filtration slopes then increase past previous active regeneration studies.

The conclusions drawn from this study are listed below:

1. Continuous regeneration did not show pressure drop advantage over passive regenerations in the cases studied. It also showed a pressure drop trend (abrupt up-shift), which was not explainable by DPF performance fundamentals.
2. The effect on DPFs of DOC operation during passive regeneration did not display significant effects. This requires further analysis of the ash formation and distribution to examine differences.
3. Depth filtration during passive regeneration proves to be less significant than that of active regeneration.

It is possible that passive regeneration early in operation of a diesel engine could offer the lowest flow restriction, therefore the lowest backpressure and lowest efficiency loss due to the ATS. Then it could be possible to switch to active regeneration for the remaining life of the DPF. This could take advantage of passive regeneration's early benefits with the lower pressure drops late in life to keep the pressure drop increases to a minimum. Ideally this would be to minimize depth filtration and build a small evenly distributed ash layer, and then prior to the layer becoming too restrictive switch to loading ash to the end plug. This would take the advantages of both passive and active regeneration into one hybrid system.

7.2 Future Work Considerations

The depth filtration of passive regeneration deserves further investigation. A study focused on loading a filter passively to around 5 g/L at small weight increments would show increased fidelity of the early stages of passive regeneration and how that affects the filter later in life. This coupled with ash analysis could be beneficial to understanding early ash formation undergoing passive regeneration.

A hybrid regeneration test plan could investigate the opportunity to utilize passive regeneration early in the DPF lifecycle and then switch to active regeneration before the adverse effects of late lifecycle passive regeneration. This would verify that switching to active regeneration adds benefit to a previously passive loaded system. On the other hand this system might be infeasible if the early ash development under passive regeneration leads the filter down an irreversible path to higher-pressure losses. If this is the case than switching to active regeneration would be wasteful and useless.

This study into the long-term aging effects of passive regeneration has broadened the view of passive regeneration methods and offers many further studies for the future. The diesel particulate filters loaded during this study will be used further as core samples on flow and catalyst bench studies to pinpoint the ash effects on regeneration with optical studies and effects on the catalyst with soot oxidation measurements.

Now that the pressure drop curves have been established and the DPFs have been loaded to 25 g/L investigation into the ash formation and deposition will provide greater insight to the mechanism of ash transport and affect on pressure drop. These characteristics of ash composition and morphology will be found by traditional post-mortem analysis previously conducted at MIT. This method includes coring the DPF and destructively splitting these sections into smaller pieces to measure the ash layer thickness and location of the start of the ash end plug. Before this destructive test the filters will be sent to Advantest

America to be scanned with the TAS7000. This system utilizes Terahertz wave to conduct three dimensional image analyses. Early work with this system can be seen following in Figure 52 and Figure 53. This early work was done with a filter loaded to two different soot levels and it shows great promise at a nondestructive view of the ash distribution. It could provide faster method of comparing different ash distributions between filters and especially between different regeneration methods.

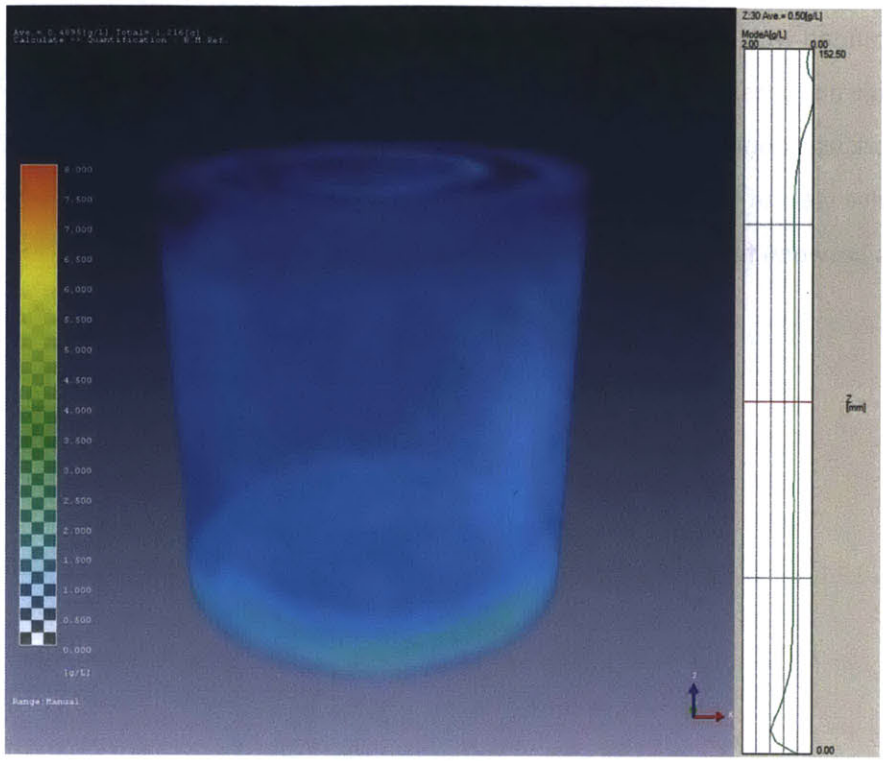

Figure 52: Advantest image of 0.5 g/L sample (scale 0-8 g/L concentration) [63]

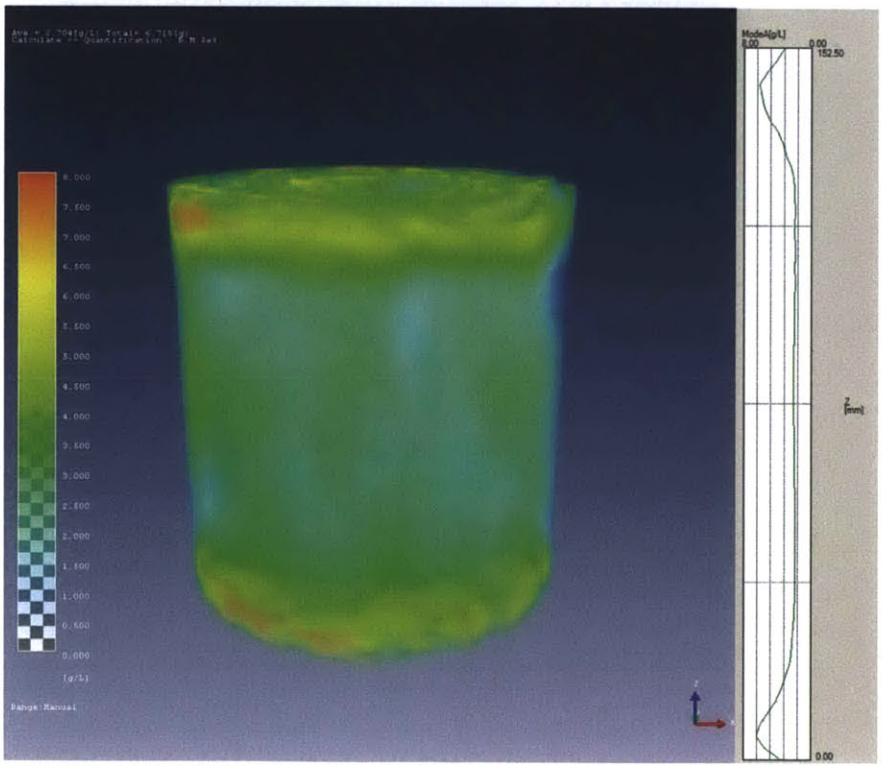

Figure 53: Advantest image 2.5 g/L sample (scale 0-8 g/L concentration) [63]

9 REFERENCES

[1] J. Heywood, *Internal Combustion Engine Fundamentals*, 1st ed. McGraw-Hill Science/Engineering/Math, 1988.

[2] R. B. GmbH, *Bosch Automotive Handbook - 8th Edition*, 8th ed. Bentley Publishers, 2011.

[3] "Technology Guide: Reference Papers on Diesel Engine and Emission Technologies." [Online]. Available: http://www.dieselnet.com/tg.php#basics. [Accessed: 17-Apr-2013].

[4] "Diesel Technology Forum: Cars,Trucks & SUVs." [Online]. Available: http://www.dieselforum.org/diesel-at-work/cars-trucks-and-suvs. [Accessed: 17-Apr-2013].

[5] "Refining Crude Oil - Energy Explained, Your Guide To Understanding Energy - Energy Information Administration." [Online]. Available: http://www.eia.gov/energyexplained/index.cfm?page=oil_refining. [Accessed: 17-Apr-2013].

[6] Charles River Associates, "Diesel Technology and the American Economy," Diesel Technology Forum Report D02378-00, 2000.

[7] A. G. (Alexander G. Sappok, "Emissions and in-cylinder combustion characteristics of Fischer-Tropsch and conventional diesel fuels in a modern CI engine," Thesis, Massachusetts Institute of Technology, 2006.

[8] "Health Assessment Document for Diesel Engine Exhaust (Final 2002) | Environmental Assessment | US EPA." [Online]. Available: http://cfpub.epa.gov/ncea/cfm/recordisplay.cfm?deid=29060#Download. [Accessed: 18-Apr-2013].

[9] "Klanner: Car Emissions and EURO 5 Consumers View - Google Scholar." [Online]. Available: http://scholar.google.com/scholar?cluster=17714664793592776130&hl=en&as_sdt=0,22&sciodt=0,22. [Accessed: 18-Apr-2013].

[10] "Gasoline Boats and Personal Watercraft | Nonroad Engines, Equipment, and Vehicles | US EPA." [Online]. Available: http://www.epa.gov/oms/marinesi.htm. [Accessed: 01-Jun-2012].

[11] "Meeting EPA 2010 | Facts About SCR." [Online]. Available: http://www.factsaboutscr.com/environment/epa2010.aspx. [Accessed: 17-Apr-2013].

[12] "Substainable development and annual report 2011 | PSA PEUGEOT CITROËN." [Online]. Available: http://annualreport.psa-peugeot-citroen.com/. [Accessed: 19-Apr-2013].

[13] *sm_diesel_particulate.jpg (JPEG Image, 300 × 303 pixels)*. .

[14] *f2008-06-058.jpg (JPEG Image, 290 × 168 pixels) - Scaled (0%)*. .

[15] Z. N. Mogaka, V. W. Wong, and S. M. Shahed, "Performance and Regeneration Characteristics of a Cellular Ceramic Diesel Particulate Trap," 1982.

[16] O. Salvat, P. Marez, and G. Belot, "Passenger Car Serial Application of a Particulate Filter System on a Common Rail Direct Injection Diesel Engine," 2000.

[17] A. G. Sappok and V. W. Wong, "Detailed Chemical and Physical Characterization of Ash Species in Diesel Exhaust Entering Aftertreatment Systems," 2007.

[18] K. Aravelli and A. Heibel, "Improved Lifetime Pressure Drop Management for Robust Cordierite (RC) Filters with Asymmetric Cell Technology (ACT)," 2007.

[19] T. Ishizawa, H. Yamane, H. Satoh, K. Sekiguchi, M. Arai, N. Yoshimoto, and T. Inoue, "Investigation into Ash Loading and Its Relationship to DPF Regeneration Method," SAE International, Warrendale, PA, 2009-01-2882, Oct. 2009.

[20] C. Chiou, *X-ray CT DPF Scan*. 2012.

[21] "Catalyzed Diesel Filters [subscription]." [Online]. Available: http://www.dieselnet.com/tech/dpf_cat.php. [Accessed: 01-Jun-2012].

[22] *~th-reg.png (PNG Image, 307 × 157 pixels) - Scaled (0%). .*

[23] "Diesel Oxidation Catalyst [subscription]." [Online]. Available: http://www.dieselnet.com/tech/cat_doc.php. [Accessed: 01-Jun-2012].

[24] K. M. Bodek and V. V. Wong, "The Effects of Sulfated Ash, Phosphorus and Sulfur on Diesel Aftertreatment Systems - A Review," 2007.

[25] A. G. Konstandopoulos, D. Zarvalis, E. Kladopoulou, and I. Dolios, "A Multi-Reactor Assembly for Screening of Diesel Particulate Filters," 2006.

[26] "Emission Control Retrofit of Diesel Particulate Filter Maintenance: Current Practices and Experience," Washington, DC, 2005.

[27] W. A. Givens, W. H. Buck, A. Jackson, A. Kaldor, A. Hertzberg, W. Moehrmann, S. Mueller-Lunz, N. Pelz, and G. Wenninger, "Lube Formulation Effects on Transfer of Elements to Exhaust After-Treatment System Components," 2003.

[28] E. A. Bardasz, S. Cowling, A. Panesar, J. Durham, and T. N. Tadrous, "Effects of Lubricant Derived Chemistries on Performance of the Catalyzed Diesel Particulate Filters," 2005.

[29] J. A. Mc Geehan, J. Moritz, G. Shank, S. Kennedy, D. Stehouwer, M. Urbank, M. Belay, S. Goodier, A. Cassim, B. Runkle, H. DeBaun, S. Harold, K. Chao, S. Herzog, R. Stockwell, C. Passut, P. Fetterman, D. Taber, L. Williams, W. M. Kleiser, J. Zalar, P. Scinto, E. Santos, and J. A. Rutherford, "API CJ-4: Diesel Oil Category for Both Legacy Engines and Low Emission Engines Using Diesel Particulate Filters," 2006.

[30] *Standard Test Method for Ash from Petroleum Products*. 2000.

[31] M. Sutton, N. Britton, B. Otterholm, P. Tengström, C. Frennfelt, A. Walker, and I. Murray, "Investigations into Lubricant Blocking of Diesel Particulate Filters," 2004.

[32] J. R. Warner, J. H. Johnson, S. T. Bagley, and C. T. Huynh, "Effects of a Catalyzed Particulate Filter on Emissions from a Diesel Engine: Chemical Characterization Data and Particulate Emissions Measured with Thermal Optical and Gravimetric Methods," 2003.

[33] M. Manni, A. Pedicillo, and F. Bazzano, "A Study of Lubricating Oil Impact on Diesel Particulate Filters by Means of Accelerated Engine Tests," 2006.

[34] K. Kimura, M. Lynskey, E. R. Corrigan, D. L. Hickman, J. Wang, H. L. Fang, and S. Chatterjee, "Real World Study of Diesel Particulate Filter Ash Accumulation in Heavy-Duty Diesel Trucks," 2006.

[35] G. Gaiser and P. Mucha, "Prediction of Pressure Drop in Diesel Particulate Filters Considering Ash Deposit and Partial Regenerations," SAE International, Warrendale, PA, 2004-01-0158, Mar. 2004.

[36] A. Sappok, R. Rodriguez, and V. Wong, "Characteristics and Effects of Lubricant Additive Chemistry on Ash Properties Impacting Diesel Particulate Filter Service Life," *Sae Int J Fuels Lubr*, vol. 3, no. 1, pp. 705–722, 2010.

[37] A. G. (Alexander G. Sappok, "The nature of lubricant-derived ash-related emissions and their impact on diesel aftertreatment system performance," Thesis, Massachusetts Institute of Technology, 2009.

[38] S. Munnis, "Synergistic effects of lubricant additive chemistry on ash properties impacting diesel particulate filter flow resistance and catalyst performance," Massachusettes Institute of Technology, 2011.

[39] "Wall-Flow Monoliths." [Online]. Available: http://www.dieselnet.com.libproxy.mit.edu/tech/dpf_wall-flow.php. [Accessed: 07-May-2013].

[40] "Cellular Monolith Substrates." [Online]. Available: http://www.dieselnet.com.libproxy.mit.edu/tech/cat_substrate.php. [Accessed: 07-May-2013].

[41] G. A. Merkel, W. A. Cutler, and C. J. Warren, "Thermal Durability of Wall-Flow Ceramic Diesel Particulate Filters," 2001.

[42] F. Mao and C. G. Li, "Performance Validation of an Advanced Diesel Particulate Filter With High Catalyst Loading Capacity," 2005.

[43] N. Miyakawa, H. Maeno, and H. Takahashi, "Characteristics and Evaluation of Porous Silicon Nitride DPF," 2003.

[44] A. G. Konstandopoulos, M. Kostoglou, E. Skaperdas, E. Papaioannou, D. Zarvalis, and E. Kladopoulou, "Fundamental Studies of Diesel Particulate Filters: Transient Loading, Regeneration and Aging," 2000.

[45] D. M. Young, D. L. Hickman, G. Bhatia, and N. Gunasekaran, "Ash Storage Concept for Diesel Particulate Filters," 2004.

[46] J. A. McGeehan, S. Yeh, M. Couch, A. Hinz, B. Otterholm, A. Walker, and P. Blakeman, "On The Road to 2010 Emissions: Field Test Results and Analysis with DPF-SCR System and Ultra Low Sulfur Diesel Fuel," 2005.

[47] V. Harlé, C. Pitois, L. Rocher, and F. Garcia, "Latest Development and Registration of Fuel Borne Catalyst for DPF Regeneration," 2008.

[48] K. O. Lee, J. Zhu, S. Ciatti, A. Yozgatligil, and M. Y. Choi, "Sizes, Graphitic Structures and Fractal Geometry of Light-Duty Diesel Engine Particulates," 2003.

[49] K. O. Lee and J. Zhu, "Effects of Exhaust System Components on Particulate Morphology in a Light-duty Diesel Engine," 2005.

[50] E. A. Kladopoulou, S. L. Yang, J. H. Johnson, G. G. Parker, and A. G. Konstandopoulos, "A Study Describing the Performance of Diesel Particulate Filters During Loading and Regeneration - A Lumped Parameter Model for Control Applications," 2003.

[51] F. Family and D. P. Landau, *Kinetics of Aggregation and Gelation*. Elsevier Science, 1984.

[52] M. Tassopoulos, J. A. O'Brien, and D. E. Rosner, "Simulation of microstructure/mechanism relationships in particle deposition," *Aiche J.*, vol. 35, no. 6, pp. 967–980, 1989.

[53] M. Tassopoulos, "Relationships between particle deposition mechanism, deposit microstructure and effective transport properties," 1991.

[54] A. G. Konstandopoulos, M. Kostoglou, P. Housiada, N. Vlachos, and D. Zarvalis, "Multichannel Simulation of Soot Oxidation in Diesel Particulate Filters," 2003.

[55] P. Karin, L. Cui, P. Rubio, T. Tsuruta, and K. Hanamura, "Microscopic Visualization of PM Trapping and Regeneration in Micro-Structural Pores of a DPF Wall," *Sae Int J Fuels Lubr*, vol. 2, no. 1, pp. 661–669, 2009.

[56] Y. Takeuchi, S. Hirano, M. Kanauchi, H. Ohkubo, M. Nakazato, M. Sutherland, and W. van Dam, "The Impact of Diesel Engine Lubricants on Deposit Formation in Diesel Particulate Filters," 2003.

[57] E. Bardasz, D. Mackney, N. Britton, G. Kleinschek, K. Olofsson, I. Murray, and A. P. Walker, "Investigations of the Interactions between Lubricant-derived Species and Aftertreatment Systems on a State-of-the-Art Heavy Duty Diesel Engine," 2003.

[58] M. Manni, A. Pedicillo, G. Del Piero, and E. Previde Massara, "An Experimental Evaluation of the Impact of Lubricating Oils and Fuels on Diesel Particulate Filters," 2007.

[59] "PRAMAC - S 5500." [Online]. Available: http://www.pramac.com/United-States/ie/portable-generator-s-5500-USA.asp. [Accessed: 01-Jun-2012].

[60] O. US EPA and O. of A. and R. US EPA, "Engine Certification Data." [Online]. Available: http://www.epa.gov/oms/certdata.htm#largeng. [Accessed: 01-Jun-2012].

[61] Kathi Bahr, *Sloan Automotive Lab Photos*. 2012.

[62] "YANMAR | L100V." [Online]. Available: http://us.yanmar.com/products/industrial-engines/air-cooled/epa-certified/l-v-series/l100v/. [Accessed: 01-Jun-2012].

[63] Advantest America Inc, "DPF Analysis Report by TAS7000, A New Non-Destructive 3D Imaging Analysis System," 20-Sep-2012.

10 APPENDIX

Model	L100V
Engine Type	Air Cooled, 4 cycle, Vertical Cylinder
Fuel	Diesel
Number of Cylinders	1
Bore x Stroke	86mm x 75 mm
Combustion Type	Direct Injection
Total Displacement	435 cc
Aspiration	Natural Aspiration
Valves per Cylinder	2
Rated Speed	3600 rpm
Net Intermittent	9.1 Hp[6.8kW]/3600rpm
Net Continuous HP	8.3hp [6.2kW]/3600rpm
Direction of Rotation	Counter Clockwise, Viewed from PTO Side
Crankshaft Type	Straight Keyed, Tapered or Threaded
Starting System	Recoil or Recoil/12 V Electric
Decompression System	Manual Type with Auto-return Lever
Charging System	12 Volt, 15 Amps (for Electric Start Models)
Electric Stop Device	Optional, Fuel Stop Solenoid (for Electric Start Models)
Cold Start Aid	Optional, Intake Air Heater (for Electric Start Models)
Fuel Tank Capacity	4.7 liters
Brake Specific Fuel Consumption at Rated Output	279 g/kW-hr
Lubrication System	Pressure Lubrication with Trochoid Pump
Oil Capacity	1.60 Liters [0.60 Effective]
Exhaust System	Expansion Silencer with Cover
Air Cleaner	Dry-Type with Paper Element
Balancing System	Single, Counter-Rotating Balance Shaft
Length	16.2 in (412mm)
Width	18.6 in (472mm)
Height	19.4in (493mm)
Dry Weight (Recoil Start)	106.9 Lbs (48.5 kg)
Dry Weight (Electric Start)	117.9 Lbs (53.5 kg)
Noise Output @ Continuous Rating, Mean of Four Directions at 1 Meter	97 dB(A)

Table 14: Yanmar L100V specifications [62]

Figure 54: Test facility front [61]

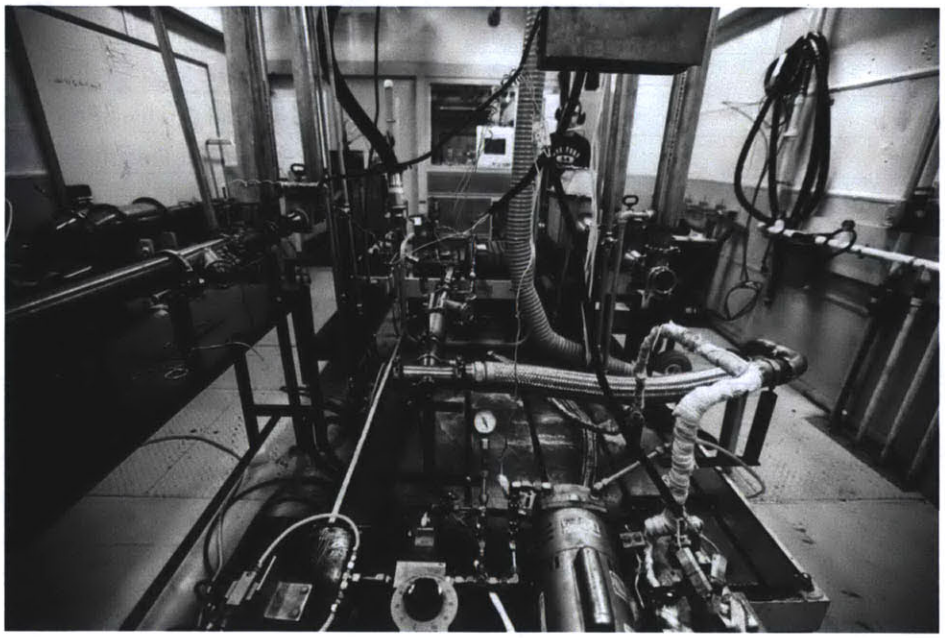

Figure 55: Test facility back [61]